EVALUATION OF SURFACE ENERGY BALANCE MODELS FOR MAPPING EVAPOTRANSPIRATION USING VERY HIGH RESOLUTION AIRBORNE REMOTE SENSING DATA

by

GEORGE PAUL

B.Tech., Allahabad Agricultural Institute, Allahabad, U.P., India, 2002
M.Tech., National Institute of Technology, Allahabad, U.P., India, 2004

AN ABSTRACT OF A DISSERTATION

submitted in partial fulfillment of the requirements for the degree

DOCTOR OF PHILOSOPHY

Department of Agronomy
College of Agriculture

KANSAS STATE UNIVERSITY
Manhattan, Kansas

2013

Abstract

Agriculture is the largest (90%) consumer of all fresh water in the world. The consumptive use of water by vegetation represented by the process evapotranspiration (ET) has a vital role in the dynamics of water, carbon and energy fluxes of the biosphere. Consequently, mapping ET is essential for making water a sustainable resource and also for monitoring ecosystem response to water stress and changing climate. Over the past three decades, numerous thermal remote sensing based ET mapping algorithms were developed and these have brought a significant theoretical and technical advancement in the spatial modeling of ET. Though these algorithms provided a robust, economical, and efficient tool for ET estimations at field and regional scales, yet the uncertainties in flux estimations were large, making evaluation a difficult task. The main objective of this study was to evaluate and improve the performance of widely used remote sensing based energy balance models, namely: the Surface Energy Balance Algorithm for Land (SEBAL), Mapping Evapotranspiration at high Resolution and with Internalized Calibration (METRIC), and Surface Energy Balance System (SEBS). Data used in this study was collected as part of a multi-disciplinary and multi-institutional field campaign BEAREX (Bushland Evapotranspiration and Agricultural Remote Sensing Experiment) that was conducted during 2007 and 2008 summer cropping seasons at the USDA-ARS Conservation and Production Research Laboratory (CPRL) in Bushland, Texas. Seventeen high resolution remote sensing images taken from multispectral sensors onboard aircraft and field measurements of the agro-meteorological variables from the campaign were used for model evaluation and improvement. Overall relative error measured in terms of mean absolute percent difference (MAPD) for instantaneous ET (mm h^{-1}) were 22.7%, 23.2%, and 12.6% for SEBAL, METRIC, and SEBS, respectively. SEBAL and METRIC performances for irrigated fields representing higher ET with limited or no water stress and complete ground cover surfaces were markedly better than that for dryland fields representing lesser ET and greater soil water deficits with sparser vegetation cover. SEBS algorithm performed equally well for both irrigated and dryland conditions but required accurate air temperature data. Overall, this study provides new insights into the performance of three widely used thermal remote sensing based algorithms for estimating ET and proposed modifications to improve the accuracy of estimated ET for efficient management of water resources.

EVALUATION OF SURFACE ENERGY BALANCE MODELS FOR MAPPING EVAPOTRANSPIRATION USING VERY HIGH RESOLUTION AIRBORNE REMOTE SENSING DATA

by

GEORGE PAUL

B. Tech., Allahabad Agricultural Institute, Allahabad, U.P., India, 2002
M. Tech., National Institute of Technology, Allahabad, U.P., India, 2004

A DISSERTATION

submitted in partial fulfillment of the requirements for the degree

DOCTOR OF PHILOSOPHY

Department of Agronomy
College of Agriculture

KANSAS STATE UNIVERSITY
Manhattan, Kansas

2013

Approved by:

Major Professor
Dr. P.V. Vara Prasad

Copyright

Abstract

Agriculture is the largest (90%) consumer of all fresh water in the world. The consumptive use of water by vegetation represented by the process evapotranspiration (ET) has a vital role in the dynamics of water, carbon and energy fluxes of the biosphere. Consequently, mapping ET is essential for making water a sustainable resource and also for monitoring ecosystem response to water stress and changing climate. Over the past three decades, numerous thermal remote sensing based ET mapping algorithms were developed and these have brought a significant theoretical and technical advancement in the spatial modeling of ET. Though these algorithms provided a robust, economical, and efficient tool for ET estimations at field and regional scales, yet the uncertainties in flux estimations were large, making evaluation a difficult task. The main objective of this study was to evaluate and improve the performance of widely used remote sensing based energy balance models, namely: the Surface Energy Balance Algorithm for Land (SEBAL), Mapping Evapotranspiration at high Resolution and with Internalized Calibration (METRIC), and Surface Energy Balance System (SEBS). Data used in this study was collected as part of a multi-disciplinary and multi-institutional field campaign BEAREX (Bushland Evapotranspiration and Agricultural Remote Sensing Experiment) that was conducted during 2007 and 2008 summer cropping seasons at the USDA-ARS Conservation and Production Research Laboratory (CPRL) in Bushland, Texas. Seventeen high resolution remote sensing images taken from multispectral sensors onboard aircraft and field measurements of the agro-meteorological variables from the campaign were used for model evaluation and improvement. Overall relative error measured in terms of mean absolute percent difference (MAPD) for instantaneous ET (mm h^{-1}) were 22.7%, 23.2%, and 12.6% for SEBAL, METRIC, and SEBS, respectively. SEBAL and METRIC performances for irrigated fields representing higher ET with limited or no water stress and complete ground cover surfaces were markedly better than that for dryland fields representing lesser ET and greater soil water deficits with sparser vegetation cover. SEBS algorithm performed equally well for both irrigated and dryland conditions but required accurate air temperature data. Overall, this study provides new insights into the performance of three widely used thermal remote sensing based algorithms for estimating ET and proposed modifications to improve the accuracy of estimated ET for efficient management of water resources.

Table of Contents

List of Figures

List of Tables

Acknowledgements

At last the time has come to write this section. The journey was long and exhausting, yet was a memorable and fruitful one. I attribute the successful completion of this research and dissertation to three groups, namely; Professional, Community, and Family, each one I would like to acknowledge here.

I owe everything to my mentor Dr. Prasanna Gowda. He literally picked me up from nowhere and nurtured me into a scientist. Dr. Gowda gave me his 'Time', provided 'Opportunities', 'Supported' me in every aspect of life, treated me like a 'Friend', and has already made big plans for my 'Career'. Thank you, Dr. Gowda. Sincere gratitude to my advisor Prof. Vara Prasad, the several discussions we had were instrumental in shaping my thought process and thanks for the exceptional financial support to my program. I would like to thank the members of my advisory committee, Prof. Scott Staggenborg, Dr. Stacy Hutchinson and Dr. Rob Aiken for their guidance, cooperation and support. Heartfelt gratitude to my colleagues Sruthi, Rachel, Raymond, Maiga, Mahama, Gautam, Kyle, and Amal; thank you for making Crop Physiology Lab the best workplace. I highly appreciate the devoted efforts of Sruthi in teaching me the many aspects of crop stress physiology. My sincere thanks to the friendly and supportive faculty and staff of the Department of Agronomy; special mention of Prof. Mary Beth Kirkham, Prof. Steve Welch and Prof. Loyd Stone.

My performance and growth as a researcher was the result of the large supportive community of friends. The student community who became friends over the years, Sowmya, Spoorthy, Anusha, Lamuel, Venkat, Vijay, Sankar, Smita, and many more, thank you for standing beside me. Friends from church, David, Anita, Steve, Rod, Jane, Robin, Lowell and other friends at Faith E Free were always there as elders to guide through daily life. Ginny, Tony, Sunil, Aisal, Dennis, Anuskha, Sruthi, Predeesh, Vinod, Abhaya and several others of the Indian-Keralite group who made our stay so enjoyable. No words to describe the love and support received from Ranjni and Philip, thanks for being my family.

Express my wholehearted gratitude to my parents, my sister Smita, niece Fiona and brother-in-law Thomas for their affection, sacrifices, and blessings. Last but not the least, my wife Amy who is my strong pillar; my Ph.D. is because of her un-matching sacrifice, leaving behind a glorious career to support me and my family.

Dedication

I dedicate my dissertation to the two great women of my life. My brilliant, loving, generous and supportive wife Amy George, who's been my inspiration and strength. My mother Elsy Paul, who taught me the three P's (Pillars) of research life, Perseverance, Practicality and Perfectionism.

Chapter 1 - General Introduction

1.1 Introduction

The Ogallala Aquifer, also known as the High Plains Aquifer, covers approximately 174,000 square miles from Texas High Plains to the southwestern South Dakota in the central United States, and is the major source of water for irrigated agriculture in the overlying region. More than 90% of the ground water withdrawals from the Ogallala aquifer is used to irrigate at least one fifth of all US cropland (Guru et al., 2000). Over exploitation of the Ogallala's water resources for irrigated agriculture has resulted in withdrawals from the aquifer far exceeding the natural recharge. Once considered as an unlimited source of fresh water is now fast depleting and threatening the sustainability of agricultural and allied operations in the Ogallala Aquifer Region. Therefore, all water conservation efforts needs to be focused on irrigated agriculture as it is the largest consumer of groundwater in the region. Sustainable irrigated agriculture demands for safeguarding profitability, productivity, and food security which could only be achieved through development and implementation of innovative technologies. Irrigation application efficiency is reaching its attainable limits, however, the computation of crop water requirement still relies heavily on the traditional empirical ratio of actual crop evapotranspiration (ET_a) to reference crop evapotranspiration (ET_r).

Irrigation scheduling using crop coefficient, K_c, values where ET_a is determined as, $ET_a=K_c \times ET_r$, was adopted widely owing to its simplistic two-step approach (Payero and Irmak, 2011). While ET_r was a function of weather data alone, K_c values were constrained to unique crop managed under given climate and site specific crop management. Uncertainties in the generalized K_c values were too many as K_c values for the same crop showed significant variation between locations due to differences in crop variety, soil properties, irrigation method and frequency, climate, and crop management practices (Payero and Irmak, 2011). The ASCE-EWRI (Allen et al., 2005) or the FAO 56 (Allen at al., 1998) standardized Penman-Monteith equation was used to compute the ET_r, however, requirement of large number of spatially variable meteorological parameters limits their usage to point scale applications.

Remote sensing methods for calculating the actual ET based on the equilibrium between the radiation balance and energy balance at the surface of the earth is recognized as the only viable means to map regional- and meso-scale patterns of ET. At field scale, ET can be measured

over a homogenous surface using conventional techniques such as Bowen Ratio (BR), eddy covariance (EC), water balance, and lysimeter systems; however, these systems do not provide spatial trends at the regional scale, especially in heterogeneous landscapes. Over the past three decades, numerous remote sensing based ET mapping algorithms were developed. These algorithms provided a robust, economical, and efficient tool for ET estimations at field and regional scales. ET maps have large utility ranging from crop water management, climate change impact assessment, hydrological modeling, recharge prediction, irrigation performance and land use planning, to name a few applications. A detailed review of different remote sensing based ET algorithms is presented in Gowda et al. (2008). They reported that ET estimation accuracy varied from 67 to 97% for daily ET and above 94% for seasonal ET, indicating that remote sensing technology with appropriate algorithms has the potential to estimate ET at regional scale adequate for irrigation scheduling.

Precision farming (PF) or site specific management is currently promoted by several sectors of agribusiness. High-resolution thermal imaging systems have been used to evaluate water status of cotton (Alchanatis et al., 2010), wheat (Tilling et al., 2007), vineyards (Grant et al., 2007) and olives (Berni et al., 2009). There is a growing interest to use energy balance algorithms to develop ET maps at field scale to support intelligent irrigation systems. Airborne remote sensing provides high resolution visible and thermal spectral data which could be utilized towards irrigation, fertilizer applications and pest management strategies, thus providing opportunities to decrease input costs and potentially increase net income.

Regional scale ET maps with daily and seasonal coverage would enhance water resources managers' ability to plan and manage limited water resources. Remote sensing based methods applied to the estimation of ET over large areas provide water managers with new tools for the assessing crop water demand accurately. Numerous remote sensing based ET models have been developed in the last three decades to make use of the visible, near-infrared (NIR), shortwave infrared (SWIR), and most importantly, thermal infrared data acquired by sensors onboard satellite platforms. Some of the commonly used remote sensing based ET algorithms are:

- Surface Energy Balance Algorithm for Land (SEBAL; Bastiaanssen et al., 1998a; 1998b)
- Mapping Evapotranspiration at High Resolution with Internalized Calibration (METRIC; Allen et al., 2007a,b)

- Surface Energy Balance System (SEBS; Su, 2002)
- Two-Source Model (TSM; Norman et al., 1995)
- Surface Energy Balance Index (SEBI; Menenti and Choudhury 1993)
- Simplified Surface Energy Balance (SSEB; Senay et al., 2007)
- Trapezoid Interpolation Model (TIM; Le Jiang and Shafiqul Islam, 2001)

1.2 A brief history of remote sensing based evapotranspiration algorithms

In the last three decades, numerous remote sensing based ET algorithms have been developed. Among those methods, some are simple and use remote sensing data to calculate only the available radiation on the surface, and then apply conventional equations such as Priestley-Taylor or P-M model to calculate ET. Complex methods include a detailed and lengthy procedure for calculating sensible heat flux. A brief review of literature for the three four major single source energy balance algorithms namely SEBAL, METRIC and SEBS is provided in the following paragraphs.

Surface Energy Balance Algorithm for Land (SEBAL) is an energy-partitioning algorithm over the land surface, which estimates the actual evaporation using satellite images (Bastiaanssen et al., 1998a, Bastiaanssen et al., 1998b,). SEBAL has been applied in more than 30 countries worldwide, with 26 research studies and 17 application studies (Bastiaanssen et al., 2005). SEBAL has been applied for ET estimation, calculation of crop coefficients and evaluation of basin wide irrigation performance under various agro-climatic conditions. Average deviation of SEBAL ET estimates using NOAA images compared with LAS for 10 day period was 17%, and decreased to 1% for monthly estimates (Hemakumara et al., 2003). MODIS level 3 data, used to estimate regional ET over wheat growing region showed relative deviation of 25% with respect to pan evaporation measurements (Patel et al., 2006). Comparison between a highly parameterized two source model (TSM) and SEBAL (single source model) over a range of environmental conditions showed similar agreements with tower observations. However, SEBAL performance over bare soil and dry sparsely vegetated areas were poor as compared to TSM (Timmermans et al., 2007). Using Landsat images, it was observed that the difference between SEBAL calculations and field measurements of accumulated actual ET was less than 1% and 5% for irrigated mango orchard and natural vegetation, respectively, when the equations are locally calibrated (Teixeira et al., 2009). Performance of Landsat based SEBAL was

evaluated over Texas High Plains by comparing estimated ET with measured value from four large monolithic lysimeters. Results show good agreement for irrigated fields but poor prediction for fields under dryland management (Gowda et al., 2008). One of the main considerations in SEBAL, when evaluating pixel by pixel sensible and latent heat fluxes, is to establish the linear relationships between surface temperature (Ts) and the surface-air temperature difference (dT) on each pixel with the coefficients of the linear expressions determined from the extremely dry (hot) and wet (cold) points. This requires subjective specifications of representative hot/dry and wet/cool pixels within the scene to determine model parameters 'a' and 'b' (Li et al., 2009).

Mapping Evapotranspiration at High Resolution with Internalized Calibration (METRIC) uses SEBAL as its foundation (Allen et al., 2007a). The main distinction between various single-source surface energy balance methods is in the estimation of sensible heat flux. METRIC utilizes the pioneering concept (dT calculated from extreme pixels) of SEBAL in the estimation of sensible heat. For this reason METRIC and SEBAL has been grouped under similar model class (Li et al., 2009). However, METRIC does come with certain additions and improvements over SEBAL and thus can rightly be called as an improved version of SEBAL. The developers of METRIC (Allen et al., 2007a) states that "the model is internally calibrated using ground-based reference ET to reduce computational biases inherent to remote sensing-based energy balance and to provide congruency with traditional methods for ET". METRIC uses alfalfa reference ET at two instances: (1) for the wet pixel, ET is set to 1.05 ETr, and (2) instantaneous ET to daily value is based on the alfalfa ETrF (defined as the ratio of instantaneous ET to the reference ETr) instead of the actual evaporative fraction. METRIC claims to account for regional advection effects through the use of reference ET. Consequently, METRIC requires computation of alfalfa reference ET for each image. Readily available high quality hourly agricultural weather data is required for calculation of ETr (Tasumi et al., 2005; Tasumi and Allen, 2007). The inclusion of water balance model for determination of residual moisture in the dry pixel again makes METRIC more data dependent and computationally complex than SEBAL. ET estimates from METRIC model, using Landsat 5 TM data for the Texas High Plains, were compared with derived ET from soil water balance model; results showed deviation of 8-10% for daily ET values (Gowda et al., 2008c). Daily ET values with good prediction indicated that METRIC performed well for the advective conditions of the Texas High Plains (Chávez et al., 2007 and Gowda et al., 2008c). Seasonal estimates of METRIC-ET used within

an irrigation scheme in southwest Spain helped to identify specific agricultural fields, experiencing problems in water management (Santos et al., 2008). A detailed evaluation of METRIC using Landsat TM data against lysimeter and other traditional methods showed an average standard deviation error between 13 to 20% (Allen et al., 2007b). Comparative study of METRIC, TSEB and TIM algorithms yielded reasonable agreement with measured energy fluxes at tower locations, with root-mean-square errors of 50-75 W/m^2; however, spatial inter-comparison revealed significant discrepancies (Choi et al., 2009).

Surface Energy Balance System (SEBS) was developed by Su (2002) for the estimation of atmospheric turbulent fluxes using satellite earth observation data. SEBS adopts the concept from the SEBI (Surface Energy Balance Index) scheme (Menenti and Choudhury, 1993). A better parameterization of turbulent heat transfer, bulk atmospheric similarity theory and algorithms to infer spectrally integrated hemispherical reflectance and brightness temperature has been integrated in SEBS (Menenti et al., 2003). At large spatial scales, SEBS requires reference potential temperature and humidity of air at an appropriate height above heterogeneous land (Jia et al., 2003). This requirement of reference height taken at the planetary boundary layer (PBL) and observation values of potential temperature and humidity at this height can be seen as a bottleneck for application over heterogeneous land surfaces. Fields of wind, potential temperature and humidity of air generated by weather prediction model integrated over the planetary boundary layer has been used successfully to execute SEBS over large heterogeneous land (Jia et al., 2003). Validation using annual ET computed from simple water balance model suggested effective estimation of annual ET (Jin et al., 2009).

1.3 Problem Statement

Remote sensing based ET models are better suited for estimating crop water use at both field and regional scales (Allen et al., 2007a). Over the past four decades various intensive field campaigns were undertaken to understand the turbulent exchanges of mass and energy at the land surface. Many multidisciplinary, multi-institutional campaigns including EAGLE2006 (Su et al., 2009), SGP97 (Menenti, et al., 2003), SPARC 2004 (Su, et al., 2008), SEN2FLEX 2005 (Sobrino et al., 2008), SMACEX (French et al., 2005), and BEAREX (Chavez et al., 2009) were taken up for further understanding and improving the parameterization of land surface hydro-meteorological processes.

To enhance the understanding of the land surface hydro-meteorological processes, the Bushland Evapotranspiration and Agricultural Remote Sensing Experiment (BEAREX) field campaign was conducted at the USDA-ARS Conservation and Production Research Laboratory. During this campaign high resolution data from the multispectral sensor onboard aircraft and ancillary ground data were acquired for summer cropping season of 2007 and 2008.

The **goal** of this research was to utilize the BEAREX dataset to evaluate single source remote sensing based algorithms for estimating ET over the semi-arid Texas High Plains (THP) region. The validation was carried out against measurements from 4 large precision weighing lysimeters installed in the center of two irrigated and two dryland fields of approximately 4.7 ha, this formed a unique and important aspect of the present study.

Specific Objectives:

1. Evaluate the variability in the 'a' and 'b' coefficients of the dT function due to the presence of multiple pixels fulfilling the hot and cold pixel selection criteria and how much influence this variability has on the final instantaneous ET (ET_i) estimates.
2. Compare SEBAL ET_i estimates with lysimetric data.
3. Incorporate a physically based parameterization for excess resistance (kB^{-1}) into SEBAL and test its performance.
4. Test the relationships to compute the various aerodynamic roughness parameters.
5. Investigate the influence of four different z_{oh} values on the flux estimations from SEBAL. The four z_{oh} values used are as follows:
   (1) $z_{oh} = z_{om}/\exp(kB^{-1})$, where $kB^{-1} = 2.3$
   (2) $z_{oh}(z_1) = 0.1$ m (spatial constant)
   (3) $z_{oh}(z_1) = 0.01$ m (spatial constant) and
   (4) $z_{oh} = z_{om}/\exp(kB^{-1})$, where kB^{-1} parameterization is used to get spatially varying z_{oh}.
6. Analyze the performance of a model that utilizes the hot and cold pixel concept (METRIC) and compares it against an algorithm (GSS) which utilizes the kB^{-1} parameter.
7. Evaluate the Surface Energy Balance System (SEBS) to estimate hourly ET fluxes.

1.4 References

Allen, R.G., Luis, S.P., Dirk, R., Martin, S., 1998. Crop evapotranspiration- Guidelines for computing crop water requirements. FAO Irrigation and Drainage Paper 56, FAO, Rome

Alchanatis, V., Cohen, Y., Cohen, S., Moller, M., Sprinstin, M., Meron, M., 2010. Evaluation of different approaches for estimating and mapping crop water status in cotton with thermal imaging. Precision Agriculture, 11, 27–41

Anderson, M.C., Norman, J.M. Diak, G.R. Kustas, W.P., Mecikalski J.R., 1997. A two-source time-integrated model for estimating surface fluxes using thermal infrared remote sensing. Remote Sensing Environment, 60, 195–216

Allen, R.G., Tasumi, M., Trezza, R., 2007a. Satellite-based Energy Balance for Mapping Evapotranspiration with Internalized Calibration (METRIC)- Model. Journal of Irrigation and Drainage Engineering ASCE, 133, 380–394

Allen, R.G., Tasumi, M., Morse, A., Trezza, R., Wright, J.L., Bastiaanssen, W., Kramber, W., Lorite, I., Robison, C.W., 2007b. Satellite-based Energy Balance for Mapping Evapotranspiration with Internalized Calibration (METRIC)-Applications. Journal of Irrigation and Drainage Engineering ASCE, 133, 395–406

ASCE-EWRI, 2005. The ASCE Standardized Reference Evapotranspiration Equation. Report 0-7844-0805-X, ASCE Task Committee on Standardization of Reference Evapotranspiration. Reston, VA., American Soc. Civil Engineers.

Berni, J.A.J., Zarco-Tejada, P.J., Sepulcre-Canto, G., Fereres, E., Villalobos, F., 2009. Mapping canopy conductance and CWSI in olive orchards using high resolution thermal remote sensing imagery. Remote Sensing of Environment, 113, 2380–2388

Bastiaanssen, W.G.M., Menenti, M., Feddes, R.A., Holtslag, A.A.M., 1998a. A remote sensing surface energy balance algorithm for land (SEBAL)- 1 Formulation. Journal of Hydrology, 213, 198–212

Bastiaanssen, W.G.M., Pelgrum, H., Wang, J., Ma, Y., Moreno, J.F., Roerink, G.J., van der Wal, T., 1998b. A remote sensing surface energy balance algorithm for land (SEBAL)- 2 Validation. Journal of Hydrology, 212, 112–229

Bastiaanssen, W.G.M., Noordman, E.J.M., Pelgrum, H., Davids, G., Thoreson, B.P., Allen, R.G., 2005. SEBAL Model with Remotely Sensed Data to Improve Water-Resources Management under Actual Field Conditions. Journal of Irrigation and Drainage Engineering, 131, 85–93

Cha´vez, J.L., Gowda, P.H., Howell, T.A., Neale, C.M.U., Copeland, K.S., 2009. Estimating hourly crop ET using a two-source energy balance model and multispectral airborne imagery. Irrigation Science, 28, 79–91

Chávez, J.L., Gowda, P.H., Howell, T.A., 2007. Evapotranspiration Mapping Using METRIC^{TM} for a Region with Highly Advective Conditions. ASABE paper no. 072146

Choi, M., Kustas, W.P., Anderson, M.C., Allen, R.G., Li F., Kjaersgaard, J.H., 2009. An intercomparison of three remote sensing-based surface energy balance algorithms over a corn and soybean production region (Iowa, U.S.) during SMACEX. Agriculture and Forest Meteorology, 149, 2082– 2097

French, A.N., Jacob, F., Anderson, M.C., Kustas, W.P., Timmermans, W., Gieske, A., Su, Z., Su, H., McCabe, M.F., Li, F., 2005. Surface energy fluxes with the Advanced Spaceborne Thermal Emission and Reflection radiometer (ASTER) at the Iowa 2002 SMACEX site (USA). Remote Sensing of Environment, 99, 55–65

Gowda, P.H., Chavez, J.L., Colaizzi, P.D., Evett, S.R., Howell, T.A., Tolk, J.A., 2008. ET mapping for agricultural water management: present status and challenges. Irrigation Science, 26, 223–237

Gowda, P.H., Howell, T.A., Chavez, J.L., Copeland, K.S., Paul, G., 2008a. Comparing SEBAL ET with lysimeter data in the Semi-arid Texas High Plains. Proceedings of the World Environmental & Water Resources Congress 2008b, Environmental & Water Resources Institute, American Society of Civil Engineers, May 12-16, Honolulu, HI, 10.

Gowda, P.H., Chávez, J.L., Howell, T.A., Marek T.M., New, L.L., 2008c. Surface Energy Balance Based Evapotranspiration Mapping in the Texas High Plains. Sensors, 8, 5186–5201

Guru, M.V., and Horne, J.E., 2000. The Ogallala Aquifer. In: Report of the Kerr Center for Sustainable Agriculture, Inc.

Grant, O.M., Tronina, L., Jones, H.G., Chaves, M.M., 2007. Exploring thermal imaging variables for the detection of stress responses in grapevine under different irrigation regimes. Journal of Experimental Botany, 58, 815–825

Hemakumara, H.M., Chandrapala, L., Moene, A.F., 2003. Evapotranspiration fluxes over mixed vegetation area measured from large aperture scintillometer, Agricultural Water Management, 58: 109–122

Jia, L., Su, Z., van den Hurk, B., Menenti, M., Moene, A., De Bruin, H.A.R., Javier, J., Yrisarry, B., Ibanez, M., Cuesta, A., 2003. Estimation of sensible heat flux using the Surface Energy Balance System (SEBS) and ATSR measurements. Physics and Chemistry of Earth, Part B: Hydrology, Ocean & Atmosphere, 28, 75–88

Jin, X., Schaepman, M.E., Clevers J.G.P.W., Su, Z., 2009. Impact and consequences of evapotranspiration changes on water resources availability in the arid Zhangye Basin, China. International Journal of Remote Sensing, 30, 3223–3238

Jiang, L. and Islam, S., 2001. Estimation of surface evaporation map over southern Great Plains using remote sensing data. Water Resource Research, 37, 329–340

Kustas,W.P., and Norman, J.M., 1999. Evaluation of soil and vegetation heat flux predictions using a simple two-source model with radiometric temperatures for partial canopy cover. Agricultural and Forest Meteorology, 94, 13−29

Kustas, W.P., & Norman, J.M., 2000. A two-source energy balance approach using directional radiometric temperature observations for sparse canopy covered surfaces. Agronomie Journal, 92, 847–854

Kustas, W.P., Anderson, M.C., Norman, J.M., Li, F., 2007. Utility of radiometric–aerodynamic temperature relations for heat flux estimation. Boundary Layer Meteorology, 122, 167–187

Kustas, W. and Anderson, M., 2009. Advances in thermal infrared remote sensing for land surface modeling. Agricultural and Forest Meteorology, 149, 2071–2081

Li, Z.L., Tang, R., Wan, Z., Yuyun , Zhou, C., Tang, B., Yan, G, Zhang, X., 2009. A Review of Current Methodologies for Regional Evapotranspiration Estimation from Remotely Sensed Data. Sensors, 9, 3801–3853

Menenti M., and Choudhury, B.J., 1993. Parameterization of land surface evapotranspiration using a location dependent potential evapotranspiration and surface temperature range. In: H.J. Bolle et al. (editors), Exchange processes at the land surface for a range of space and time scale, IAHS Publ. No. 212, 561–568

Menenti, M., Jia, L., Su, Z., 2003. On SEBI-SEBS validation in France, Italy, Spain, USA and China. In proceedings of ICID workshop on remote sensing of ET for large regions, Sep 17

Moran, M. S., Clarke, T. R., Inoue, Y., Vidal, A., 1994. Estimating crop water deficit using the relation between surface-air temperature and spectral vegetation index. Remote Sensing of Environment 49, 246–263.

Norman, J.M., Kustas,W.P., Humes, K. S., 1995. A two-source approach for estimating soil and vegetation energy fluxes in observations of directional radiometric surface temperature. Agricultural and Forest Meteorology, 77: 263 – 293

Norman, J.M.; Kustas, W.P.; Prueger, J.H.; Diak, G.R., 2000. Surface flux estimation using radiometric temperature: A dual temperature difference method to minimize measurement errors. Water Resources Research, 36, 2263–2273

Norman, J.M., Anderson, M.C., Kustas, W.P., French, A.N., Mecikalski, J., Torn, R., Diak, G.R., Schmugge, T.J., Tanner, B.C.W., 2003. Remote sensing of surface energy fluxes at 10^1 m pixel resolutions. Water Resource Research, 39, 1–19

Payero, J.O., Irmak, S., 2011. Daily crop evapotranspiration, crop coefficient and energy balance components of a surface-irrigated maize field. In: Evapotranspiration – From Measurements to Agricultural and Environmental Applications, Edited by Giacomo Gerosa.

Patel, N.R., Rakhesh, D., Mohammed, A.J., 2006. Mapping of regional evapotranspiration in wheat using Terra/MODIS satellite data. Hydrological Sciences Journal, 51, 325–335

Su, Z., 2002. The Surface Energy Balance System (SEBS) for estimation of turbulent heat fluxes. Hydrology and Earth System Sciences, 6, 85–99

Su, Z., Timmermans, W.J., van der Tol, C., Dost, R., Bianchi, R., G´omez, J.A., House, A., Hajnsek, I., Menenti, M., Magliulo, V., Esposito, M., Haarbrink, R., Bosveld, F., Rothe, R., Baltink, H.K., Vekerdy, Z., Sobrino, J.A., Timmermans, J., van Laake, P., Salama, S., van der Kwast, H., Claassen, E., Stolk, A., Jia, L., Moors, E., Hartogensis, O., Gillespie, A., 2009. EAGLE 2006 – Multi-purpose, multi-angle and multi-sensor in-situ and airborne campaigns over grassland and forest. Hydrology and Earth System Sciences, 13, 833–845

Su, Z., Timmermans, W., Gieske, A., Jia, L., Elbers, J.A., Olioso, A., Timmermans, J., Velde, R.V., Jin, X., van der Kwast, H., Nerry, F., Sabol, D., Sobrino, J. A., Moreno J., Bianchi, R., 2008. Quantification of land–atmosphere exchanges of water, energy and carbon dioxide in space and time over the heterogeneous Barrax site. International Journal of Remote Sensing, 29, 5215–5235

Santos, C., Lorite, J., Tasumi, M., Allen, R.G., Fereres, E., 2008. Integrating satellite-based evapotranspiration with simulation models for irrigation management at the scheme level. Irrigation Science, 26, 277–288

Sobrino, J.A., Jiménez Muñoz, J.C., Sòria, G., et al., 2008 Thermal remote sensing in the framework of the SEN2FLEX project: field measurements, airborne data and applications. International Journal of Remote Sensing, 29, 4961–4991

Senay, G.B., Budde, M., Verdin J.P., Melesse, A.M., 2007. A Coupled Remote Sensing and Simplified Surface Energy Balance Approach to Estimate Actual Evapotranspiration from Irrigated Fields. Sensors, 7, 979–1000

Timmermans, W.J., Kustas, W.P., Anderson, M.C., French, A.N., 2007. An inter-comparison of the Surface Energy Balance Algorithm for Land (SEBAL) and the Two-Source Energy Balance (TSEB) modeling schemes. Remote Sensing of Environment, 108, 369–384

Teixeira, A.H.C., Bastiaanssen, W.G.M., Ahmad, M.D., Bos, M.G., 2009. Reviewing SEBAL input parameters for assessing evapotranspiration and water productivity for the Low-Middle Sa˜o Francisco River basin, Brazil Part B: Application to the regional scale. Agriculture and Forest Meteorology, 149, 477–490

Tasumi, M., and Allen, R.G., 2007. Satellite-based ET mapping to assess variation in ET with timing of crop development. Agricultural Water Management, 88, 54–66

Tasumi, M., Trezza, R., Allen, R.G., Wright, J.L., 2005. Operational aspects of satellite-based energy balance models for irrigated crops in the semi-arid U.S. Irrigation and Drainage Systems, 19, 355–376

Tilling, A.K., O'Leary, G.J., Ferwerda, J.G., Jones, S.D., Fitzgerald, G.J., Rodriguez, D., 2007. Remote sensing of nitrogen and water stress in wheat. Field Crops Research, 104, 77–85

Chapter 2 - A comprehensive evaluation of SEBAL using high resolution airborne imagery from BEAREX08

2.1 Abstract

In this study, Surface Energy Balance Algorithm for Land (SEBAL) was evaluated for its ability to derive aerodynamic components and surface energy fluxes from very high resolution airborne remote sensing data acquired during the Bushland Evapotranspiration and Agricultural Remote Sensing Experiment 2008 (BEAREX08) in Texas, USA. Issues related to hot and cold pixel selection and the underlying assumptions of difference between air and surface temperature (dT) being linearly related to the surface temperature were also addressed. Estimated instantaneous evapotranspiration (ET) and other components of the surface energy balance were compared with measured data from four large precision weighing lysimeter fields, two each managed under irrigation and dryland conditions. Instantaneous ET was estimated with overall mean bias error and root mean square error (RMSE) of 0.13 and 0.15 mm h^{-1} (23.8 and 28.2%) respectively, where relatively large RMSE was contributed by dryland field. Sensitivity analysis of the hot and cold pixel selection indicated that up to 20% of the variability in ET estimates could be attributed to differences in the surface energy balance and roughness properties of the anchor pixels. Adoption of an excess resistance to heat transfer (kB^{-1}) model into SEBAL significantly improved the instantaneous ET estimates.

2.2 Introduction

Evapotranspiration (ET) mapping has many applications including crop water management, climate change impact assessment, hydrological modeling, groundwater recharge studies, irrigation performance, and land use planning (Bastiaanssen et al., 2005). At field scales, ET can be measured over a homogenous surface using conventional techniques such as the Bowen ratio (BR), eddy covariance (EC), water balance, and lysimeter systems; however, these systems do not provide spatial trends at the regional scale, especially in heterogeneous landscapes. Generally, large weighing lysimeters are considered the most accurate instrument for direct ET measurement in field (Allen et al., 2011; Howell et al., 1995), while the tower based measurements of EC and BR, and water balance methods are commonly employed; each differ in their achievable accuracy range and operational capabilities (Allen et al., 2011a, 2011b). With

the advent of earth observing satellites, numerous remote sensing based ET (RS-ET) algorithms were developed and validated. The need for spatial ET mapping was great and therefore it became imperative to keep developing, modifying, and improving these RS-ET algorithms. Surface Energy Balance Algorithm for Land (SEBAL) developed by Bastiaanssen (1995) in early 90's, is considered as one the important RS-ET algorithm, that has continuously evolved and received wide acceptance around the world. According to the developers, by 2005, SEBAL was applied in more than 30 countries for mapping ET (Bastiaanssen et al., 2005), indicating that SEBAL is one of the widely used RS-ET algorithms.

Numerous validation studies of SEBAL have taken place involving: (a) satellite sensors with different spatial and spectral image resolutions such as MODIS (Moderate Resolution Imaging Spectroradiometer), AVHRR (Advanced Very High Resolution Radiometer), ASTER (Advanced Spaceborne Thermal Emission and Reflection) and ETM/TM (Enhanced Thematic Mapper); (b) ET measurement techniques with varying accuracy such as BR, EC, lysimeter, and scintillometer; (c) time integration such as instantaneous, daily, monthly, and annual; (d) space integration such as field to watershed scale; and (e) agroclimatic regions. A large number of unique combinations of validation scenarios remain unexplored. In a performance comparison between a two source model (TSM) and SEBAL using airborne sensors, yielded relatively large discrepancies over bare soil and dry/sparsely vegetated areas, where TSM was in better agreement with the observations (Timmermans et al., 2007). Another model intercomparison study (Gao and Long, 2008) concluded that SEBAL is highly sensitive to the parameter kB^{-1}, leading to large errors for sparsely vegetated drier regions. A summary of SEBAL validation studies provided by Bastiaanssen et al. (2005) and numerous other recent studies (Singh et al., 2008; Choi et al., 2009; Long and Singh, 2012) revealed that this algorithm has been extensively applied. However, the range of typical accuracy across these studies corroborated the reported range (67-97%) by review studies (Gowda et al., 2008; Kalma et al., 2008; Li et al., 2009). SEBAL has come a long way since its inception in 1995 (Bastiaanssen, 1995) with several variant algorithms' like METRIC (Mapping Evapotranspiration at high Resolution and with Internalized Calibration; Allen et al., 2005), SSEB (Simplified Surface Energy Balance; Senay et al., 2007), ReSET (Remote Sensing of Evapotranspiration; Elhaddad et al., 2008), M-SEBAL (Modified SEBAL; Long and Singh, 2012), SEBTA (Surface Energy Balance with Topography Algorithm; Gao et al. 2011) being developed over the years.

Evaluation of uncertainties in remote sensing based models for estimation of surface energy fluxes is not an easy task (Norman et al., 2006), while at the same time the need for validation studies across hydrological regimes and agroclimatological regions is advocated by review studies (Gowda et al., 2008; Kalma et al., 2008; Li et al., 2009). Single source models like SEBAL considers the exchange of heat and water in the soil-vegetation-atmosphere continuum as a lumped composite of the underlying surface. Studies have reported the biased performance of single source models in handling extremes in moisture/vegetation cover conditions (Gao and Long, 2008; Kustas and Anderson, 2009). The indigenous approach of SEBAL, in the determination of the temperature gradient using two extreme pixels representing the hydrological end members (wet and dry) has been found to be subjective to analyst decision and domain size (Timmermans et al., 2007; Long et al., 2011). While the approach of generating single linear temperature gradient function for the complete scene (study region) may be simplistic, however, the uncertainty in surface energy flux estimation resulting from this assumption is very large (Timmermans et al., 2007; Singh et al., 2008; Bastiaanssen et al., 2010). Testing and validation of RS-ET algorithms across a range of hydrometeorological and surface cover conditions is important to fill in the existing gap in the operationalization of these algorithms.

The Bushland Evapotranspiration and Agricultural Remote Sensing Experiment 2008 (BEAREX08) conducted during the 2008 summer growing season in Bushland, Texas, provided a unique opportunity to evaluate the turbulent exchange of mass and energy at the land surface. In the past decade, numerous multi-disciplinary, multi-institutional, intensive field campaigns including, Southern Great Plains Hydrology Experiment (SGP97; Jackson et al., 1999), Exploitation of Angular effects in Land surface observations from satellite (EAGLE 2006; Su et al., 2009), Surface Processes and Ecosystem Changes Through Response Analysis SPECTRA Barrax Campaign (SPARC 2004; Su et al., 2008), SENtinel-2 and Fluorescence Experiment (SEN2FLEX 2005; Sobrino et al., 2008), Soil Moisture Atmosphere Coupling Experiment (SMACEX; Kustas et al. 2003), and BEAREX07 (Chavez et al., 2009), were undertaken to augment the understanding and improving the parameterization of land surface hydrometeorological processes. These campaigns provide datasets acquired over a diverse hydrological regimes, well suited for evaluating remote sensing based evapotranspiration models.

The main objective of this study was to assess the performance of SEBAL under both dryland and irrigated agricultural conditions in the Texas High Plains using high resolution airborne images. Specific objectives of this evaluation study were to: (a) evaluate the variability in the 'a' and 'b' coefficients of the dT function due to the presence of multiple pixels fulfilling the hot and cold pixel selection criteria and how much influence this variability has on the final instantaneous ET (ET_i) estimates, (b) compare SEBAL ET_i estimates with lysimetric data, (c) incorporate a physically based parameterization for excess resistance (kB^{-1}) into SEBAL and test its performance, and (d) test the relationships to compute the various aerodynamic roughness parameters.

2.3 Materials and Methods

SEBAL was applied to five high resolution airborne images and validated against large precision weighing lysimeters. Validation points consisted of two irrigated and two dryland cotton fields situated in the semi-arid Texas High Plains region known for significant advection and nighttime ET (Tolk et al., 2006). Detailed information on the experimental set-up, algorithm description and evaluation process follows.

2.3.1 Study area and data acquisition

The BEAREX08 was conducted at the USDA-ARS Conservation and Production Research Laboratory (CPRL) during the 2008 summer cropping season. The CPRL is located in Bushland, TX (Fig. 2.1) with geographic coordinates of 35° 11' N, 102° 06' W and elevation of 1170 m above mean sea level. It is within the Texas High Plains, where semi-arid climatic conditions and strong advective currents prevail during the summer cropping season. The CPRL has four large weighing lysimeters (3 m long x 3 m wide x 2.4 m deep), each located in the middle of 4.3 ha fields arranged in a block pattern. The two lysimeter fields located on the east (NE and SE) were managed under irrigation and planted to cotton on 21 May, and the other two lysimeters on the west (NW and SW) were under dryland management and planted to cotton on 5 June. Cotton (variety Delta Pine 117) was seeded at 15.8 plants/m^2 on raised beds spaced at 0.76 m. Each lysimeter field was equipped with an automated weather station that provided measurements for net radiation, radiometric surface temperature, soil heat flux, air temperature, relative humidity, and wind speed (refer Chávez et al., 2009 for details of field instrumentation). In addition, a grass reference ET weather station field (0.31 ha), which is a part of the Texas

High Plains ET Network was located on the eastern edge of the irrigated lysimeter fields (Marek et al., 2009) (Fig. 2.1).

Flying expeditions during BEAREX08 were conducted to collect remotely sensed imagery using the Utah State University (USU) airborne digital multispectral system at high resolutions. The system acquired high resolution imagery in the green (0.545-0.555 μm), red (0.665-0.675 μm), near infrared (0.790-0.810 μm), and thermal infrared (8-12 μm) portions of the electromagnetic spectrum. Visible and near infrared images were acquired at 1 m spatial resolution, and the thermal images were acquired at 3 m. Five images were acquired from early to mid-cropping season for dates June 26 (178), July 12 (194), July 20 (202), July 28 (210), and August 5 (218). All images were acquired close to 12 noon central standard time from an altitude of 2000 m agl (above ground level). Description of the post processing including geometric corrections, radiometric calibration and atmospheric correction can be found in Neale et al., 2012. SEBAL was coded using Python programming language and executed in the Arc-GIS 10.0. The five images provided conditions from a near bare soil situation to near complete canopy cover. Fig. 2.2 shows the digital picture of the field taken on 26 June and 5 August. On 26 June, only isolated seedlings are seen on both irrigated and dryland fields, and the surface is dominated by bare soil. On 5 August, the crops in the irrigated field had attained a near complete canopy, whereas, the dryland fields exhibited high reflectance from soil. The lysimeter fields were considered homogeneous, and the centre of the field with the lysimeter and instrument cluster was used to validate all the estimates. A 12 x 12 (1 m) pixel grid covering the lysimeter location was marked (in the image) in all 4 lysimeter fields to extract average values of estimated ET, net radiation, soil heat flux, surface temperature and aerodynamic parameters. The performance statistics used for the evaluation of surface energy fluxes and instantaneous ET are provided in Table 2.1.

2.4 SEBAL

Two versions of SEBAL, SEBAL2000 and SEBAL2008 have been identified by the developers with claims of several unpublished advances incorporated into the later version (Bastiaanssen et al., 2010). In this study, we have used the published SEBAL (SEBAL2000 and SEBAL2008) versions and efforts were made to report the sub-models and approaches taken.

SEBAL utilizes the widely applied residual approaches of surface energy balance to estimate ET at different temporal and spatial scales. The energy coming from the sun and atmosphere in the form of short- and long-wave radiation is transformed and used for (a) heating the soil (soil heat flux into the ground), (b) heating the surface environment (sensible heat flux to the atmosphere), and (c) transforming water into vapor (latent heat flux from the crop/soil surfaces). All the energy involved in the soil-vegetation-atmosphere interface can be given as the Energy Balance (EB) equation:

$$R_n = G_o + H + LE \tag{2.1}$$

where, R_n is the net radiation, G_o is the soil heat flux, H is the sensible heat flux, and LE is the latent heat flux, with all units expressed in W m^{-2}. Latent heat was expressed as hourly ET (mm) (by dividing LE by the latent heat of vaporization and the density of water). Net radiation (R_n) expressed as an electromagnetic balance of all incoming and outgoing fluxes, which constitutes a key driver for heating the atmosphere and the ground, is given by:

$$R_n = S\downarrow - S\uparrow + L\downarrow - L\uparrow = (1-\alpha_s)S\downarrow + \varepsilon_a\,\sigma\,T_a^4 - \varepsilon_s\,\sigma\,T_s^4 \tag{2.2}$$

In Eq. (2.2), S denotes short-wave radiation (0.3 – 3 μm) and L is the long-wave radiation (3-100 μm). The arrows show the direction of the flux entering (↓) or leaving (↑) the system. Each term in Eq. (2) can be either determined directly from models or obtained from the ground weather station. The incoming short-wave radiation (S↓) and the air temperature (T_a) are measured at weather stations. T_s is the surface radiometric temperature obtained from the inversion of Plank's law in 10-12 μm band width. Other terms in Eq. (2.2) are broadband surface albedo (α_s), apparent emissivity of atmosphere (ε_a), surface emissivity (ε_s), and the Stefan-Bolzmann constant (σ = 5.67 E-08 W m^{-2} K^{-4}).

Broadband planetary albedo (α_p) was calculated as the sum of the individual in-band planetary albedos with different weighing factors. The weighing factor for each band is proportional to its solar exoatmospheric irradiance ($ESUN_\lambda$) which is an average solar irradiance weighted by the corresponding spectral band response function. The weight for each band was calculated and the equation for broadband planetary albedo (α_p) was derived as:

$$\alpha_p = 0.303\,green + 0.400\,red + 0.296\,NIR \tag{2.3}$$

where green, red, and NIR are the reflectance of the respective bands. Because low flying airborne images were used with primary atmospheric corrections, the need for converting

planetary albedo into surface albedo was evaded and planetary broadband albedo (α_p) was considered equivalent to the surface broadband albedo (α_s).

The apparent emissivity of the atmosphere was estimated from equations based on vapor pressure and air temperature at the standard meteorological stations. For clear skies, the Brutsaert (1975) formulation was used as:

$$\varepsilon_a = 0.892 \left(\frac{e_a}{T_a}\right)^{1/7} \tag{2.4}$$

where ea is vapor pressure near the surface (actual vapor pressure) in kPa and T_a is in Kelvin. Actual vapor pressure (e_a) can be calculated from relative humidity and air temperature at reference level as:

$$e_a = \frac{RH}{100\ e_s} \tag{2.5}$$

where e_a is in kPa and e_s is the saturation vapor pressure in kPa given by:

$$e_s = 0.6108\, exp\left(\frac{17.27\ \times T_a}{T_a + \ 237.3}\right) \tag{2.6}$$

T_a is the air temperature in degree Celsius [°C].

The surface emissivity (ε_s) is calculated from NDVI (Normalized Difference Vegetation Index) as given by Van de Griend and Owe (1993):

$$\varepsilon_s = 1.009 + 0.047 \ln\ (NDVI) \tag{2.7}$$

The above relationship is valid only for NDVI values over 0.16. For NDVI values below 0.16 (usually bare soils), emissivity was assumed to be 0.92 and for NDVI values below –0.1 (usually water), it was assumed to be 1.0.

The mathematical formulation of H is based on the single source resistance scheme of mass transport of heat and momentum between the surface and the overlying atmosphere. H is directly related to the difference between the surface aerodynamic temperature (T_o) and above canopy air temperature (T_a):

$$H = \rho_a\, C_p\, \frac{T_o - T_a}{r_{ah}} \tag{2.8}$$

where ρ_a is the density of air (~1.17 kg m^{-3}), C_p is the air specific heat at constant pressure (~1,005 J kg^{-1} K^{-1}), and r_{ah} is the aerodynamic resistance to heat between the surface and the reference level (s m^{-1}). Since T_o cannot be measured directly at source height, in single-source

models the radiometric surface temperature (T_s) measured by the remote sensing thermal sensors, is used as a surrogate. To accommodate this approximation, a dimensional parameter for excess resistance to heat transfer (kB^{-1}) is incorporated into the calculation of r_{ah}. Studies (Kustas et al., 1989; Stewart et al., 1994) have shown that if an appropriate value of kB^{-1} is determined, H can be estimated accurately using T_s. The SEBAL model has used an areal constant kB^{-1} value of 2.3 for all surfaces and emphasized that the approach of hot and cold pixel for scaling thermal inertia would reduce the consequences of aerodynamic temperature inaccuracy on H estimation (Bastiaanssen et al., 1998). The classical aerodynamic resistance to heat transfer (r_{ah}) equation is given by

$$r_{ah} = \frac{1}{ku_*}\left[ln\left(\frac{z_{ref} - d_o}{z_{oh}}\right) - \psi_h\right] \tag{2.9}$$

where $u*$ is the friction velocity defined by

$$u_* = \frac{ku_b}{ln\left[\frac{z_b - d_o}{z_{om}}\right] - \psi_m} \tag{2.10}$$

The d_o is the zero plane displacement height, z_{om} is the roughness length for momentum transport, z_{oh} is the roughness length for heat transport, z_{ref} (2 m) is the reference level at which the wind speed (u_{ref}) and T_a are measured, k is the von Karman's constant (~0.41), z_b is the blending height (~100 m), u_b is the wind speed at blending height, and ψ_h and ψ_m are the stability correction functions for heat and momentum as a function of Monin-Obukhov length (L). Equations developed by Paulson (1970) were used to determine ψ_h and ψ_m . Sensible heat flux (H) can be calculated from Eqs. (2.8), (2.9), and (2.10) by simultaneously solving for the stability functions through an iterative process. Soil heat flux was derived from the relationship developed by Bastiaanssen et al. (1998), given as:

$$\frac{G_o}{R_n} = \frac{(T_s - 273.15)}{100\alpha_s}(c_1\alpha_s + c_2\alpha_s^2)(1 - 0.98NDVI^4) \tag{2.11}$$

where c_1 and c_2 are locally calibrated coefficients with values of 0.12 and 0.42, respectively. Other variables such as d_o, z_{om}, u_b, and kB^{-1} can be solved with empirical or physically based models. Appendix A lists the various parameterizations used in the intermediate steps.

2.5 The excess resistance parameter (kB^{-1})

In equation 2.8, the aerodynamic temperature T_o, is defined as the extrapolation of air temperature down to an effective height within the canopy at which the vegetation component of H and LE fluxes arise given by d_o+z_{oh} (Chehbouni et al., 1996). From the Monin-Obukhov (M-O) similarity theory, the aerodynamic resistance, r_{ah}, is defined as the resistance from height $z_{oh}+d_o$ having an aerodynamic temperature, to the height z_{ref}. Eq. (2.9) can be written as:

$$r_{ah} = r_a + r_r = \frac{1}{ku_*}\left[ln\left(\frac{z-d_o}{z_{om}}\right) - \psi_h\right] + \frac{1}{ku_*} ln\left(\frac{z_{om}}{z_{oh}}\right) \quad (2.12)$$

where, r_a is the aerodynamic resistance between the air temperature at a height d_o+z_{om} and the reference height (z_{ref}). The formulation of H using the definition of T_o requires an additional resistance called the excess resistance and denoted by r_r in equation 2.12. Following many authors (Chehbouni et al., 1996; Kustas et al., 1989), the r_{ah} is greater than resistance to momentum transfer. Consequently, the roughness length for heat transfer (z_{oh}) is lower than the roughness length for momentum transfer (z_{om}). The excess resistance (rr) is an integral part of the aerodynamic resistance formulation (Eq.2.12) and takes into account the fundamental difference in the mechanism determining heat and momentum transfer. It is important to understand that the excess resistance is attached to the aerodynamic temperature, however, a practical problem arises when neither the T_o nor the z_{oh} could be measured. An alternative is to use the radiometric surface temperature from the infrared sensors as a surrogate for T_o and to accommodate this substitution a correction is performed on the excess resistance term. Excess resistance (r_r) formulation from Eq. (2.12) can be written as:

$$r_r = \frac{1}{ku_*} ln\left(\frac{z_{om}}{z_{oh}}\right) \quad (2.13)$$

Eq. (2.13) is commonly expressed as a function of the dimensionless bulk parameter B^{-1} (Chamberlain, 1968):

$$kB^{-1} = ln\left[\frac{z_{om}}{z_{oh}}\right] \quad (2.14)$$

It must be emphasized here that kB^{-1} is the parameter describing the excess resistance and should not be confused with the excess resistance (r_r). In context to heat transfer estimation from T_s, kB^{-1} is a mere fitting parameter no longer connected to its theoretical background and largely an empirical parameter (Chamberlain, 1968; Lhomme et al., 2000).

In SEBAL, we see two different approaches for handling excess resistance accounting for the discrepancy between T_o and T_s: (i) use of an areal constant kB^{-1} value of 2.3 (Timmermans et al., 2007; Bastiaanssen et al., 1998; Bastiaanssen et al., 2000; Jacob et al., 2002) and (ii) use of scalar roughness length for heat transfer (z_{oh}) value of 0.1 (Bastiaanssen et al., 2005; Bastiaanssen et al., 2002; Wang et al. 2009) or 0.01 (Singh et al., 2008; Gieske and Meijninger, 2005; Chandrapala and Wimalasuriya, 2003; Allen et al., 2001). In a study by Long and Singh (2011), they concluded that specifying z_{oh} as 0.1 or introducing a fixed kB^{-1} parameter of 2.3 had appreciable difference in the magnitude of resulting H fluxes. Numerous studies on kB^{-1} can be found in the literature; for more detail, readers can refer to Verhoef et al. (1997a), Su et al. (2001), and Lhomme et al. (2000). It has been categorically stated that for remote sensing based single source bulk transfer schemes, a kB^{-1} parameterization is required (Stewart et al., 1994; Verhoef et al., 1997a). Furthermore, a widely used kB^{-1} value of 2 has been found to be too low in most cases (Kustas et al., 1989; Stewart et al., 1994; Verhoef et al., 1997a). Under both sparse and full vegetation conditions, an appropriate value of kB^{-1} is required for accurate estimation of H using T_s (Kustas et al., 1989; Kustas et al., 2007; Jia et al., 2003).

In SEBAL, the kB^{-1} value of 2.3 (Bastiaanssen et al., 1998) sets the value of roughness length for heat to 1/10 of roughness length for momentum. Several studies have shown that the value of kB^{-1} can range from 1 to 10 depending on the dominant surface cover (Kustas et al., 1989; Beljaars and Holtslag 1991; Stewart et al., 1994; Su et al., 2001). A physically based model for z_{oh} expressed in terms of kB^{-1} was incorporated into SEBAL to see its influence on the estimation of ET. The kB^{-1} model developed by Su et al. (2001) that consists of terms representing the contribution of the soil alone, the canopy and the canopy-soil interaction to resistance to heat transfer (Appendix B) was selected.

2.6 Aerodynamic roughness parameters

Roughness height for momentum (z_{om}) greatly influences the turbulent characteristics near the surface where the heat fluxes originate. The z_{om} depends on various factors such as wind speed and direction, vegetation height, canopy cover, vegetation type, and row spacing. Estimating these factors using an empirical equation as a function of NDVI might be an over simplification; however, such estimates are reasonably accurate for uniform cover and fairly flat terrains (Kustas et al., 1989). Although remote sensing observations provide vegetation

information, estimation of roughness height remains a challenge for regional modeling of turbulent transport because of highly variable topographic and canopy structures, and wind behaviors. There are numerous methods to retrieve this parameter including wind profile methods, vegetation height, lookup table based on the land use classification, and empirical relationship using NDVI. Calibrating the empirical relationship for the study region from the data collected during the campaign would be the best available option. The following exponential relationship derived using NDVI and crop height information (Bastiaanssen, 1995) was used to estimate z_{om}.

$$z_{om} = \exp(C_1 + C_2\, NDVI) \tag{2.15}$$

where C_1 and C_2 are regression constants derived separately for each image from a plot of $ln(z_{om})$ versus NDVI for pixels representing varied vegetation heights and extremes of NDVI (Fig. 2.3). For generating the relationship, z_{om} was calculated from the height of vegetation (z_{om}=0.13 h) (Brutsaert, 1982) recorded for different crops during the campaign. One single set of coefficients for all five images, C_1 = -5.5 and C_2 = 5.8, from (Bastiaanssen, 1995) was used to test the coefficient's sensitivity on the ET estimation.

2.7 Selection of a dry (hot) and wet (cold) pixel

A distinctive approach in SEBAL is the calculation of a single temperature gradient (dT; defined as the difference between T_o and T_a) function for the study region using two points denoting the hydrological contrast. The two pixels representing the hydrological contrast were termed as 'Hot' (dry) and 'Cold' (wet) pixels, was first introduced in SEBAL, and adopted into at least five other energy balance algorithms. Hot and cold pixel selection ('a' and 'b' coefficients of the linear relation) forms the backbone of SEBAL (Timmermans et al., 2007; Singh et al., 2008; Bastiaanssen et al., 2010) and other similar single-source algorithms; however, a very few studies have explored the sensitivity of 'a' and 'b' calculation (Norman et al., 2006) process in SEBAL and how errors are propagated into the ET estimation. SEBAL uses the extreme pixels of the image (dry and wet pixel), to develop a relationship between T_s and the difference between T_o and T_a given in the form of:

$$T_o - T_a = dT = a + b.T_s \tag{2.16}$$

where 'a' and 'b' are the regression constants. The basic assumption behind this relationship is that the difference between T_o and T_a is linearly related to the T_s. A second assumption of the

existence of hydrological contrast (dry and wet area) in the study region must be implemented. Fig. 2.4 illustrates the process of deriving the coefficients from extreme dry and wet pixels. For the wet pixel, dT was considered zero while for the dry pixel, dT was iteratively determined by Eq. (2.8–2.10) adjusting for the stability functions. Physically, the wet pixel should be the surface transpiring at its potential limit (LE = LEmax and H = 0), and therefore dT=0. The ideal location of a wet pixel is a surface with full canopy vegetation growing under no soil moisture limitation. A dry pixel physically represents a surface with dry conditions and ET equal to zero. (LE= 0 or H = Hmax= Rn – Go). Ideally, bare soil with no residual moisture for evaporation should fit the dry pixel requirements. Selection of these two extreme pixels in the image causes a bottleneck in the implementation of SEBAL as it involves a subjective decision of the analyst. Generally, the wet pixel is selected on the criteria of low temperature and high NDVI, whereas the dry pixel is characterized by high temperature, low NDVI, and low albedo. Scatter plots of NDVI-Ts and albedo-Ts along with histograms have been used to identify the group of pixels fulfilling the extreme pixel criteria (Timmermans et al., 2007; Choi et al., 2009) however, these methods do not help in secluding a single set of pixels, which again largely depends on the analyst's decision. Furthermore, different sets of pixels fulfilling the dry and wet pixel criteria may exhibit entirely different surface energy balance and roughness properties and lead to variations in the 'a' and 'b' coefficients. In the present study, we harnessed the capability of the GIS environment wherein classification, histogram generation, and overlaying of the surface temperature, NDVI, and albedo maps could be done easily, leading to identification of a group of pixels that fulfilled the criteria. The identification of the wet pixel was easier because of the presence of a grass reference ET weather station in the study region (Fig. 2.1) that typically exhibited the lowest surface temperature and greatest NDVI for all five images. Selection of the hot pixel was not easy because multiple pixels satisfied the conditions. We selected three sets of hot pixels well spread in the study domain to test the variations in the determination of 'a' and 'b' coefficients and further its influence on final ET estimation.

2.8 Results and Discussion

2.8.1 Net radiation, soil heat flux and surface temperature

Performance statistics for R_n, G_o, and T_s for the complete data set (n=20) are provided in Table 2.4. The T_s retrieved from the airborne thermal images was compared against the observed

IRT (infra-red thermometer) values with a small RMSE value of 1.16°C (3.36%). It is within the range of T_s values (1-1.5°C) reported in the literature for thermal imagery acquired from various airborne and satellite platforms (Sobrino et al., 2008). Net radiation was under predicted with a small RMSE of 17.98 W m^{-2} (3.1%) and an MBE of 6.61 W m^{-2} (1.14%), which was well within the typical error range of 5 to 10% (~ 30-60 W m^{-2}) (Timmermans et al., 2007; Singh et al., 2008; Choi et al., 2009) and most instrument measurement uncertainty (Field et al., 1992). The R_n estimates were comparable to those observed by Jacob et al. (2002), who attributed the low R_n estimation errors to use of relatively accurate albedo estimates derived from aircraft data. An overestimation error of 9.87 W m^{-2} (36.2%) and RMSE of 13.5 W m^{-2} (49.6%) was recorded for G_o estimates. A large discrepancy was evident from the low R^2 value, with negative NSE indicating the model's unsatisfactory performance in estimating G_o. Similar results with RMSE ranging from 20 to 40 W m^{-2} have been reported by various studies (Jacob et al., 2002; Singh et al., 2008) for the present parameterization (Eq. 2.11) using NDVI and R_n. Although G_o estimates were not accurate, it was not a major concern because the magnitude of error was small (± 13 W m^{-2}) and was expected to have negligible effect on the ET estimates. Moreover, the available energy (R_n – G_o) for convective fluxes resulting from the underestimation of R_n and overestimation of G_o was 16.5 W m^{-2} (MBE), which was a small underestimation. Nevertheless, several causes can explain the poor performance of G_o estimates in the evaluation's statistics including the spatial variability of G_o, inaccuracies in the soil heat flux plate measurements and the limitations of NDVI based G_o parameterization.

2.8.2 ET flux variability due to selection of different dry and wet pixel end members

Three sets of 'a' and 'b' coefficients generated per image with their temperature, NDVI, albedo, and roughness properties are presented in Table 2.2. It is evident from the Table 2.2 that end member pixels of particular image exhibiting same temperature could still produce a different set of coefficients owing to their different surface energy balance and roughness properties. SEBAL was executed for each set of 'a' and 'b' coefficients, and the estimated instantaneous ET was analyzed using standard deviation and coefficient of variation (Table 2.3). The coefficient of variation (CV in %; SD x 100/Mean) for the irrigated lysimeter fields (SE and NE, Fig. 1) ranged from 0 to 22% while for the dryland lysimeter fields (NW and SW, Fig. 2.1), the CV ranged from 4 to 80%. Consistently larger deviations (CV) were associated with dryland

(sparse vegetation) ET_i estimations compared with irrigated fields (more complete vegetative cover). The reason for this biased behavior of the algorithm for irrigated (full cover) and dryland (sparse cover) cropping systems lies in the fact T_s - T_o is minimal for full cover canopies (Chehbouni et al., 1996), and a nominal correction of 2.3 (kB^{-1}) provide good ET estimates (Kustas et al., 1989). However, on sparse canopy cover, the T_s - T_o is always greater, and the correction applied (kB^{-1}=2.3) could not account for the larger differences, thus providing unreliable ET estimates. This shows that the temperature gradient relationship cannot completely address the spatial variability of kB^{-1}. Therefore, inherent assumption that hot and cold pixel for scaling thermal inertia (dT) accommodates the consequences of aerodynamic temperature inaccuracy on H estimation may not be true.

2.8.3 Instantaneous ET by SEBAL

For each image, the average ET_i derived from the three set of 'a' and 'b' was compared against lysimeter values for the performance evaluation of SEBAL. Evaluation statistics for the complete data set as well as for the irrigated and dryland fields are presented separately in Table 2.5a for thorough evaluation. An overall RMSE of 0.15 mm h^{-1} (28.1%) and MBE of 0.13 mm h^{-1} (23.8%) were observed for ET_i estimates from all four lysimeter fields. The positive bias indicated underestimation of ET_i. This result is similar to the accuracy (27.1% RMSE) that Tasumi et al. (2005) reported for semi-arid Idaho conditions in their comparison of ET_i versus lysimeter values using Landsat imagery. In a comprehensive evaluation study by the SEBAL developer, the overall accuracy of daily ET for scale of the order of 100 ha has been reported as ±15%, further stating that time and space integration would improve accuracy (Bastiaanssen et. al., 2005). SEBAL ET_i estimates explained 86% of the variability in the observed lysimeter data with slope close to unity (0.98) and an intercept of -0.11 mm h^{-1}, both significant at the 0.05 probability level (Fig. 2.5).

The evaluation of SEBAL model for irrigated and dryland lysimeter fields with the high resolution imagery revealed an interesting bias in the model's performance for the two agricultural water management regimes. The ET_i from the irrigated fields showed an RMSE of 0.14 mm h^{-1} contributing to 21.5% error, however, the dryland fields gave an RMSE of 0.15 mm h^{-1} which accounted for 39.5% error, nearly double the error as compared to the irrigated field. The NSE value for the dryland field ET_i estimates was -0.81 and R^2 was 0.35, as compared to

NSE of 0.55 and R^2 of 0.95 from the irrigated field. Clearly, the biased performance of SEBAL for dryland conditions affected the overall performance. Similar gross under prediction results in relatively dry areas are reported by Timmermans et al. (2007), Gowda et al. (2008), and Gao and Long (Gao and Long, 2008). Timmermans et al. (2007) made unsuccessful attempt to fix this problem by adjusting the end-member temperatures and momentum roughness length. In their study, they articulated that errors in H estimation over sparsely vegetated surfaces in single source models can be reduced by adjusting the kB^{-1} parameter.

2.8.4 SEBAL with kB^{-1} parameterization

Overall underperformance of SEBAL with variable accuracies for irrigated and dryland crops could be attributed to one or a combination of reasons. In the present agriculture dominant landscape with no forest cover and flat topography, the empirical parameterization of z_{om} could not be the reason for deviations in ET estimates. At the same time, the aircraft image covered a small area with a relatively less heterogeneous landscape, hence the assumption of linearity of dT versus T_s could be considered valid. However, there are no studies to prove that the dT versus T_s linearity assumption could adequately address the spatial variation of z_{oh} (kB^{-1}), or in other words address the differences between T_o and T_s; we believe that this could be a reason for the biased results.

Results of SEBAL model estimates with kB^{-1} parameterization showed improvement in the ET_i estimation (Fig. 2.6). Overall RMSE of 0.08 mm h^{-1} (16.3%) and MBE of -0.02 mm h^{-1} (-3.6%) were observed for the complete dataset (Table 2.5b). A 1:1comparison of Table 2.5a and 2.5b clearly indicates that the SEBAL with kB^{-1} parameterization substantially improved its performance in estimating ET_i. The overall underestimation errors decreased considerably from 24% to -3.6% (PBIAS). This can be seen clearly in plots of ET_i for the irrigated and dryland field separately with and without the kB^{-1} modifications (Fig. 2.7). Underestimated ET_i associated with partial canopy covers, moved closer to the observed values after the introduction of kB^{-1} parameterization, while it did not affect the higher ET_i estimates associated with near complete canopy cover in the irrigated fields. This could be explained from Fig. (2.2), where the images under analysis are from early crop stage to near complete canopy cover stage; hence, a sparse vegetation condition existed in most images. A nominal kB^{-1} value of 2.3 did not work well under sparse vegetation conditions and generated lower ET_i estimates. SEBAL is known to have

problems estimating ET under dry and sparse vegetation conditions (Gao and Long, 2008; Timmermans et al., 2007). Under these conditions, the difference between T_s and T_o was relatively large, and this could not be adequately addressed by the nominal kB^{-1} value of 2.3, whereas the converse was true for complete canopies. Therefore, the improvement in the ET_i estimates was solely due to an appropriate representation of spatially variable roughness length for heat transport (z_{oh}). Table 2.6 gives a comprehensive list of aerodynamic roughness parameter estimates from the four fields. Marked difference in the z_{oh} values with and without kB^{-1} parameterization was observed.

2.8.5 Roughness length for momentum transport, excess resistance, and roughness length for heat transport

Questions have been raised about the simplistic approach of determining the complex roughness length for momentum transport (z_{om}) from the empirical relationship, Eq. (2.16), as a function of NDVI (Timmermans et al., 2007; Norman et al., 2006). SEBAL developers suggested deriving local coefficients for the z_{om} relationship from the observed plant height over varied canopy structure. Although the requirements of plant height add to the inputs, our results show that the relationship generated realistic z_{om} values under the present agricultural landscape setup (Table 2.6). Furthermore, applying a single pair of coefficients for the z_{om} relationship (derived from the Tomelloso super site, Cas de Las Carascas, Spain; Bastiaanssen, 1995) for all the images did not result in any noticeable difference in the ET_i estimation; however, we must caution that the Tomelloso super site was also an agricultural region, and these coefficients cannot be universally applied. The z_{om} values compared well with the estimates obtained over an incomplete canopy cover of cotton using the profile method (Kustas et al., 1989). Also, the z_{om} values were comparable with the Brutsaert (1982) relationship ($z_{om} = 0.13h$) (Table 2.6).

The kB^{-1} parameter representing the excess resistance to heat transfer has been a matter of controversy since its inception into the single source model. Nevertheless, the term cannot be avoided because it accounts for the fact that T_s is frequently greater than T_o (Lhomme et al., 2000). In this study, the parameterized kB^{-1} values produced more accurate ET_i estimates compared with the constant kB^{-1} value of 2.3 proposed by the SEBAL developers. The value for kB^{-1} for all four lysimeter fields is presented in Table 2.6. The value of kB^{-1} varied between 2

and 13 for most cases, with higher values associated with low canopy cover conditions. On 26 June, exceptionally high kB^{-1} values were found due to the fact that image was acquired early in the cropping season when the surface was bare soil with isolated cotton seedlings (see Fig. 2.2); such a surface is classified as bluff rough element with no consensus on appropriate kB^{-1} value (Verhoef et al., 1997a). The kB^{-1} value for the irrigated fields were always less than that in the dryland fields (Table 2.6).This is because, at any point during the cropping season, irrigated fields had larger canopy cover than the dryland fields. Consequently, the value of around 2.3 was suitable for irrigated fields when the crop attained near complete canopy cover conditions. The minimum value of kB^{-1} for the dryland fields was 5.3, which was estimated with the 5August image. These results corroborate the conclusions from numerous studies on the excess resistance parameter (kB^{-1}), that: (i) over a sparsely vegetated surface, the difference between T_s and T_o can exceed 10°C (Chehbouni et al., 1997), so an adjustment is required (through kB^{-1}), (ii) kB^{-1} value should range from 1 to 10, to obtain accurate estimates of H (Kustas et al., 1989; Stewart et al., 1994), and (iii) H is more sensitive to kB^{-1} value of 2 than a value of about 6 (Verhoef et al., 1997a).

Roughness length for heat transport, $z_{oh,}$ expressed in terms of kB^{-1} [$z_{oh} = z_{om}/\exp(kB^{-1})$] for four lysimeter fields over the five image acquisition dates are presented in Table 2.6. Comparison of z_{oh} values obtained from kB^{-1} parameterization and a constant kB^{-1} (of 2.3) reveals significant differences. To address the high kB^{-1} values obtained for the sparse vegetation conditions, we restricted the lower limit of z_{oh} to 10^{-5} m.

2.9 Conclusions

The BEAREX08 provided the opportunity to evaluate SEBAL at very high spatial resolution with extensive crop and ET data from fields equipped with large weighing lysimeters provided new insight into the performance of the algorithm. The main distinguishing feature of this study was the simultaneous evaluation of SEBAL for both irrigated and dryland crops covering a range of conditions from sparse vegetation to near complete canopy cover. This study also examined the issues of subjective selection of extreme pixels, dealt with aerodynamic roughness parameters, and showed improvement in ET estimates through the introduction of kB^{-1} parameterization into the SEBAL model. On an average 20% uncertainty in term of CV was observed as a result of subjectivity in the end member selection process. The sensitivity to end

member pixel selection is crucial to the performance of SEBAL; hence, a clear methodology for the selection process is required to remove the subjective decision and make the process more robust. A rigorous sensitivity analysis of the 'a' and 'b' coefficients estimation in the temperature gradient relationship is necessary because this forms the backbone of SEBAL. SEBAL ETi estimates compared reasonably well against the lysimeter values with underestimation error and RMSE close to 0.15 mm h 1 (28%). Errors were relatively small for the irrigated fields as compared with the dryland fields. Modifying the SEBAL algorithm by introducing kB^{-1} parameterization considerably improved the accuracy of ETi estimation, with an overall RMSE of 0.08 mm h^{-1} (16%). It can be concluded that the temperature gradient (dT) and (T_a-T_o) linear relationship does not have any component to consider for the differences arising due to use of T_s for T_o and hence a realistic correction factor in the form of kB^{-1} has to be incorporated into SEBAL. Furthermore, a kB^{-1} value of 2.3 would grossly underestimate ET for sparse vegetation conditions. Locally calibrated coefficients for the aerodynamic roughness parameters are crucial to the performance of the algorithm. SEBAL is a physically based algorithm, but the numerous empirical sub-models and requirement for image specific calibrations, limits its operational capabilities. Nevertheless, results of the present study with the suggested improvements in the algorithm make it a viable tool for regional scale ET mapping. The temperature gradient approach (dT estimation) is a novel approach indigenous to the SEBAL algorithm, however, the underlying assumptions are many necessitating a detailed sensitivity study.

2.10 Acknowledgments

This research was supported by the Ogallala Aquifer Program, a consortium between USDA−Agricultural Research Service, Kansas State University, Texas AgriLife Research, Texas AgriLife Extension Service, Texas Tech University, and West Texas A&M University. This is contribution number 12-284-J from the Kansas Agricultural Experiment Station.

2.11 References

Allen, R.G., Pereira, L.S., Howell, T.A., Jensen, M.E., 2011a. Evapotranspiration information reporting: I. Factors governing measurement accuracy. Agric. Water Manage., 98, 899–920.

Allen, R.G., Pereira, L.S., Howell, T.A., Jensen, M.E.,2011b. Evapotranspiration information reporting: II. Recommended documentation. Agric. Water Manage., 98, 921–929.

Allen, R.G., Tasumi, M., Morse, A.T., Trezza, R., 2005. A Landsat-based Energy Balance and Evapotranspiration Model in Western US Water Rights Regulation and Planning. Irrig. Drain. Syst., 19, 251–268.

Allen, R.G., Bastiaanssen, W.G.M., Tasumi, M., Morse, A., 2001. Evapotranspiration on the watershed scale using the SEBAL model and landsat images. ASAE Meeting Paper No.01–2224 St. Joseph, Michigan.

Bastiaanssen, W., Thoreson, B., Clark, B., David, G., 2010. Discussion of "Application of SEBAL Model for Mapping Evapotranspiration and Estimating Surface Energy Fluxes in South-Central Nebraska" by R. K. Singh, Ayse Irmak, Suat Irmak, and Derrel L. Martin. J. Irrig. Drain. Eng., 134, 282–283.

Bastiaanssen, W.G.M., Noordman, E.J.M., Pelgrum, H., Davids, G., Thoreson, B.P., Allen, R.G., 2005. SEBAL model with remotely sensed data to improve water-resources management under actual field conditions. J. Irrig. Drain. Eng.,131, 85–93.

Bastiaanssen, W.G.M., Ahmad, M.D., Chemin, Y., 2002. Satellite surveillance of evaporative depletion across the Indus Basin. Water Resour. Res., 38, 1273–1281.

Bastiaanssen, W.G.M., 2000. SEBAL-based sensible and latent heat fluxes in the irrigated Gediz Basin, Turkey. J. Hydrol., 229, 87–100.

Bastiaanssen, W.G.M., Menenti, M., Feddes, R.A., Holtslag, A.A.M., 1998. A remote sensing surface energy balance algorithm for land (SEBAL) 1. Formulation. J. Hydrol., 213, 198–212.

Bastiaanssen, W.G.M., 1995. Regionalization of surface flux densities and moisture indicators in composite terrain. Ph.D Thesis, Wageningen Agriculture University.

Beljaars, A.C.M. & Holtslag, A.A.M., 1991. Flux parameterization over land surfaces for atmospheric models. J. Appl. Meteorol., 30, 327–341.

Brutsaert, W., 1982. Evaporation into the atmosphere. Holland: D. Reidel Pub. Co.

Brutsaert, W. 1975. On a derivable formula for long-wave radiation from clear skies. Water Resour. Res., 11, 742–744.

Chávez, J.L., Gowda, P.H., Howell, T.A., Neale, C.M.U., Copeland, K.S., 2009. Estimating hourly crop ET using a two-source energy balance model and multispectral airborne imagery. Irrig. Sci. 28, 79–91.

Chamberlain, A.C., 1968. Transport of gases to and from surfaces with bluff and wave-like roughness elements. Q. J. R. Meteorol. Soc. 94, 318–332.

Chandrapala, L., Wimalasuriya, M., 2003. Satellite measurement supplemented with meteorological data to operationally estimate evapotranspiration in Sri Lanka. Agric. Water Manage., 58, 89–107.

Chehbouni, A., Seen, D.L., Njoku, E.G., Monteny, B.M., 1996. Examination of the difference between radiative and aerodynamic surface temperatures over sparsely vegetated surfaces. Remote Sens. Environ. 58, 177–186.

Choi, M., Kustas, W.P., Anderson, M.C., Allen, R.G., Li, F., Kjaersgaard, J.H., 2009. An intercomparison of three remote sensing-based surface energy balance algorithms over a corn and soybean production region (Iowa, U.S.) during SMACEX . Agric. For. Meteorol., 149, 2082–2097.

Elhaddad, A., Garcia, L.A., 2008. Surface energy balance-based model for estimating evapotranspiration taking into account spatial variability in weather. J. Irrig. Drain. Eng., 134, 681–689.

Field, R.T., Fritschen, L.J., Kanemasu, E.T., Smith, E.A., Stewart, J.B., Verma, S.B., Kustas, W.P., 1992. Calibration, comparison, and correction of net radiation instruments used during FIFE. J. Geophys. Res., 18, 681–695.

Gao Y. and Long D., 2008. Intercomparison of remote sensing-based models for estimation of evapotranspiration and accuracy assessment based on SWAT. Hydrol. Process. 22, 4850–4869.

Gao, Z.Q., Liu, C.S., Gao, W., Chang, N.B., 2011. A coupled remote sensing and the Surface Energy Balance with Topography Algorithm (SEBTA) to estimate actual evapotranspiration over heterogeneous terrain. Hydrol. Earth Syst. Sci. 15, 119–139.

Gieske, A., Meijninger, W., 2005. High density NOAA time series of ET in the Gediz Basin, Turkey. Irrig. Drain. Syst., 19, 285–299.

Gowda, P.H., Chavez, J.L., Colaizzi, P.D., Evett, S.R., Howell, T.A., Tolk, J.A., 2008. ET mapping for agricultural water management: present status and challenges. Irrig. Sci. 26, 223–237.

Gowda, P.H., Howell, T.A., Chavez, J.L., Copeland, K.S., Paul, G., 2008. Comparing SEBAL ET with Lysimeter data in the semi-arid Texas High Plains. In: Proceedings of World Environmental and Water Resources Congress.

Gowda, P.H., Chavez, J.L., Colaizzi, P.D., Howell, T.A., Schwartz, R.C., 2007. Relationship between LAI and Landsat TM spectral vegetation indices in the Texas Panhandle. In: proceedings of the ASABE Annual Meeting.

Howell, T.A., Schneider, A.D., Dusek, D.A., Marek, T.M., Steiner, J.L., 1995. Calibration and scale performance of bushland weighing lysimeters. Trans. ASAE 38, 1019–1024.

Jackson, T.J., Vine, D.M.L., Hsu, A.Y., Oldak, A., Starks, P.J., Swift, C.T., 1999. Soil moisture mapping at regional scales using microwave radiometry: The Southern Great Plains Hydrology Experiment. IEEE Trans. Geosci. Remote Sens. 37, 2136–2151.

Jacob. F., Olioso, A., Gu, X.F., Su, Z., Seguin, B., 2002. Mapping surface fluxes using airborne visible, near infrared, thermal infrared remote sensing data and a spatialized surface energy balance model. Agronomie, 22, 669–680.

Jia, L., Su, Z., van den Hurk, B., Menenti, M., Moene, A., De Bruin, H.A.R., 2003. Estimation of sensible heat flux using the Surface Energy Balance System (SEBS) and ATSR measurements. Phys. Chem. Earth Pt B., 28, 75–88.

Kalma, J.D., McVicar, T.R., McCabe, M.F., 2008. Estimating land surface evaporation: A review of methods using remotely sensed surface temperature data. Surv. Geophys, 29, 421–469.

Kustas, W., Anderson, M., 2009. Advances in thermal infrared remote sensing for land surface modeling. Agric. For. Meteorol., 49, 2071–2081.

Kustas, W.P., Anderson, M.C., Norman, J.M., Li, F., 2007. Utility of radiometric–aerodynamic temperature relations for heat flux estimation. Bound Layer Meteorol., 122, 167–187.

Kustas, W.P., Jackson, T.J., Prueger, J.H., Hatfield, J.L., Anderson, M.C., 2003. Remote sensing field experiments for evaluating soil moisture retrieval algorithms and modeling land-atmosphere dynamics in central Iowa. EOS Trans. Am. Geophys. Union, 84, 485–493.

Kustas, W.P., Choudhury, B.J., Kunkel, K.E., Gay, L.W., 1989. Estimation of the aerodynamic roughness parameters over an incomplete canopy cover of cotton. Agric. For. Meteorol., 46, 91–105.

Kustas, W.P., Choudhury, B.J., Moran, M.S., Reginato, R.J., Jackson, R.D., Gay, L.W., Weaver, H.L., 1989. Determination of sensible heat flux over sparse canopy using thermal infrared data. Agric. For. Meteorol., 44, 197–216.

Long, D. and Singh, V.P., 2012. A modified surface energy balance algorithm for land (M-SEBAL) based on a trapezoidal framework. Water Resour. Res., 48, W02528, doi:10.1029/2011WR010607

Long, D., Singh, V.P., Li. Z.L., 2011. How sensitive is SEBAL to changes in input variables, domain size and satellite sensor. J. Geophys. Res., 116: D21107, doi 10.1029/2011JD016542.

Li, Z.L., Tang, R., Wan, Z., Bi, Y., Zhou, C., Tang, B., 2009. A review of current methodologies for regional evapotranspiration estimation from remotely sensed data. Sensors, 9, 3801–3853.

Lhomme, J.P., Chehbouni, A., Monteny, B., 2000. Sensible heat flux-radiometric surface temperature relationship over sparse vegetation: Parameterizing B^{-1}. Bound Layer Meteorol. 97, 431–457.

Marek, T.H., Porter, D.O., Howell, T.A., Kenny, N., and Gowda, P.H., 2009. Understanding ET 4 and its use in irrigation scheduling (a TXHPET Network series user manual). Texas 5

AgriLife Research at Amarillo, Publication No. 09-02, Texas A&M University, Amarillo, Texas, 60 p.

Neale, C.M.U., Geli, H., Kustas, W.P., Alfieri, J.G., Gowda, P.H., 2012. Modeling the Soil Water Content Profile using a Remote Sensing Based Hybrid Evapotranspiration Modeling Approach. Adv. in Water Resour., 50, 152-161.

Norman, J.M., Anderson, M.C., Kustas, W.P., 2006. Are single-source, remote-sensing surface-flux models too simple? In: D'Urso G, Jochum MAO, Moreno J, Editors. Proceedings of the international conference on earth observation for vegetation monitoring and water management. American Institute of Physics, 852, 170–177.

Paulson, C.A., 1970. The mathematical representation of wind speed and temperature profiles in the unstable atmospheric surface layer. J. Appl. Meteorol. 9, 856–861.

Singh, R.K., Irmak, A., Irmak, S., Martin, D.L., 2008. Application of SEBAL model for mapping evapotranspiration and estimating surface energy fluxes in south-central Nebraska. J. Irrig. Drain. Eng. 134, 273–285.

Senay, G.B., Budde, M.E., Verdin, J.P., Melesse, A.M., 2007. A coupled remote sensing and Simplified Surface Energy Balance approach to estimate actual evapotranspiration from irrigated fields. Sensors, 7, 979–1000.

Sobrino, J.A., Muñoz, J.J.C., Sòria, G., Gómez, M., Ortiz, A.B., Romaguera, M., 2008. Thermal remote sensing in the framework of the SEN2FLEX project: field measurements, airborne data and applications. Int. J. Remote Sens. 29, 4961–4991.

Stewart, J.B., Kustas, W.P., Humes, K.S., Nichols, W.D., Moran, M.S., De Bruin, H.A.R., 1994. Sensible heat flux-radiometric surface temperature relationship for eight semi arid areas. J. Appl. Meteorol. 33, 1110–1117.

Su, Z., Timmermans, W.J., van der Tol, C., Dost, R., Bianchi, R., G´omez, J.A., 2009. EAGLE 2006 – Multi-purpose, multi-angle and multi-sensor in-situ and airborne campaigns over grassland and forest. Hydrol. Earth Syst. Sci. 13, 833–845.

Su, Z., Timmermans, W., Gieske, A., Jia, L., Elbers, J.A., Olioso, A., 2008. Quantification of land atmosphere exchanges of water, energy and carbon dioxide in space and time over the heterogeneous Barrax site. Int. J. Remote Sens., 29, 5215–5235.

Su, Z., Schmugge, T., Kustas, W.P., Massman, W.J., 2001. An evaluation of two models for estimation of the roughness height for heat transfer between the land surface and the atmosphere. J. Appl. Meteorol., 40, 1933–1951.

Tasumi, M., Trezza, R., Allen, R.G., Wright, J.L., 2005. Operational aspects of satellite-based energy balance models for irrigated crops in the semi-arid U.S. Irrig. Drain. Syst. 19, 355–376.

Timmermans, W.J., Kustas, W.P., Anderson, M.C., French, A.N., 2007. An intercomparison of the Surface Energy Balance Algorithm for Land (SEBAL) and the Two-Source Energy Balance (TSEB) modeling schemes. Remote Sens. Environ. 108, 369–84.

Tolk, J.A., Evett, S.R., Howell, T.A., 2006. Advection influences on evapotranspiration of Alfalfa in a semiarid climate. Agron. J., 98, 1646–1654.

Verhoef, A., De Bruin, H.A.R., Van Den Hurk, B.J.J.M., 1997a. Some practical notes on the parameter kB^{-1} for sparse vegetation. J. Appl. Meteorol. 36, 560–572.

Verhoef, A., McNaughton, K.G., Jacobs, A.F.G., 1997b. A parameterization of momentum roughness length and displacement height for a wide range of canopy densities. Hydrol. Earth Syst. Sci., 1, 81–91.

Van de Griend, A.A., and Owe, M., 1993. On the relationship between thermal emissivity and normalized difference vegetation index for natural surfaces. Int. J. Remote Sens. 14, 1119–1131.

Wang, J., Sammis, T.W., Gutschick, V.P., Gebremichael, M., Miller, D.R., 2009. Sensitivity analysis of the Surface Energy Balance Algorithm for Land (SEBAL). Trans. ASABE. 52, 801–811.

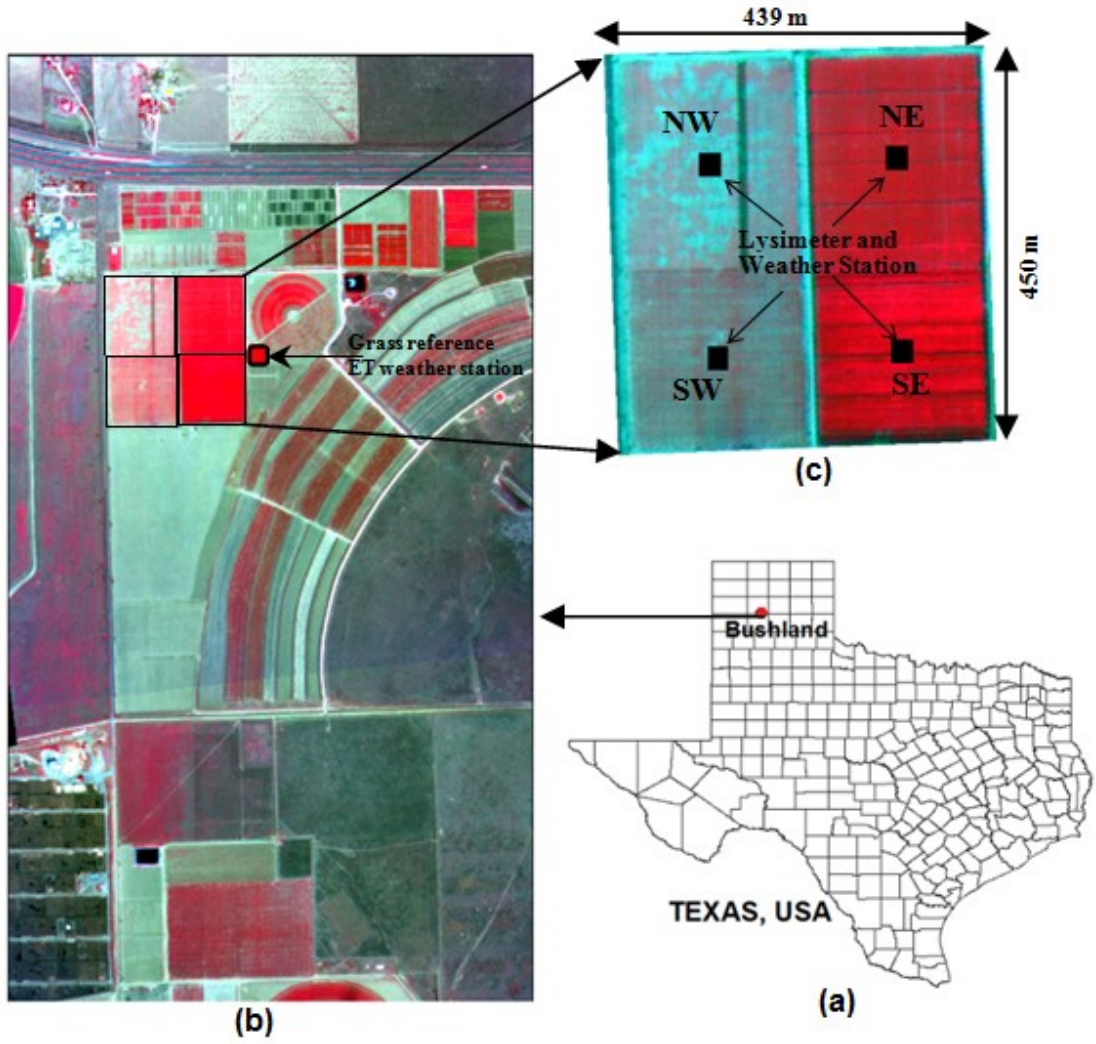

Figure 2.1 False color composite aircraft image of 5 August, 2008, showing the BEAREX08 study region. (a) location of the study area in reference to the state of Texas, USA. (b) aircraft scene covering a region of close to 5km^2 and (c) exploded view of the lysimeter field.

Figure 2.2 Canopy cover from the first image acquisition date to the last. A1–26 June irrigated field, A2–26 June dryland field, B1– 5 August irrigated field, and B2– 5 August dryland field.

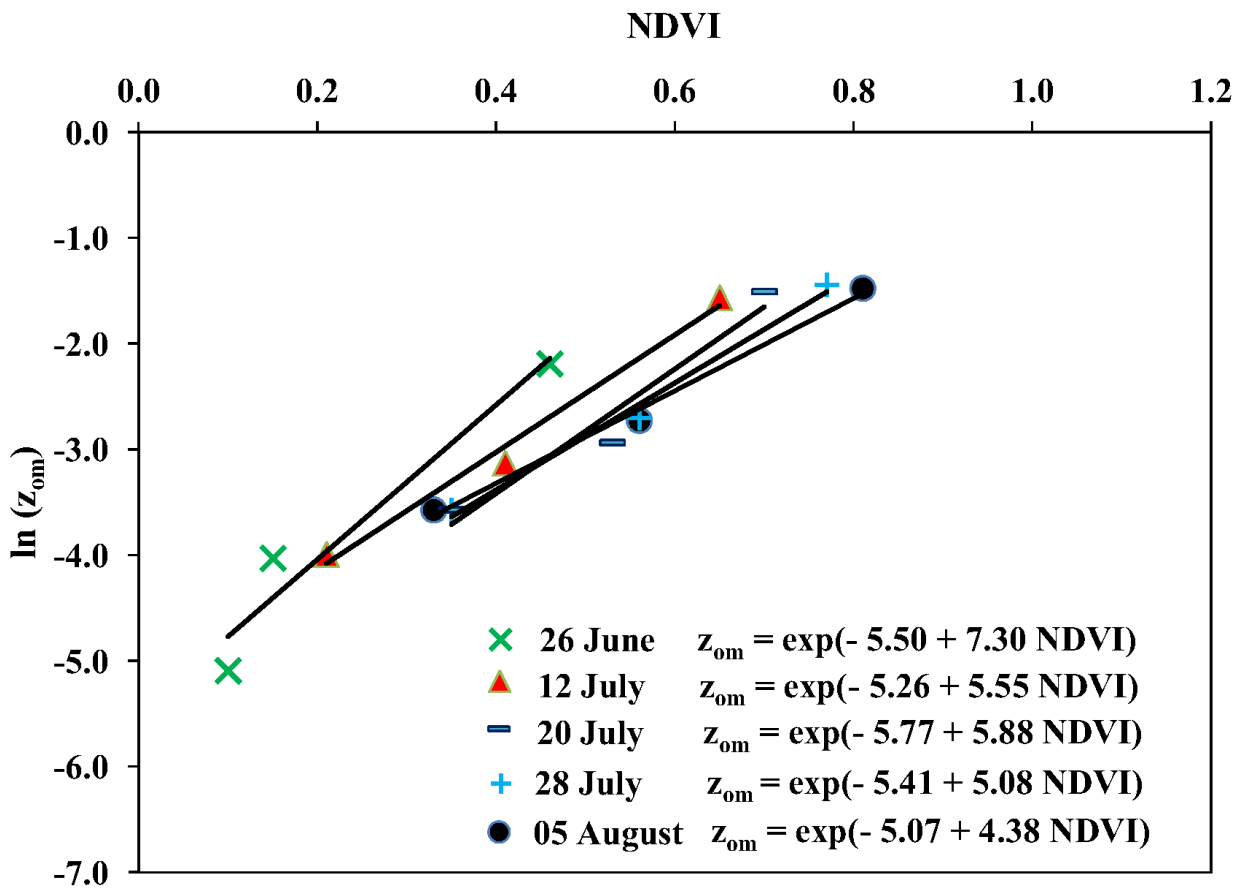

Figure 2.3 Relationship for roughness length for momentum transport generated from plant height information for each image.

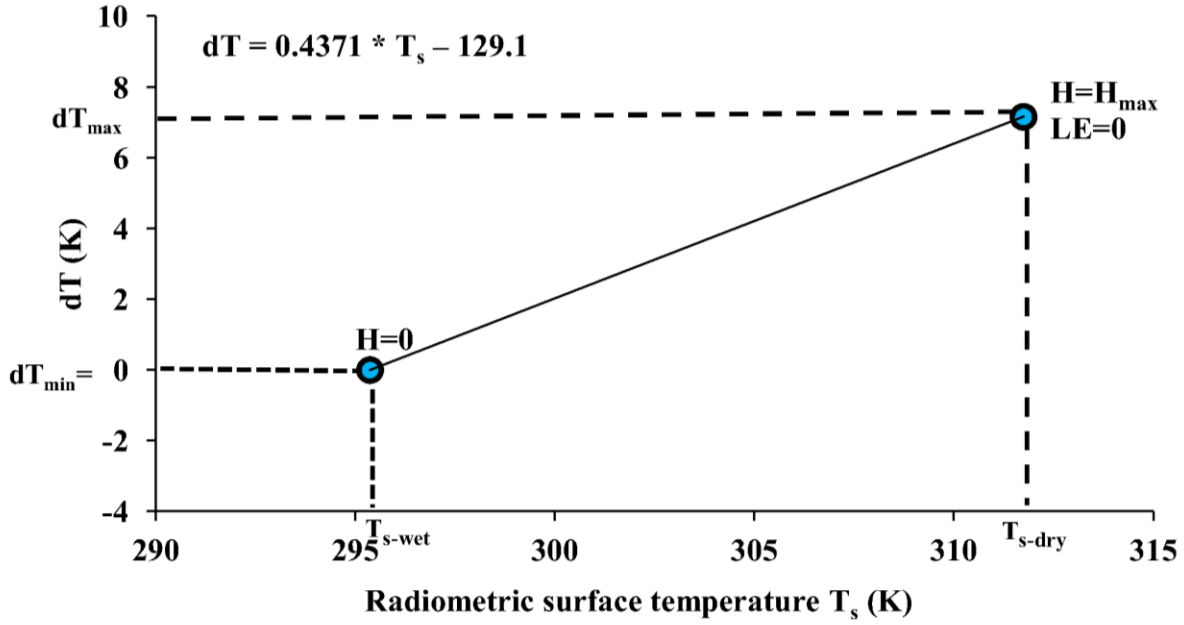

Figure 2.4 Solving for coefficients 'a' and 'b' using the wet and dry pixel concept.

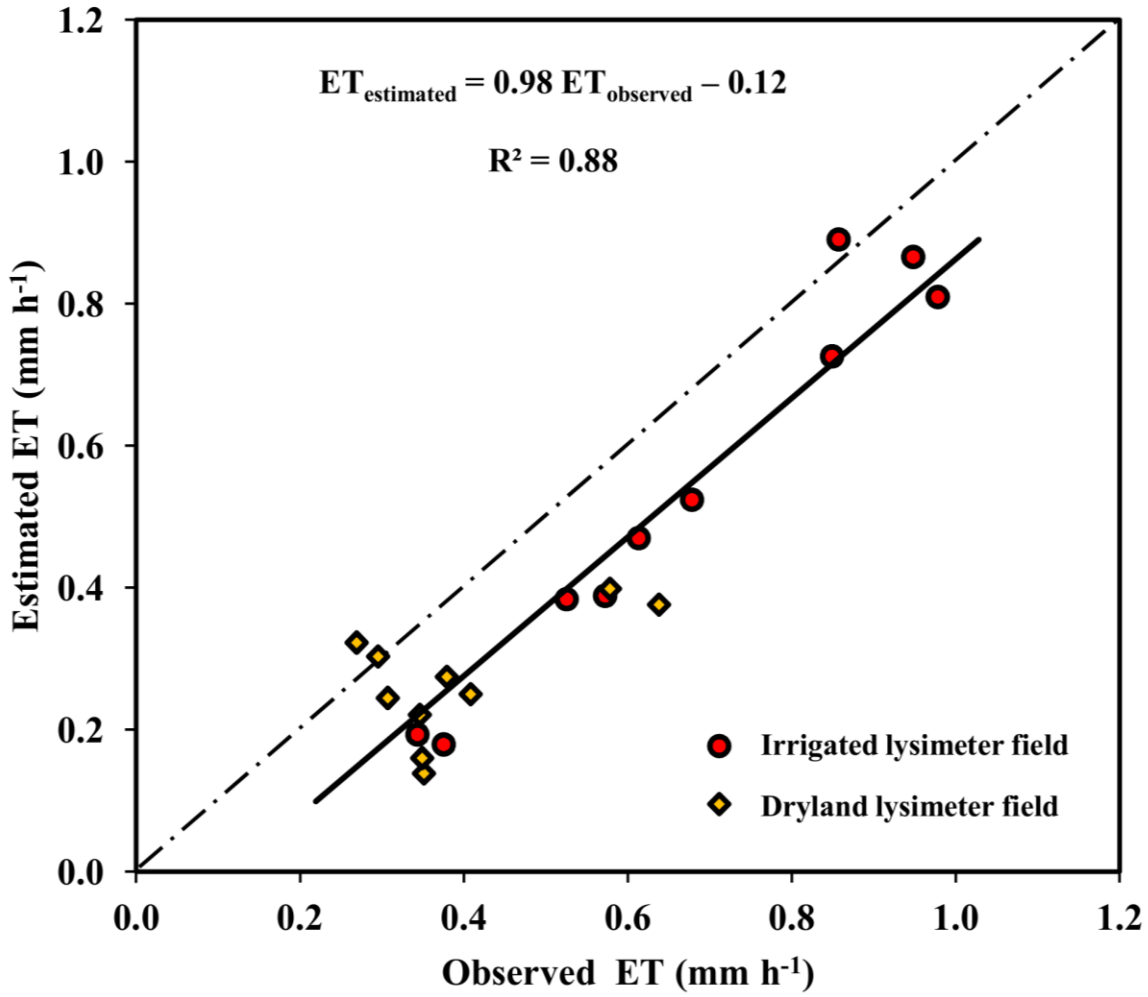

Figure 2.5 SEBAL modeled versus observed instantaneous ET comparison for cotton fields under dryland and irrigation management.

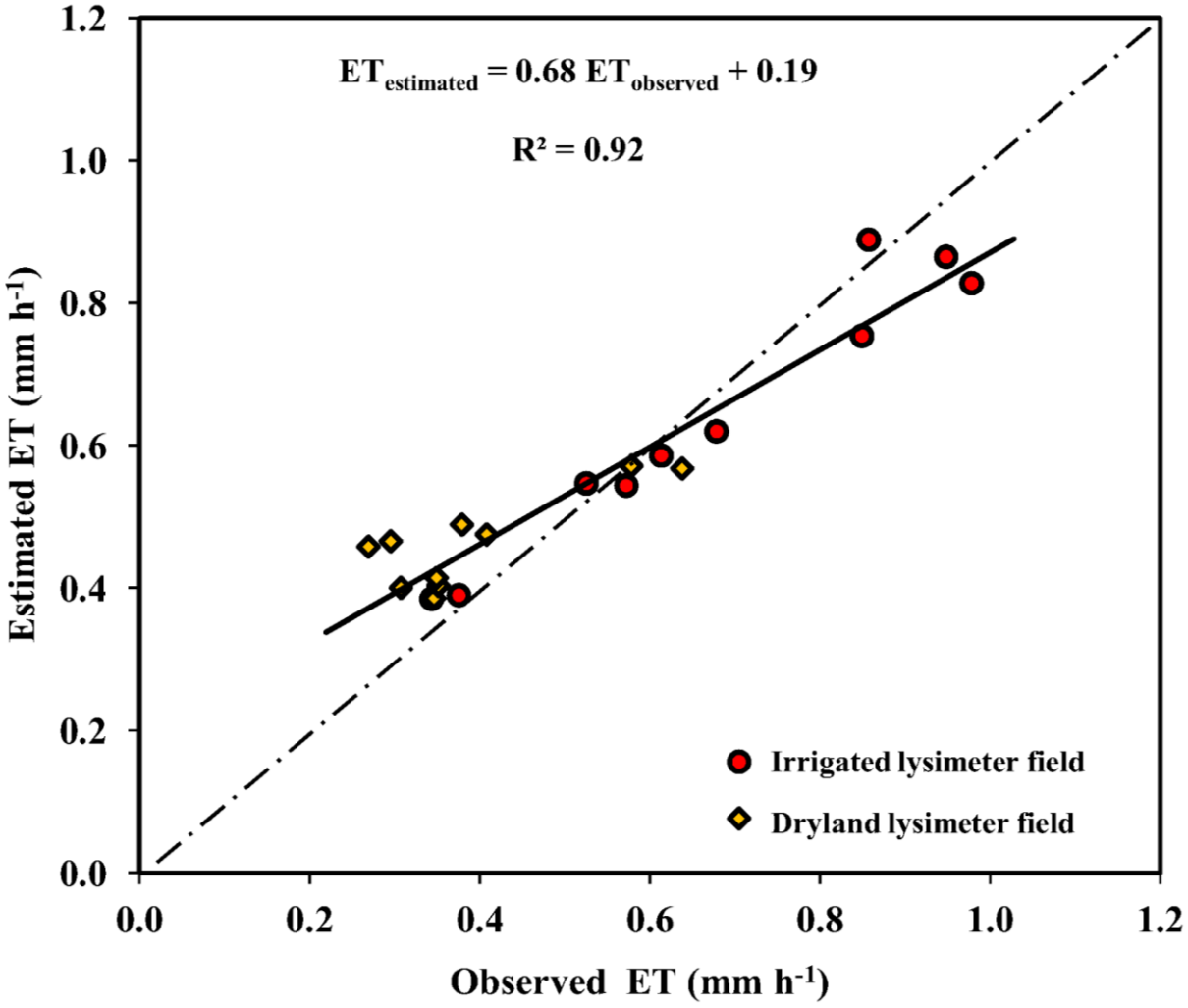

Figure 2.6 SEBAL with kB-1 parameterization modeled ET versus observed instantaneous ET comparison for cotton fields under dryland and irrigation management.

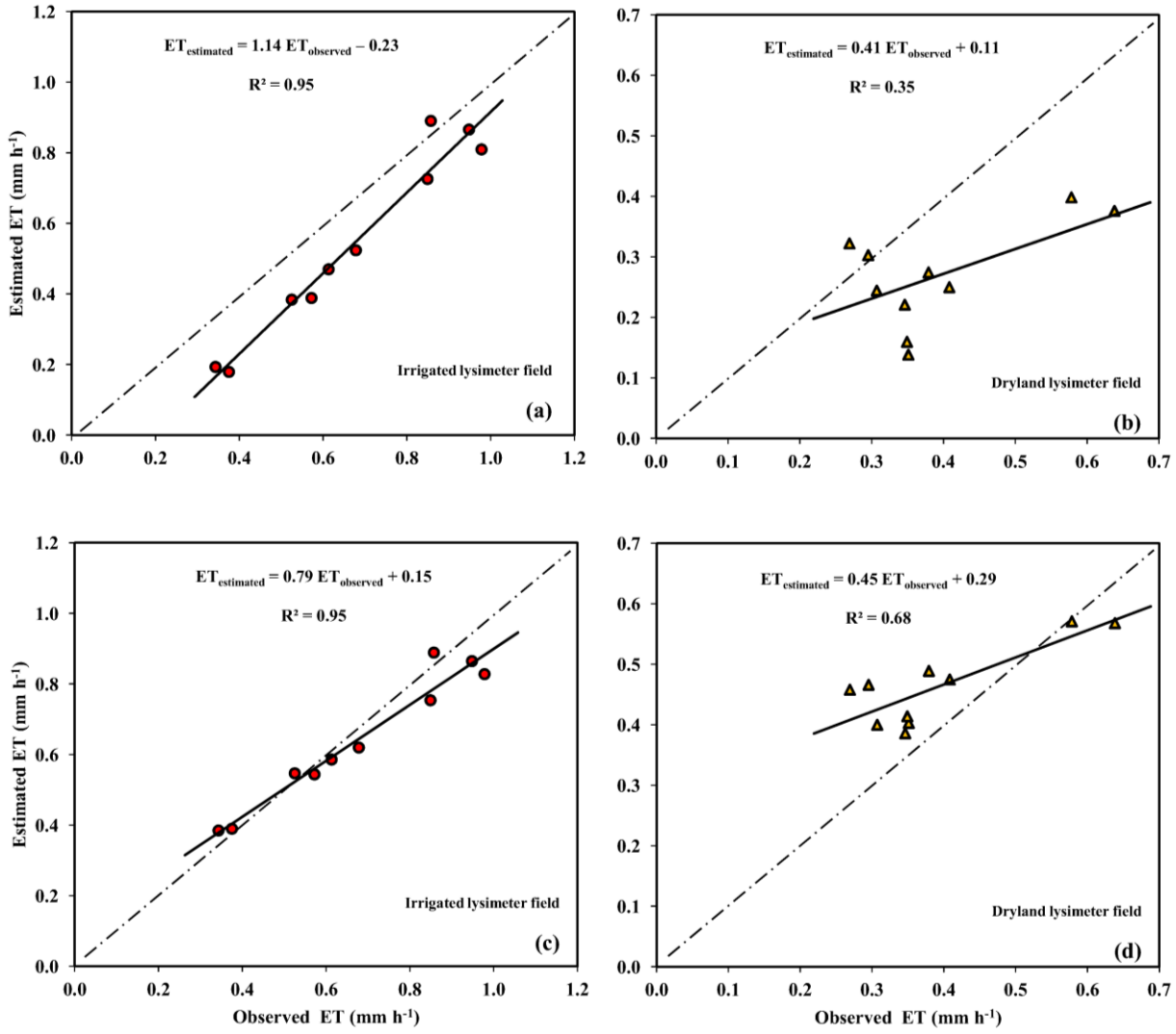

Figure 2.7 Observed instantaneous ET comparison with (a) SEBAL ET for irrigated cotton field, (b) SEBAL ET for dryland cotton field, (c) SEBAL with kB-1 parameterization–ET for irrigated cotton field, and (d) SEBAL with kB-1 parameterization–ET for dryland cotton field.

Table 2.1 Performance statistics used for evaluating model performance.

Statistical variable	Description	Equation	Use and desired value
n	Number of observations	-	-
R^2	Coefficient of determination	$\frac{\left(\sum_{i=1}^{n}(O_i-\bar{O})\,(M_i-\bar{M})\right)^2}{\sum_{i=1}^{n}(O_i-\bar{O})^2.\sum_{i=1}^{n}(M_i-\bar{M})^2}$	Degree of collinearity +1or -1
m	Slope of the best fit regression line	$\frac{M_1-M_2}{O_1-O_2}$	Relative relationship between modeled and observed value ~1
y-intercept	y-intercept of the best fit regression line	-	Lag or lead indicator ~0
MBE	Mean bias error	$\frac{1}{N}\sum_{i=1}^{n}(O_i-M_i)$	Error in the constituents unit with underestimation/ overestimation indication ~0
PBIAS	Percentage bias	$\frac{\sum_{i=1}^{n}(O_i-M_i)}{\sum O_i}\times 100$	Bias expressed as percentage error ~0
RMSE	Root mean square error	$\sqrt{\frac{1}{N}\sum_{i=1}^{n}(M_i-O_i)^2}$	Indicates error in the constituents unit ~0
% RMSE	Percentage root mean square error	$\frac{RMSE}{\frac{\sum_{i=1}^{n}O_i}{n}}\times 100$	RMSE expressed as percentage deviation from mean ~0
NSE	Nash-Sutcliffe efficiency	$\frac{\sum_{i=1}^{n}(O_i-\bar{O})^2-\sum_{i=1}^{n}(M_i-O_i)^2}{\sum(O_i-\bar{O})^2}$	Indicative of the strength of model to predict the observed ~0-1

Table 2.2 Selection of hot and wet pixel and the variability in the 'a' and 'b' coefficient.

Image acquisition date	Cold/wet pixel		Hot/dry pixel				$dT = a + b.T_s$	
	T_{wet}	NDVI	T_{dry}	NDVI	Albedo	z_{om}	a	b
26 June, 2008	301.09	0.704	315.42	0.143	0.162	0.012	-198.46	0.659
	301.09	0.704	315.42	0.122	0.180	0.010	-199.25	0.662
	301.09	0.704	315.98	0.153	0.185	0.013	-177.12	0.588
12 July, 2008	295.36	0.805	310.14	0.165	0.168	0.013	-172.07	0.582
	295.36	0.805	310.50	0.162	0.151	0.013	-172.41	0.583
	295.36	0.805	311.74	0.206	0.220	0.016	-129.09	0.437
20 July, 2008	297.47	0.790	317.42	0.232	0.178	0.012	-185.71	0.624
	297.47	0.790	316.94	0.138	0.172	0.007	-227.04	0.763
	297.47	0.790	316.99	0.176	0.166	0.009	-215.83	0.725
28 July, 2008	299.08	0.799	317.37	0.152	0.185	0.010	-220.95	0.738
	299.08	0.799	317.28	0.197	0.181	0.012	-201.89	0.675
	299.08	0.799	317.37	0.155	0.188	0.009	-212.95	0.712
05 August, 2008	300.50	0.800	334.35	0.152	0.161	0.012	-143.79	0.478
	300.50	0.800	334.59	0.150	0.146	0.012	-147.22	0.489
	300.50	0.800	335.45	0.157	0.149	0.013	-138.318	0.460

Table 2.3 Influence of 'a' and 'b' coefficients on the final ET (mm h-1) value.

Image acquisition date	Statistics	Irrigated fields		Dryland fields	
		NE	SE	NW	SW
26 June, 2008	σ	0.04	0.04	0.03	0.03
	%CV	21.10	18.22	14.11	12.29
12 July, 2008	σ	0.08	0.08	0.11	0.11
	%CV	21.02	21.88	79.93	68.52
20 July, 2008	σ	0.04	0.04	0.05	0.05
	%CV	6.70	8.59	21.25	19.21
28 July, 2008	σ	0.01	0.01	0.02	0.02
	%CV	0.74	1.18	5.60	5.17
05 August, 2008	σ	0.00	0.00	0.01	0.01
	%CV	0.12	0.06	4.33	4.23

Table 2.4 Performance statistics for T_s, R_n, and G_o (no. of observations = 20).

Estimated parameter	MBE	PBIAS	RMSE	%RMSE	NSE	Regression		
						R^2	m	y-intercept
T_s (^{o}C)	0.04	0.13	1.16	3.36	0.96	0.96	0.95	1.59
R_N (W m^{-2})	6.61	1.14	17.98	3.10	0.86	0.91	1.10	-65.04
G_S (W m^{-2})	-9.87	-36.24	13.51	49.58	-3.96	0.02	0.18	32.19

Table 2.5 Performance statistics for Instantaneous ET (mm h^{-1}) computed from SEBAL.

Observation points	n	MBE	PBIAS	RMSE	%RMSE	NSE	Regression		
							R^2	m	y-intercept
All fields	20	0.13	23.82	0.15	28.15	0.55	0.88	0.98	-0.12
Irrigated field	10	0.13	19.38	0.14	21.48	0.55	0.95	1.14	-0.23
Dryland field	10	0.12	31.44	0.16	39.55	-0.80	0.35	0.41	0.11

Table 2.6 Performance statistics for SEBAL Instantaneous ET (mm h^{-1}) computed from SEBAL with kB^{-1} parameterization.

Observation points	n	MBE	PBIAS	RMSE	%RMSE	NSE	Regression		
							R^2	m	y-intercept
All fields	20	-0.02	-3.56	0.08	16.27	0.85	0.92	0.68	0.19
Irrigated field	10	0.03	4.89	0.07	10.15	0.89	0.95	0.79	0.12
Dryland field	10	-0.07	-18.11	0.10	25.97	0.22	0.68	0.45	0.29

Table 2.7 Aerodynamic roughness parameters for the four cotton fields under irrigation (NE and SE) and dryland (NW and SW) management.

Date	Field	z_{om}_D (m)	z_{om}_E (m)	z_{oh}_C (m)	kB^{-1} (m)	z_{oh}_S (m)	C_ht (m)	C_ht_O (m)	z_{om}_B (m)
26 Jun	NE	0.011	0.009	0.0009	19.21	0.00001	0.084	0.152	0.020
	SE	0.010	0.008	0.0008	24.67	0.00001	0.076	0.178	0.023
	NW	0.008	0.007	0.0007	44.51	0.00001	0.063	0.089	0.012
	SW	0.008	0.007	0.0007	58.86	0.00001	0.060	0.114	0.015
12 Jul	NE	0.052	0.044	0.0044	5.39	0.00026	0.382	0.457	0.059
	SE	0.048	0.041	0.0041	5.55	0.00020	0.352	0.330	0.043
	NW	0.018	0.015	0.0015	8.54	0.00001	0.137	0.356	0.046
	SW	0.026	0.022	0.0022	6.99	0.00003	0.190	0.292	0.038
20 Jul	NE	0.082	0.102	0.0102	3.50	0.00268	0.602	0.559	0.073
	SE	0.073	0.092	0.0092	3.65	0.00213	0.540	0.406	0.053
	NW	0.009	0.011	0.0011	13.04	0.00001	0.066	0.432	0.056
	SW	0.019	0.025	0.0025	6.55	0.00008	0.142	0.356	0.046
28 Jul	NE	0.123	0.182	0.0182	2.78	0.00780	0.902	0.559	0.073
	SE	0.115	0.168	0.0168	2.86	0.00717	0.843	0.610	0.079
	NW	0.012	0.013	0.0013	11.87	0.00001	0.087	0.508	0.066
	SW	0.021	0.024	0.0024	6.78	0.00007	0.153	0.457	0.059
05 Aug	NE	0.146	0.265	0.0265	2.18	0.01662	1.073	0.635	0.083
	SE	0.199	0.401	0.0401	2.02	0.02684	1.468	0.559	0.073
	NW	0.017	0.016	0.0016	8.53	0.00003	0.126	0.533	0.069
	SW	0.028	0.030	0.0030	5.32	0.00023	0.207	0.432	0.056
MEAN		0.051	0.074	0.0074	12.14	0.00321	0.378	0.401	0.052

z_{om}_D = Roughness length for momentum estimated from Eq.(16) using coefficients derived for each image as given in Figure 2.3

z_{om}_E = Roughness length for momentum estimated from Eq. (16) using constant coefficients C1 = -5.5 and C2 = 5.8, from (Bastiaanssen, 1995)

z_{oh}_C = Roughness length for heat estimated from Eq. (15) using constant kB-1 value of 2.3.

kB-1 = Excess resistance parameter for heat transfer estimated from parameterization given by Su et. al (2001), Appendix B.

z_{oh}_S = Roughness length for heat estimated from Eq. (15) using kB-1 value from Su et. al (2001), Appendix B.

C_ht = Canopy height from Eq. (A2) (= zom_D/0.13)

C_ht_O = Field measurement of canopy height

z_{om}_B = Roughness length for momentum estimated from Brutsaert relationship, Eq. (A2) (= 0.13*C_ht_O)

Appendix A - Various intermediate parameterizations used in the SEBAL algorithm

Displacement height was computed from the model given by Verhoef et al. (1997b):

$$d_o = h\left(1 - \frac{1 - e^{-\sqrt{c_1 .\ LAI}}}{\sqrt{c_{1\ .LAI}}}\right) \tag{2.17}$$

where h is the canopy height and c_1 is a free parameter with the value 20.6

Roughness length for momentum transport as given by Brutsaert (1982):

$$z_{om} = 0.13\ h \tag{2.18}$$

Leaf Area Index model developed specifically for the Texas High Plains region given by Gowda et al. (2007):

$$LAI = 8.768 \times NDVI^{3.616} \tag{2.19}$$

Fractional cover was derived from relationship taken from Jia et al. (2003):

$$f_c = 1 - \left[\frac{NDVI - NDVI_{max}}{NDVI_{min} - NDVI_{\max}}\right]^K \tag{2.20}$$

where K is taken as 0.4631

Blending height

$$u_b = u_{ref}\left[\frac{\ln(z_b - d_o) - \ln(z_{om})}{\ln(z_{ref}\ - d_o) - \ln(z_{om})}\right] \tag{2.21}$$

Monin Obukhov Length (L)

$$L = -\frac{\rho_a C_p u_*^3 T_s}{kgH} \tag{2.22}$$

where density of air (ρ_a) = ~1.17 kg m^{-3}, specific heat capacity of air (C_p) =~1,005 J kg^{-1} K^{-1}, gravitational acceleration (g) = 9.81 m s^{-2}.

Momentum transfer correction factor under unstable condition from Paulson (1970):

$$\psi_m = 2ln\left[\frac{1 + x_m}{2}\right] + ln\left[\frac{1 + x_m^2}{2}\right] - 2\arctan(x_m) + \frac{\pi}{2} \tag{2.23}$$

where x_m is defined as:

$$x_m = \left(1 - 16\frac{z_b - d_o}{L}\right)^{0.25} \tag{2.24}$$

Heat transfer correction factor under unstable condition from Paulson (1970):

$$\psi_h = 2ln\left[\frac{1+x_h^2}{2}\right] \tag{2.25}$$

where x_h is defined as:

$$x_h = \left(1 - 16\frac{z_{ref} - d_0}{L}\right)^{0.25} \tag{2.26}$$

Appendix B - Excess resistance to heat transfer formulation

Excess resistance to heat transfer formulation as given by Su.et al. (2001)

$$kB^{-1} = \frac{kC_d}{4C_t\frac{u_*}{u(h)}\left(1 - e^{-\frac{n_{ec}}{2}}\right)}f_c^2 + \frac{k.\frac{u_*}{u(h)}.\frac{z_{om}}{h}}{C_t^*}f_c^2 f_s^2 + kB_s^{-1}f_s^2 \tag{2.27}$$

In Eq. (B1), kB_s^{-1} is the bare soil surface excess resistance computed as:

$$kB_s^{-1} = 2.46(Re_*)^{\frac{1}{4}} - \ln(7.4) \tag{2.28}$$

In Eq. (B1), n_{ec} is within-canopy wind speed profile extinction coefficient given by:

$$n_{ec} = \frac{C_d.LAI}{\frac{2u_*^2}{u(h)^2}} \tag{2.29}$$

In Eq. (B1) and (B3), the ratio $u_*/u(h)$ is parameterized as:

$$\frac{u_*}{u(h)} = c_1 - c_2.e^{-c_3.C_d.LAI} \tag{2.30}$$

where c_1=0.320, c_2=0.264 and c_3=15.1

In Eq. (B1), C_t^* is heat transfer coefficient of the soil given as:

$$C_t^* = \Pr^{-\frac{2}{3}} Re_*^{-\frac{1}{2}} \tag{2.31}$$

In Eq. (B2) and Eq. (B5), Re_* is roughness Reynolds number calculated as:

$$Re_* = \frac{h_s u_*}{\nu} \tag{2.32}$$

where h_s is the roughness height for soil taken here as 0.009 m.

In Eq. (B1), ν is kinematic viscosity of the given by:

$$\nu = 1.327 \times 10^{-5} \left(\frac{p_0}{p}\right)\left(\frac{T_a}{T_{a0}}\right)^{1.81} \tag{2.33}$$

where, p and T_a are ambient pressure and temperature and p_o=101.3 kPa and T_{ao}=273.15 K. Other terms in Eqs. (B1) to (B7) are: C_d is the drag coefficient of the foliage elements taken as 0.2, C_t is heat transfer coefficient of the leaf with value 0.01, P_r is Prandtl number with value 0.71, u(h) is the horizontal wind speed at the canopy height, f_c is the fractional canopy coverage and f_s is its compliment, and k is von Karman's constant taken as 0.41.

Chapter 3 - Investigating the influence of roughness length for heat transport (z_{oh}) on the performance of SEBAL in semi-arid irrigated and dryland agricultural systems

3.1 Abstract

Satellite-based thermal infrared remote sensing has greatly contributed to the development and improvement of remote sensing–based evapotranspiration (RS-ET) mapping algorithms. Radiometric temperature (T_s) derived from thermal sensors is inherently different from the aerodynamic temperature (T_o) required for solving the bulk formulation of sensible heat (H) based on the Monin-Obukhov similarity (MOS) posing an ill-fated problem. The scalar roughness length z_{oh}, representing heat transport mechanism and described by the dimensionless parameter kB^{-1}, was used to account for the discrepancy between radiometric and aerodynamic temperatures. Surface Energy Balance Algorithm for Land (SEBAL) with its indigenous approach of linearly relating dT (near-surface temperature gradient) with T_s across the imagery, maintained that this approach would absorb the impacts of differences between T_s and T_o. SEBAL utilized a constant kB^{-1} value of 2.3 in its initial version, and later switched to a constant z_{oh} (z_1) value of 0.1. In this study, we investigated the influence of this change in SEBAL by testing four approaches: (i) z_{oh} derived from a constant kB^{-1} of 2.3, (ii) constant z_{oh} (z_1) = 0.1, (iii) constant z_{oh} (z_1) = 0.01, and (iv) spatially variable z_{oh} from kB^{-1} parameterization. SEBAL was applied on 10 high-resolution airborne images acquired during BEAREX07-08 (Bushland Evapotranspiration and Agricultural Remote Sensing Experiment) field campaigns and validated against measurements from four large precision weighing lysimeters installed on two irrigated and two dryland fields. The spatially variable kB^{-1} produced statistically different and improved ET estimates compared to that with constant kB^{-1} and constant z_1 (z_{oh}) approaches. SEBAL performance for irrigated fields representing high ET, limited soil water deficits, and complete ground cover surfaces was markedly different from the dryland fields representing less ET, greater soil water deficits with sparser vegetation cover. A variable kB^{-1} value derived from a physical model incorporated into SEBAL generated good overall estimates while delivering better performance for dryland agricultural systems. Overall, this study focused on the classical problem of estimating heat transfer from two contrasting hydrological regimes i.e. irrigated and

dryland agriculture and illustrated the existing need for a realistic consideration of excess resistance to heat transfer in single-source resistance modeling frameworks.

3.2 Introduction

There is an imminent need for a settlement and clarity on the usage of roughness length for heat transport (z_{oh}) in the estimation of evapotranspiration (ET) using SEBAL (Surface Energy Balance Algorithm for Land). Before addressing the real issue, a brief history of SEBAL will provide helpful background for this problem. SEBAL was developed by Bastiaanssen (1995) in the early 90's, and soon it became one of the widely used algorithms around the world for estimating ET using thermal remote sensing data (Bastiaanssen et al., 2005). In its earlier version (Bastiaanssen, 1995), SEBAL derived z_{oh} based on a constant excess resistance parameter to heat transfer (kB^{-1}) value of 2.3 (Bastiaanssen et al., 1998; Bastiaanssen, 2000). In recent versions (Bastiaanssen et al., 2002; Bastiaanssen et al., 2005), it redefined the z_{oh} into a purely empirical height and renamed it as z_1 with a constant value of 0.1. Although the impact of this change on the final ET estimates were never investigated; there were still some studies where the z_{oh} (z_1) value was taken as 0.01 (Allen et al., 2001; Singh et al., 2008). With the variations in the usage of z_{oh} values, one could conclude that z_{oh} was not a sensitive parameter, and its influence on ET estimates as negligible. However, a study by Long et al. (2011) has shown that z_{oh} was a sensitive parameter in the estimation of ET in SEBAL. In their study, they used both the original (derived from constant kB^{-1} of 2.3) and updated value of z_{oh} (z_{oh}=0.1 m), and found a significant influence on the final ET estimates; however, this study lacked validation. In another research study, the same authors (Long and Singh, 2012a), refuted their claim of variable z_{oh} value by saying "*this study (by Timmermans et al., 2007) mistakenly took kB^{-1} = 2.3 as a part of the SEBAL algorithm; in fact, SEBAL does not use a fixed kB^{-1} parameter, but rather takes the roughness length for heat transfer (z_{oh}) as 0.1 m*". SEBAL studies with z_{oh} derived from constant kB^{-1} of 2.3 (Jacob et al., 2002; Timmermans et al., 2007; Gao and Long, 2008; French et al., 2005), and those with z_{oh}= 0.1 m (Allen et al., 2007; Wang et al., 2009), further the ones with z_{oh}=0.01 m (Gieske and Meijninger, 2005; Chandrapala and Wimalasuriya, 2003), and the more recent use of kB^{-1} parameterization (Paul et al., 2012; Wu et al., 2012), elucidate the need for a study that can be validated. Several studies using SEBAL were ambiguous on how the z_{oh} was handled (Teixeira et al., 2009; Elhaddad and Garcia, 2011).

The radiometric surface temperature (T_s) derived from satellite and airborne sensors have brought forth a significant technical and theoretical advancement in the spatial modeling of ET. However, there remains some skepticism over the usage of remotely sensed T_s in ET algorithms (Hall et al., 1992; Cleugh et al., 2007; Mu et al., 2007, 2011). The reason for this criticism was the non-unique relationship between aerodynamic temperature (T_o) as defined in the bulk parameterization based on the Monin-Obukhov similarity (MOS) and T_s. Since most remote sensing based algorithms used the MOS parameterization procedures (Su et al., 2001) and calculate ET as the residual of the surface energy balance, this criticism seems valid. However, there have been remarkable progresses made in the conceptualization and parameterization of the soil-canopy-air heat exchange mechanism addressing the issue arising from aerodynamic-radiometric temperature differences (Lhomme et al., 2012, Gokmen et al., 2012). In general, the residual surface energy balance scheme utilizing the MOS formulation for ET estimation can be categorized into both a single-source model and a dual-source model, differing in their treatment of soil and vegetation source contribution as composite or distributed respectively. The single source and dual source approaches, both utilize T_s from the thermal sensors and have comparable computational complexities and input requirements (Kustas et al., 2007). Both approaches have demonstrated incredible capabilities in solving regional water resources problems by providing accurate and economical spatial ET information (Anderson et. al., 2012; Bastiaanssen et al., 2005). Several intercomparison studies, of single-source and dual-source scheme (Tang et al., 2012; Long and Singh, 2012b; Gonzalez-Dugo et al., 2009; Choi et al., 2009; Gao and Long, 2008; Timmermans et al., 2007) has reported comparable accuracy of surface flux retrievals with mixed performances. Comprehensive reviews on the various remote sensing based ET (RS-ET) algorithms (Gowda et al., 2008; Kalma et al., 2008; Li et al., 2009) suggests that these methods have the potential to be developed as an operational tool in the planning, monitoring and decision support of water resource systems.

Norman et al. (2006) stated that evaluating uncertainties in remote sensing based models for estimation of surface fluxes is not an easy task. One of the hurdles in advancing the RS-ET technology to an operational stage is the limited number of validation studies performed for limited numbers of test scenarios and locations. ET estimates generated by the RS-ET algorithms are usually validated against ground based measurements or SVAT (soil-vegetation-atmosphere transfer) models. Errors from these observational measurements (eddy covariance, Bowen ratio,

lysimeter, soil water balance, sap flow, scintillometer) can range from 5–15% (Allen et al., 2011), and a similar magnitude of error is inherent in SVAT models. Review studies (Glenn et al., 2007; Gowda et al., 2008, Kalma et al., 2008, Li et al., 2009) have pointed out that this uncertainty in the validation dataset has plagued the performance evaluation of various RS-ET algorithms. Large weighing lysimeters are generally considered the most direct and accurate field measurement technique (Allen et al., 2011); however, most validation studies have been performed against tower observations of eddy covariance and/or Bowen ratio measurements which has an uncertainty or error bound of 20–30% (Kalma et al., 2008; Glenn et al., 2007) that is typically not random but systematically biased. Another limitation in the model validation studies is the inability to test the performances under varied agro-climatic conditions ranging from humid to arid regions with complex landscapes (Kustas et al., 2007). Norman et al. (2006) commented that most experimental sites used in validation studies reported in the literature do not contain both stressed (soil water deficits) and unstressed vegetation (limited soil water deficits) or significant differences in roughness within the scenes. The choice of the remote sensing data varying in spatial, spectral, temporal and radiometric resolutions has considerable influence on the final ET estimates (Batra et al., 2006; McCabe et al., 2006). Numerous testing scenarios remain unexplored. The validation of RS-ET algorithms under diverse testing scenarios is an important step in the continuous process of developing and improving, and making it more widely accessible.

This study employs 10 high resolution airborne images, lysimetric observations and variable moisture regimes across two cropping seasons to investigate the influence of four different z_{oh} values on the flux estimations from SEBAL. The four z_{oh} values used are as follows:

(1) $z_{oh} = z_{om}/\exp(kB^{-1})$, where $kB^{-1} = 2.3$

(2) $z_{oh}(z_1) = 0.1$ m (spatial constant)

(3) $z_{oh}(z_1) = 0.01$ m (spatial constant) and

(4) $z_{oh} = z_{om}/\exp(kB^{-1})$, where kB^{-1} parameterization is used to get spatially varying z_{oh}.

3.3 Theoretical basis

What does z_{oh} represent, and how was the value 0.1 (or derived from constant $kB^{-1} = 2.3$) assigned? To find the answer, we begin with the bulk formulation of sensible heat (H) based on the flux-gradient relation as:

$$H = \rho_a C_p \frac{T_o - T_a}{r_{ah}} \quad (3.1)$$

where ρ_a is the density of air (kg m^{-3}), C_p is the air specific heat at constant pressure (~1,004 J kg^{-1} K^{-1}), r_{ah} (s m^{-1}) is the aerodynamic resistance to heat transfer between the surface and the reference level, and T_a is the air temperature (°C). In Eq.(1), T_o (°C) is defined as the extrapolation of T_a down to an effective height within the canopy at which the vegetation component of H and latent heat (LE) fluxes arise given by d_o+z_{oh} (Chehbouni et al., 1996). From the Monin-Obukhov (M-O) similarity theory, the aerodynamic resistance r_{ah}, is defined as the resistance from height $z_{oh}+d_o$ having an aerodynamic temperature, to the height z_{ref}, given by:

$$r_{ah} = r_a + r_r = \frac{1}{ku_*}\left[ln\left(\frac{z_{ref} - d_o}{z_{om}}\right) - \psi_h\right] + \frac{1}{ku_*} ln\left(\frac{z_{om}}{z_{oh}}\right) \quad (3.2)$$

where, r_a (s m^{-1}) is the aerodynamic resistance to momentum transfer between height d_o+z_{om} (d_o is zero plane displacement height, and z_{om} (m) is roughness length for momentum transport), and z_{ref} (m) is the reference height. A distinction is required between z_{om} and z_{oh} due to the fact that heat transfer near the surface is mainly controlled by the molecular diffusion while momentum transfer is not only due to viscous shear but also due to pressure gradient (Brutsaert, 1982). Hence, following many authors (Owen and Thomson, 1963; Thom, 1972; Chebouni et al., 1996; Kustas et al., 1989), it is surmised that the aerodynamic resistance for heat transfer (r_{ah}) is greater than aerodynamic resistance for momentum transfer (r_a). Thus, the formulation of H using the definition of T_o requires an additional resistance called the excess resistance denoted by r_r in Eq. (2). This would also imply that the roughness length for heat transfer (z_{oh}) would be less than the roughness length for momentum transfer (z_{om}) (Troufleau et al., 1997; Kustas et al., 1989; Kalma and Jupp, 1990). The other terms in Eq. (2) are, von Karman's constant (k ; ~0.41), the friction velocity (u_*) and stability correction functions for heat (ψ_h) as a function of Monin-Obukhov length (L). Eq. (3.2) can be resolved and re-written in the more familiar way as:

$$r_{ah} = \frac{1}{ku_*}\left[ln\left(\frac{z_{ref} - d_o}{z_{oh}}\right) - \psi_h\right] \quad (3.3)$$

It is important to understand that the excess resistance (r_r) is attached to the aerodynamic temperature and can be rightly called as aerodynamic excess resistance. Excess resistance (r_r) formulation from Eq. (3.2) can be written as:

$$r_r = \frac{1}{ku_*} ln\left(\frac{z_{om}}{z_{oh}}\right) \tag{3.4}$$

Eq. (3.4) is classically expressed as a function of the dimensionless bulk parameter B^{-1} (inverse Stanton number) introduced by Owen and Thomson (1963) and used by Chamberlain (1968) and Thom (1972), given by:

$$r_r = \frac{B^{-1}}{u_*} \tag{3.5}$$

The parameter kB^{-1} is related to roughness height for heat z_{oh}, (Garratt and Hicks, 1973) as:

$$kB^{-1} = ln\left[\frac{z_{om}}{z_{oh}}\right] \tag{3.6}$$

It must be emphasized that the theoretical basis of kB^{-1} parameter is strictly aerodynamic; i.e., related to the aerodynamic surface temperature.

Despite the simplistic formulation of H, problems arise in the absence of direct measurements of T_o and z_{oh}. The T_s derived from the thermal sensors of various satellites was explored as a potential replacement for T_o. The lack of strong theoretical or experimental evidence linking T_s to T_o necessitated building strategies to address the inherent differences (Chehbouni et al., 1996; Troufleau et al., 1997). For partial canopies the difference between T_s and T_o was found to exceed 10°C (Chehbouni et al., 1996) leading to overestimation of H. For dense homogeneous crops, good agreement with H estimation was found implying that the differences between T_s and T_o was minimal (1–2°C) (Kustas et al., 1989). It was clear that both under sparse and full vegetation conditions, an appropriate value of kB^{-1} was required for accurate estimation of H using T_s (Stewart et al., 1994; Jia et al., 2003; Kustas et al., 2007). Replacing T_o with T_s in Eq. (3.1) requires a new definition for the excess resistance. The aerodynamic excess resistance defined by Eq.(3.4) would now have a radiometric component to relate H to radiometric surface temperature. In context to heat transfer estimation from radiometric surface temperature, kB^{-1} is now merely a fitting and largely empirical parameter no longer connected to its theoretical background (Lhomme et al., 2000). Consequently it would be more physically meaningful to define the excess resistance parameter kB^{-1} as radiometric kB^{-1} (Colaizzi et al., 2004). Finally, kB^{-1} should be considered as a correction factor when radiometric temperature is used.

The scalar roughness length z_{oh} represents the parameterization of heat transport and is described by the dimensionless parameter kB^{-1} and these could be again related to the excess resistance as formulated in Eqs. (3.4), (3.5) and (3.6). Several attempts were made in the last century to develop better understanding of the kB^{-1} parameter (Sverdrup, 1937; Verhoef et al., 1996), followed by a recent revived interest by the remote sensing surface energy modeling community (Su et al., 2001; Gokmen et al., 2012). Obtaining an efficient parameterization for kB^{-1} applicable over a wide range of land cover has been a challenging task. Researchers have used analytical and experimental approaches to develop relationship based on environmental variables, vegetation structural characteristics, multi layer approach, and simulation results (Brutsaert and Sugita, 1996; Lhomme et al., 2000; Massman, 1999; Blumel, 1999). Numerous studies have shown that the value of kB^{-1} can typically range from 1 to 12, depending on the dominant surface cover (Su et al., 2001; Kustas et al., 1989; Stewart et al., 1994; Beljaars and Holtslag, 1991; Troufleau et al., 1997). Finally, with all the complexity and lack of clarity in the kB^{-1} formulation it remains an unavoidable parameter both because of its physical linkage to the bulk transfer formulation and also as a correction factor when using T_s. Hence, an appropriate value of spatially variable kB^{-1} is required for accurate estimation of H using T_s, (Kustas et al., 1989; Stewart et al., 1994; Su et al., 2001; Kustas and Anderson, 2009).

SEBAL adopts a conservative value of 2.3 for kB^{-1}, which was derived for homogenous cropped surface, from Garrat and Hicks (1973). This value was found to be too low for most land covers (Kustas et al., 1989; Stewart et al., 1994; Verhoef et al., 1997; Su et al., 2001; Lhomme et al., 2000), and in general kB^{-1} values ranging from 4 to 8 were found more suitable. In the latter version, z_{oh} has been redefined and renamed as z_1, and its values were fixed at 0.1 m suggesting that this change would evade the problems originating from the definition of z_{oh} (Bastiaanssen et al., 2005; Bastiaanssen et al., 2002). METRIC (Mapping evapotranspiration at high resolution with internalized calibration) a close variant of SEBAL, also replaces z_{oh} with a height z_1 (0.1). Allen et al. (2007) suggest, "*the aerodynamic resistance formulation support the use of a temperature gradient defined between two heights that are both above the surface; allowing one to estimate* r_{ah} *without having to estimate a second aerodynamic roughness for sensible heat transfer* z_{oh}*, since height* z_1 *is defined to be at an elevation above* z_{oh}". They also added that this is an advantage because z_{oh} can be difficult to estimate for sparse vegetation. It must be understood here, that z_1 is replacing z_{oh} in Eq.(3) and simultaneously z_1 is being given a new

definition. Also, it should be noted that a constant z_1 value of 0.1 could be frequently larger than the corresponding z_{om} value, tending r_r to be negative in Eq.(3.2). However, this is not a physically possible situation and hence the height z_1 has no physical significance and remains a largely empirical parameter. The roughness length for heat transfer, z_{oh} is different and should not be confused with the empirical height z_1. However, since the literature on SEBAL has used z_{oh} and z_1 interchangeably (Long and Singh 2012a; Gieske and Meijninger, 2005), this precedent will be followed in the rest of the paper, although it is misleading if the theoretical background is considered .

3.4 Materials and Methods

The Bushland Evapotranspiration and Agricultural Remote Sensing Experiment 2007 and 2008 (BEAREX07 and BEAREX08) provided a unique opportunity to evaluate the turbulent exchange of mass and energy over agricultural landscape. SEBAL was executed for 10 high resolution airborne images acquired during the BEAREX07 and BEAREX08 field campaign and validated against large precision weighing lysimeters. Validation points consisted of two irrigated and two dryland fields located in the semi-arid Texas High Plains known for significant advection and nighttime ET (Tolk et al., 2006). Detailed information on the experimental set-up, algorithm description and evaluation process follows.

3.4.1 Study Area and instrumentations

The BEAREX07 and BEAREX08 field campaigns were conducted at the USDA-ARS Conservation and Production Research Laboratory (CPRL) during the 2007 and 2008 summer cropping season. The USDA-ARS Conservation and Production Research Laboratory is located in Bushland, TX (Fig. 1) with geographic coordinates of 35° 11' N, 102° 06' W and elevation of 1170 m above mean sea level. The area is within the Texas High Plains, where semi-arid climatic conditions and strong advective currents prevail during the summer cropping season. The CPRL has four large weighing lysimeters (3 m long x 3 m wide x 2.4 m deep), each located in the middle of 4.3 ha fields, arranged in a block pattern. The two lysimeter fields located on the east (NE and SE) were managed under irrigated conditions, and the other two lysimeters on the west (NW and SW) were under dryland management. Each lysimeter field was equipped with an automated weather station that provided measurements for net radiation (R_n), T_s, soil heat flux (G_o), T_a, relative humidity, and wind speed (refer to Chávez et al., 2009 for details of field

instrumentation). In addition, a grass reference ET weather station field (0.31 ha), which is a part of the Texas High Plains ET Network, was located on the eastern edge of the irrigated lysimeter fields (Marek et al., 2009; Fig. 3.1). In 2007 (BEAREX07), the NE field was planted with forage sorghum (on May 30), the SE field was planted with corn (on May 17) both being grown for silage. The NW field was planted with grain sorghum in rows (on June 6), and the SW field was planted with grain sorghum in clumps (on June 6). In 2008 (BEAREX08), the NE and SE fields were planted to cotton on May 21, and the NW and SW dryland lysimeters fields were planted to cotton on June 5. Cotton (variety Delta Pine 117) was seeded at 15.8 plants/m^2 on raised beds spaced at 0.76 m. The warm-season tall crop , corn, and sorghum during BEAREX07 and warm-season broadleaf short crop, cotton during BEAREX08, represented a diverse set of agricultural surface roughness with varied land surface energy balance systems. Regular measurements on the crop physiological parameters, leaf area index (LAI), crop height, and soil moisture content were recorded throughout the duration of the BEAREX campaign.

3.4.2 Airborne Remote Sensing Data

Flying expeditions were conducted during the field campaign to collect remotely sensed imagery using the Utah State University (USU) airborne digital multispectral system. The system acquired high resolution imagery in the green (0.545–0.555 μm), red (0.665–0.675 μm), near-infrared (0.790–0.810 μm), and thermal infrared (8–12 μm) portions of the electromagnetic spectrum. Image information such as spatial resolution, acquisition date, and weather parameters at the time of acquisition is tabulated and provided in Table 1. Five images per year were acquired during early to mid-cropping season and used in this study to represent the varying canopy cover (or soil cover) conditions. Description of the post processing including geometric corrections, radiometric calibration and atmospheric correction can be found in Neale et al. (2012). SEBAL was coded using Python programming language and executed in Arc-GIS 10.0. The five images analyzed in each year provided conditions from a near bare soil situation to near complete canopy cover. Crops in the irrigated field attained a near complete canopy by the last image acquisition date, whereas the dryland fields exhibited higher soil cover. Lysimeter fields were considered homogeneous, and the center of the field with the lysimeter and instrument cluster was used to validate all estimates. A 12 x 12 (1 m) pixel grid covering the lysimeter

location was marked (in the image) in all four lysimeter fields to extract average values of estimated ET, R_n, G_o, T_s and aerodynamic parameters.

3.4.3 Evaluation Statistics

Validation studies in the past have used numerous performance evaluation statistics, however, there is some inconsistency and lack of clarity in usage of these statistics. For example, some studies report only the RMSE (root mean square error) values (Singh et al., 2008; Kustas and Anderson, 2009), others report only the MBE (mean bias error) values (Tasumi et al., 2005), and still others do not report the relative error (Gonzalez-Dugo et al., 2009). Apart from the standard and regression statistics (mean, slope, intercept and coefficient of determination), we recommend using three error index statistics, MBE, MAE (mean absolute error), and RMSE, as well as a dimensionless performance statistic, NSE (Nash-Sutcliffe efficiency; Moriasi et al., 2007), for a detailed model evaluation. In MBE, the individual differences between the modeled and corresponding observed values are averaged while retaining the sign, with negative and positive sign indicating average under- or overestimation, respectively. MAE is a linear score whereby individual absolute differences are weighted equally in the average. RMSE is a quadratic scoring rule where the squared values of the differences are averaged over the sample. RMSE gives a relatively greater weight to larger errors, severely penalizing large deviations, and hence is most useful when large errors are particularly undesirable. Large differences between RMSE and MAE indicate high variance in the individual errors of the dataset. All three error indices provide errors in the constituent's unit and can also be expressed as relative error with respect to the mean. However, all three error indices serve unique purpose and should be used together to diagnose the performance of model. From the definition of these error indices, it follows that MBE≤MAE≤RMSE (Willmott and Matsuura, 2005). Willmott and Matsuura (2005), pointed out that RMSE is an inappropriate indicator of average error and that MAE is the most natural and unambiguous measure of average error magnitude, they recommended MAE for all dimensioned evaluations and inter-comparisons of average model performance. Reiterating, in this study MBE was used as the indicator of under/overestimation error, MAE was used as the primary indicator for average error and RMSE was reported as a conventional measure of error, and MAPD (mean absolute percent difference) was used as a relative error indicator expressed as percentage deviation. Nash-Sutcliffe efficiency (NSE) is a dimensionless model evaluation

statistics and indicates how well the plot of observed versus model estimated data fits the 1:1 line. NSE ranges between $-\infty$ and 1.0 (1 inclusive), with NSE=1 being the optimal value. Values between 0.0 and 1.0 are generally viewed as acceptable levels of performance, whereas values <0.0 indicates unacceptable model performance (Moriasi et al., 2007). The coefficient of determination (R^2) describes the proportion of the variance in measured data explained by the model and ranges from 0 to 1 with the greater values indicating less error variance. Although R^2 has been widely used for model evaluation, it cannot be used to reach a conclusion on the performance of model; NSE should be used instead. Reporting these statistics would not only help in better interpretation of the results but also help in future comparative/review studies. Formulations of performance statistics used in this study are provided in the footnote in Table 2.

Four sets of straight line regression fits would be derived from the four model runs, each with different z_{oh} values. A two-sided t-test was formulated to test appropriate null hypotheses for comparing the slopes and intercepts (of two straight lines) derived from the regression fits. We tested for the coincidence of two straight line regression fits. Two straight lines are coincident if their slopes and their intercepts are equal. Statistical significance of the two straight lines was tested using the null hypothesis of equal slope and equal intercept. If both null hypotheses are rejected, we would accept the alternative hypothesis. Coincidence would indicate failure to detect differences between model formulations. The statistical method used is known as comparing two straight lines using separate regression fits and is adapted from Kleinbaum (1988).

3.4.4 SEBAL

SEBAL utilizes the widely applied residual approach of surface energy balance to estimate ET at different temporal and spatial scales. The energy coming from the sun and atmosphere in the form of short- and long-wave radiation is transformed and used for (a) heating the soil (G_o into the ground), (b) heating the surface environment (sensible heat flux to the atmosphere), and (c) transforming water into vapor (LE from the crop/soil surfaces). All the energy involved in the soil-vegetation-atmosphere interface can be given as the Energy Balance (EB) equation:

$$R\_n = G\_o + H + LE \quad (3.7)$$

where all units expressed in W m^{-2}. Latent heat flux can be expressed as hourly ET (mm) (by dividing LE by the latent heat of vaporization and the density of water). Net radiation (R_n) expressed as an electromagnetic balance of all incoming and outgoing fluxes, which constitutes a key driver for heating the atmosphere and the ground, is given by:

$$R_n = S\downarrow - S\uparrow + L\downarrow - L\uparrow = (1 - \alpha_s)S\downarrow + \varepsilon_a\, \sigma\, T_a^4 - \varepsilon_s\, \sigma\, T_s^4 \quad (3.8)$$

In Eq. (3.8), S denotes short-wave radiation (0.3–3 μm); L is long-wave radiation (3–100 μm). The arrows show the direction of the flux entering (↓) or leaving (↑) the system. Each term in Eq. (8) either can be determined directly from models or obtained from the ground weather station. The incoming short-wave radiation (S↓) and the T_a are measured at weather stations. T_s is obtained from the inversion of Plank's law in 10 to 12 μm band width. Other terms in Eq. (8) are broadband surface albedo (α_s), apparent emissivity of atmosphere (ε_a), surface emissivity (ε_s), and the Stefan-Bolzmann constant (σ = 5.67 E-08 W m^{-2} K^{-4}).

Broadband planetary albedo (α_p) was calculated as the sum of the individual in-band planetary albedos with different weighing factors. The weighing factor for each band is proportional to the band-pass solar exoatmospheric irradiance ($ESUN_\lambda$) which is an average solar irradiance weighted by the corresponding spectral band response function. The weight for each band was calculated and the equation for broadband planetary albedo (α_p) was derived as:

$$\alpha_p = 0.303\, green + 0.400\, red + 0.296\, NIR \quad (3.9)$$

where green, red, and NIR are the reflectance of the respective bands. Because low flying airborne images were used with primary atmospheric corrections, the need for converting planetary albedo into surface albedo was evaluated by the planetary broadband albedo (α_p) and considered equivalent to the surface broadband albedo (α_s).

The apparent emissivity of the atmosphere was estimated from equations based on vapor pressure and air temperature at the standard meteorological stations. For clear skies, the Brutsaert (1975) formulation was used as:

$$\varepsilon_a = 0.892 \left(\frac{e_a}{T_a}\right)^{1/7} \quad (3.10)$$

where ea is vapor pressure near the surface (actual vapor pressure) in kPa and Ta is in K. Actual vapor pressure (ea) can be calculated from relative humidity and air temperature at reference level as:

$$e_a = \frac{RH}{100\ e_s} \tag{3.11}$$

where e_a is in kPa and e_s is the saturation vapor pressure in kPa given by:

$$e_s = 0.6108\ exp\left(\frac{17.27\ \times T_a}{T_a + \ 237.3}\right) \tag{3.12}$$

T_a is the air temperature in °C.

The surface emissivity (ε_s) was calculated from NDVI (Normalized Difference Vegetation Index) as given by Van de Griend and Owe (1993):

$$\varepsilon_s = 1.009 + 0.047 \ln\ (NDVI) \tag{3.13}$$

The above relationship is valid only for NDVI values over 0.16. For NDVI values below 0.16 (usually bare soils), emissivity was assumed to be 0.92 and for NDVI values below –0.1 (usually water), it was assumed to be 1.0.

Sensible heat flux (H) was calculated from Eqs. (3.1) and (3.3) by simultaneously solving for the stability functions through an iterative process. The friction velocity (u_*) in Eq. (3.2) was defined by:

$$u_* = \frac{ku_b}{ln\left[\frac{z_b - d_o}{z_{om}}\right] - \psi_m} \tag{3.14}$$

where the zero plane displacement height (d_o) was determined from the empirical relationship given by Brutsaert (1982) based on the crop height (h in m):

$$d_o = \frac{2}{3}\ h \tag{3.15}$$

The following exponential relationship was derived using NDVI and crop height (h) information (Bastiaanssen, 1995) and used to estimate z_{om}.

$$z_{om} = \exp(C_1 + C_2\ NDVI) \tag{3.16}$$

where C_1 and C_2 are regression constants derived separately for each image from a plot of $ln(z_{om})$ vs. NDVI for pixels representing varied vegetation heights and extremes of NDVI. For generating the relationship, z_{om} was calculated from the height of vegetation (z_{om}=0.13 h;

Brutsaert, 1982) recorded for the different crops during the campaigns. The blending height, z_b, was taken as 100 m and the wind speed at blending height (u_b) was given by the relation:

$$u_b = u_{ref}\left[\frac{\ln(z_b - d_o) - \ln(z_{om})}{\ln(z_{ref} - d_o) - \ln(z_{om})}\right] \quad (3.17)$$

The stability correction functions for heat and momentum transfer (ψh and ψm) were derived as a function of Monin-Obukhov length (L) using equations developed by Paulson (1970). Soil heat flux was computed using the relationship developed by Bastiaanssen et al. (1998), given as:

$$\frac{G_o}{R_n} = \frac{(T_s - 273.15)}{100\alpha_s}(c_1\alpha_s + c_2\alpha_s^2)(1 - 0.98NDVI^4) \quad (3.18)$$

where c_1 and c_2 are locally calibrated coefficients with values of 0.12 and 0.42, respectively.

3.4.5 Hot and Wet pixel selection

A distinctive approach in SEBAL is the calculation of a single temperature gradient dT function (defined as the T_o - T_a) for the study region using two points denoting the hydrological contrast. The two pixels representing the hydrological contrast, termed Hot (dry) and Cold (wet) pixels, were first introduced in SEBAL and adopted into at least five other energy balance remote sensing algorithms. SEBAL uses the extreme pixels of the image (dry and wet pixel), to develop a relationship between T_s and the difference between T_o and T_a given in the form of:

$$T_o - T_a = dT = a + bT_s \quad (3.19)$$

where 'a' and 'b' are the regression constants. In later SEBAL version (Bastiaanssen et al., 2005; Bastiaanssen et al., 2002), dT was redefined as the vertical air temperature difference between heights z_1 and z_2, [$dT = T(z_1)-T(z_2)$], where z_1 (z_{oh}) is 0.1 m and z_2 (z_{ref}) is 2 m, was fixed. The basic assumption behind this relationship is that T_o - T_a was linearly related to T_s. A second assumption of the existence of hydrological contrast (dry and wet area) in the study region must be implemented. For the wet pixel, dT was considered zero while for the dry pixel, dT was iteratively determined by adjusting for the stability functions. Physically, the wet pixel should be the surface transpiring at its potential limit (LE = LE_{max} and H = 0), and therefore, dT=0. The ideal location of a wet pixel is a surface with full canopy vegetation growing under no soil water limitation. A dry pixel physically represents a surface with dry conditions where ET equals zero (LE= 0 or H = H_{max}= R_n – G_o). Ideally, bare soil with no residual moisture for evaporation should

approximate the dry pixel characterization. Selection of these two extreme pixels in the image causes a bottleneck in the implementation of SEBAL, because it involves subjective decision of the analyst. Generally, the wet pixel is selected on the criteria of low temperature and high NDVI, whereas the dry pixel is characterized by high temperature, low NDVI, and low albedo. Scatter plots of NDVI-T_s and albedo-T_s along with histograms have been used to identify the group of pixels fulfilling the extreme pixel criteria (Timmermans et al., 2007); however, these methods do not help in secluding a single set of pixels, which again largely depends on the analyst's decision. Furthermore, different sets of pixels fulfilling the dry and wet pixel criteria may exhibit entirely different surface energy balance and roughness properties and lead to variations in the 'a' and 'b' coefficients. In the present study, we harnessed the capability of the GIS environment wherein classification, histogram generation, and overlaying of T_s, NDVI, and α_s maps can be done easily leading to identification of a group of pixels that fulfilled the criteria. The identification of the wet pixel in the agricultural landscape was relatively easier, but the identification of hot pixel was not easy because of the presence of multiple pixels that satisfied the selection criteria.

3.4.6 kB^{-1} parameterization

A physically based model for excess resistance to heat transfer parameter (kB^{-1}), developed by Su et al. (2001), was incorporated into SEBAL. This model is based on Massman (1999) and consists of terms representing the contribution of the soil alone, the canopy and the canopy-soil interaction to resistance to heat transfer. This model has been incorporated into the SEBS (Surface Energy Balance System; Su, 2002) algorithm and further validated through several studies (Gokmen et al., 2012; Jia et al., 2003). The parameterized excess resistance to heat transfer formulation is given as:

$$kB^{-1} = \frac{kC_d}{4C_t \frac{u_*}{u(h)}\left(1 - e^{-\frac{n_{ec}}{2}}\right)} f_c^2 + \frac{k.\frac{u_*}{u(h)}.\frac{z_{om}}{h}}{C_t^*} f_c^2 f_s^2 + kB_s^{-1} f_s^2 \qquad (3.20)$$

3.5 Results and discussion

All the results presented in this section pertain to SEBAL model executions with four different z_{oh} values. Model estimated H was compared against H derived as the residual of the observed components of the energy balance Eq. (3.7). The SEBAL model evaluations with

different z_{oh} values are expressed in the article as kB^{-1}=2.3, $z_{oh}(z_1)$ = 0.1 m, $z_{oh}(z_1)$ = 0.01 m and use of kB^{-1} model.

3.5.1 Net radiation, soil heat flux, and surface temperature

Performance statistics for T_s, R_n, and G_o for the complete data set (n = 40) are provided in Table 3.2. Comparison of T_s retrieved from the airborne thermal images was validated against the measured data, showed good agreement with an MAE of 1.1°C representing 3.18% (MAPD) relative error. The performance of the airborne retrieved temperature was within the typical error of 1 to 1.5°C reported for satellite and airborne sensors (Sobrino et al., 2008; Sobrino et al., 2009). Net radiation was estimated with an average error of 23.55 W m^{-2} (MAE) and RMSE of 29.55 W m^{-2}. Evaluation statistics revealed good performance of the R_n model with a small relative error of 4% (MAPD), which was better than the reported range of 5 to 10% (~ 30–60 W m^{-2}) (Timmermans et al., 2007; Choi et al., 2009; Singh et al., 2008) and most instrument measurement uncertainty (Field et al., 1992). The performance of R_n model in studies involving aircraft data has been good (Jacob et al., 2002; Kustas et al., 1994) and this could be attributed to the relatively accurate albedo input derived from the airborne imageries. Soil heat flux was smallest amongst the energy balance components in the present agricultural location, where the observed mean of G_o was 36.2 W m^{-2} which was significantly smaller than the observed means of R_n (574.6 W m^{-2}), H (170.1 W m^{-2}) and LE (368.3 W m^{-2}). Past studies have reported a large error range of 10–40 W m^{-2} (15–30%) (Jacob et al., 2002; Long and Singh, 2012a; Singh et al., 2008) in the estimation of G_o derived from the present parameterization involving fraction of R_n and a vegetative index formulation. Several reasons could explain the poor performance of the G_o model, including inadequate calibration of the empirical models and the model's incapability in capturing the large spatial variability. G_o was estimated with an overall error of 13.2 W m^{-2} (MAD), RMSE of 16.8 W m^{-2} and relative error of 36.4 % (MAPD). NSE value of 0.21 indicated average performance of the soil heat flux model. However, we articulate that the overall underperformance of G_o is not expected to influence the ET estimates because of the small magnitude of error.

3.5.2 Statistical comparison of the four approaches

The four different z_{oh} values yielded different ET estimates (see Fig. 3.2, Table 3.4). Inspection of Fig. 3.2 indicates that out of the four linear regression fits, three (kB^{-1} = 2.3, z_{oh} =

0.1 m, and z_{oh} = 0.01 m) yielded similar trends, whereas the fourth regression (the variable kB^{-1} model) was distinctly different. Results of statistical tests, intercomparing each model run are provided in Table 3.3. Intercomparison of the three model runs, kB^{-1}=2.3, z_{oh} (z_1) =0.1 m, and z_{oh} (z_1)=0.01 m, reveals that the differences in the slope and intercept were not statistically significant; in other words statistical evidence was insufficient to reject the null hypothesis of equal slope and equal intercept. Thus, the three regression fits (kB^{-1} = 2.3, z_{oh} = 0.1 m, and z_{oh} = 0.01 m) were considered coincident, implying that these models did not produce significantly different estimates. Statistical test, comparing the fourth approach (variable kB^{-1} model) with the other models, rejected the null hypothesis of a common slope and common intercept, suggesting that this approach yielded results that were significantly different from the other three approaches. By conventional criteria, the differences were statistically significant. To summarize with, a spatially constant z_{oh} (z_1) of 0.1 m or 0.01 m or a spatially constant kB^{-1} of 2.3, all yielded similar ET estimates, whereas a spatially variable z_{oh} derived from the kB^{-1} model generated ET estimates that were significantly different from the other three approaches while improving the overall model performance in estimating ET.

3.5.3 SEBAL performance evaluation

The performance statistics of the four approaches for the complete data set (irrigated and dryland combined) for instantaneous ET estimates is provided in Table 3.4. A relative error of 26.8% (MAPD) was observed for the model run with kB^{-1} = 2.3, followed by 21.4% and 21.9% for z_{oh}(z_1)=0.1 m and z_{oh}(z_1) =0.01 m, respectively, whereas the parameterized kB^{-1} model registered the smallest error of 16.5%. The negative value of y-intercept for kB^{-1} = 2.3, z_{oh}=0.1 m, and z_{oh}=0.01 m, in the regression statistics indicated the presence of lag between the model prediction and measured data; the negative MBE values suggested underestimation error. The difference between the MAE and RMSE values for the kB^{-1} model was smallest compared with the other three approaches, indicating minimal variance in the individual errors. The performance of the kB^{-1} model was the best of the four approaches, with no significant under/overestimation bias and relatively small error variance. Although the approach of kB^{-1} = 2.3 showed similar error trend, compared with constant z_{oh} = 0.1 m or z_{oh} = 0.01 m, its performance was much lower and more severely biased. Interestingly, the two constant z_{oh} (z_1) approach produced similar results, and their performances were identical in the evaluation statistics. A comparison of the

present results with previous studies cannot be justified, primarily for two reasons. First, most previous studies are validated against EC/BR tower data, which has possible inherent errors in LE, in particular, ranging from 20–30% (Kalma et al. 2008; Twine et al., 2000; Allen et al., 2011). Second, most studies lack replication in terms of number of images utilized, surface covers considered, and testing under variable soil water conditions. The evaluation statistics reported herein for instantaneous ET from the four approaches should be seen as a standalone results of SEBAL performance generated from specific set of diverse and stringent experimental conditions adopted in this study. However, the results obtained, corroborate the 15–30% range of error reported across techniques, measurement, and spatial-temporal aggregations (Gowda et al., 2008; Kalma et al., 2008; Glenn et al., 2007) applied in RS-ET algorithms.

The performance statistics for H and LE for the complete dataset form the four approaches is provided in Table 3.5. A large overestimation of H led to underestimation of LE for the first three approaches with spatially constant values for z_{oh}, or kB^{-1}=2.3, whereas model run with the variable kB^{-1} parameterization did not show any significant bias. The constant z_{oh} (z_1) approach (of 0.1 m and 0.01 m) produced identical results and performed equally well in predicting H fluxes, compared with the kB^{-1} model except for the large biases. An interesting observation is the close comparison of relative errors in H estimates from $z_{oh}(z_1)$ = 0.1 m and the kB^{-1} model, yet when it came to LE estimation, the performance of the variable kB^{-1} model far exceeded the constant $z_{oh}(z_1)$ approaches.

The observed magnitude of LE (mean: 356 W m^{-2}) was found to be considerably greater than H (mean: 182 W m^{-2}) for the agricultural landscape considered in this study. The partitioning of the available energy between H and LE provides a crucial understanding of the existing hydrological regime. In the Texas High Plains, energy is usually not the limiting factor; instead, water availability becomes a limiting factor for ET. The large observed LE value, in the present case gives a picture that there is ample availability of soil water to meet ET demand; however, this is not completely or universally true. Separating the dryland and irrigated observations indicates that the mean value of LE from the irrigated fields was 437 W m^{-2}, which was almost 3.5 times greater than the mean value of corresponding H (126 W m^{-2}); in contrast, the mean value of LE from the dryland fields was 284 W m^{-2}, which was similar to the corresponding mean value of H (232 W m^{-2}). The existing hydrological testing regime has clearly taken into consideration the two contrasting cases often encountered in arid and semi-arid

agricultural regions: a water stressed condition and a "near" potential growth condition. Hence, the model performance should also be evaluated from the three prospective viewpoints, namely: (i) achievable accuracy under the water stressed condition (dryland), (ii) achievable accuracy under the non-water stressed condition (irrigated) and (iii) achievable accuracy derived from the combined dataset. The MAE for LE ranged from 104 to 62 W m^{-2} for all four approaches, which in terms of relative error (MAPD) was consistent with the ET estimate errors given in Table 4. MAPD for LE ranged from 16.9 – 28.2%, but for H it ranged from 41.5 – 59.5% across the four approaches. Long and Singh (2012a) reported large MAPD of 70.6% for H (observed mean 86.8 W m^{-2}) and yet could estimate LE (observed mean 421.0 W m^{-2}) with a 8.9% error, using 3 Landsat TM/ETM imagery scenes and a modified SEBAL model validated with EC data. In another study (Yang et al., 2010) involving EC observation and MODIS imagery, over irrigated wheat and maize in the North China Plain had estimated LE with an error of 8–11% (observed mean range: 353–478 W m^{-2}), whereas errors in estimated H ranged from 37–125% (observed mean range: 28–83 W m^{-2}). In contrast, a more diverse hydrological regime was considered by Timmerman et al. (2007) that reported a MAPD of 26% for H (observed mean 148 W m^{-2}) and 23% for LE (observed mean 262 W m^{-2}) using aircraft imagery data and SEBAL model applied over two large scale campaigns covering sub-humid grassland and semi-arid rangeland. Clearly, in these datasets with significantly greater transpiration (3 – 4 times) the value of observed LE as compared to H denote a hydrological regime where large errors in H may not influence the accuracy of LE. Furthermore, when the magnitude of H was small, LE seemed to be influenced by the available energy (R_n-G_o). For this reason, datasets with significantly greater LE compared with H might not be desirable for testing RS-ET algorithms. RS-ET algorithms relying on that residual energy balance concept (LE=R_n-G_o-H) differ from each other based on the approach at computing H, so evaluating these algorithms for their capacity to estimate H accurately is important.

3.5.4 Performance evaluation for irrigated and dryland fields separately

The performance statistics for H and LE were calculated separately for dryland and irrigated fields and presented in Table 3.6. The tabulated results in conjunction with the regression fits of observed vs. modeled values for H and LE (Fig. 3.3 and 3.4), derived

separately for the irrigated and dryland fields, reveal several interesting features of the model, discussed point-wise herewith.

Sensible heat (H) flux estimates for two irrigated lysimeter fields representing high fractional vegetation cover and greater ET, produced a relative error (MAPD) from 34–62%, indicating a large sensitivity involved across four approaches used in estimating ET or LE. Use of $z_{oh}(z_1)$=0.1 m gave the best statistical performance (MAPD = 34.8%), closely followed with $z_{oh}(z_1)$=0.01 m (Fig 3.3a). The constant kB^{-1} = 2.3 approach had a trend similar to the z_{oh} = 0.1 m approach (Fig 3.3a), but it was strongly biased with large overestimation error and an MAPD of 62.8%. The poor performance was observed with the constant kB^{-1}=2.3 proving that this widely used kB^{-1} value was too low for most surfaces (Kustas et al., 1989; Stewart et al., 1994; Verhoef et al., 1997; Su et al., 2001; Lhomme et al., 2000). It must be noted here, that even though the irrigated fields are considered representative of greater canopy cover and larger ET rates, yet the surface condition during the initial days of image acquisition would be dominated by isolated seedlings forming a sparsely vegetated surface. Therefore, the large overestimation with kB^{-1} of 2.3 was partially due to the inappropriate kB^{-1} value during the initial days and partially due to the insufficient (smaller) kB^{-1} value during the growing period. The performance of the kB^{-1} model in the estimation of H for the irrigated fields (Table 3.6 and Fig 3.3a) was intermediate. Examining Fig 3.3a, we can see that the kB^{-1} approach produced differential treatment for the high and low H values. It was interesting to see that the empirical constant value of z_{oh} (z_1)=0.1 m and z_{oh} (z_1)=0.01 m, not only outperformed the other two approaches, but also produced similar performances. These results necessitate speculation about why these empirical numbers worked and why a value with as diverse a magnitude as 0.1 m and 0.01 m produced similar results. Before explaining, we need to draw attention to two points concerning a surface predominantly vegetated, growing and transpiring at (presumed) potential rate: (i) dT is always smaller compared with a surface that is sparsely vegetated and/or water stressed; which is obvious from the current study and has been shown in other research (Wang et al., 2009; Crow and Kustas, 2005) (ii) the difference between T_o and T_s is small (1–2°C) compared with the more sparsely vegetated and/or water stressed surfaces (often exceeding 10°C) (Chehbouni et al.,1996, Lhomme et al., 2000). Accordingly, it follows that the errors attributed to dT would be small, because dT is not only small in magnitude, but also measured accurately (errors due the difference between T_o and T_s is small). The constant z_1 (z_{oh}) modifies the dT (T_{z1}-T_{zref}) and

proportionally modifies the r_{ah}, so the value of z_1 = 0.1 m and z_1 = 0.01 m produced similar H estimates. This was confirmed when we ran the model with z_1=0.001 m and found that all the three (z_1 = 0.1 m, z_1 = 0.01 m, and z_1 = 0.001m) values produced similar H estimates (results with z_1=0.001 m are not shown here). Therefore, H was not sensitive to the empirical z_1 (z_{oh}) value. The empirical height z_1 (z_{oh}) does not have any property to correct for the inaccuracies between T_o and T_s which is supported by the fact that a constant overestimation error was always present. The height z_1 does not have physical significance and should not be related or considered equivalent to roughness length for heat transport, z_{oh}.

Estimates of H fluxes from two dryland lysimeter fields produced a relative error (MAPD) from 37–57% (Table 3.6), indicating the large sensitivity involved across the four approaches as in case of irrigated lysimeter fields. All four approaches generated negative NSE and very low R^2 values, indicating poor performances in predicting dryland H. SEBAL performance over dryland fields, representing a sparsely vegetated surface undergoing frequent water stress and small ET, was markedly less compared with the irrigated fields. Among the four approaches, the kB^{-1} model registered an insignificant underestimation error of 14 W m^{-2}, whereas others produced large overestimation errors ranging from 80– 116 W m^{-2}. Fig. 3.4a shows that the three approaches (kB^{-1} = 2.3, z_{oh} = 0.1 m, and z_{oh} = 0.01 m) had similar trends and identical performance, while only the kB^{-1} model generated distinct results. The performance of the kB^{-1} model in predicting dryland H was notably superior, as evidenced by the significantly smaller error indices compared with the other three approaches (Table 3.6). Although the regression statistics (R^2) and the performance index (NSE) indicate poor performance, the magnitude of the errors were comparable to the irrigated fields suggesting the model's predictive capability under dryland conditions. The gross overestimation, high relative error, and large RMSE in the H estimates from SEBAL were comparable with several studies in the literature (Long and Singh, 2012a; Choi et al., 2009; French et al., 2005; Jacob et al., 2002). The drastic and significant improvement in the dryland H estimates from the kB^{-1} model compared with other three approaches clearly indicated that the majority of the errors in the H estimate was caused by the differences between T_o and T_s. As follows from the discussion of irrigated H estimates, the converse is true in the case of dryland H estimates, where the role of dT becomes prominent and the inaccuracies associated with dT tended to be larger, resulting in less accuracy in predicting H fluxes. Errors in estimated H fluxes over sparsely vegetated surfaces when using

single source resistance model were attributed to the inappropriate correction applied in terms of kB^{-1} parameter to account for the large differences between T_o and T_s. (Kalma and Jupp, 1990; Kustas et al., 1989, Verhoef et al., 1997, Stewart et al., 1994).

The underestimation error in the LE estimates for the irrigated fields has its origin traced back to the overestimation errors of corresponding H values across the four approaches (Table 3.6 and Fig 3.3b). The error magnitudes (MBE, MAE, and RMSE) for H and LE were similar, yet the relative error (MAPD) for LE was small. The LE estimate from the $kB^{-1} = 2.3$ approach on the irrigated fields produced the highest RMSE of 88 W m^{-2} and a large MBE value of -63.7 W m^{-2}, yet the relative error was 17% (MAPD). The other three approaches produced identical results with excellent performance (11% MAPD). The magnitude of LE was significantly greater (3.5 times) compared with the H magnitude for the irrigated fields, which led to the small relative error of LE; in other words, H had a more limited role in the accuracy of LE. This is substantiated by the fact that the kB^{-1} model performance was noticeably inferior than that with $z_{oh} = 0.1$ m (or $z_{oh} = 0.01$ m) in the estimation of H, yet when it came to corresponding LE accuracy, the kB^{-1} model performed equally well, substantiating the limited role of H in LE estimates for the irrigated lysimeter fields with more complete canopy cover surfaces. Subsequently, the accuracy of LE was highly dependent on the accuracy of estimated available energy (R_n-G_o). The combined overestimation of H with the underestimation of available energy (R_n-G_o) improved the LE value; thus, in Fig. 3.3b we see the regression lines moving closer to the 1:1 line. Kalma and Jupp (1990) pointed out that LE estimates were not very sensitive to H estimate errors in studies where one-layer resistance models were applied to well-watered field crops.

The large overestimation errors from dryland H translated into large underestimation error in LE estimates for the three approaches ($kB^{-1} = 2.3$ and $z_{oh} = 0.1$ m, $z_{oh} = 0.01$ m), whereas the kB^{-1} model remained unbiased (Table 3.6 and Fig 3.5b). The performance of these three approaches ($kB^{-1} = 2.3$ and $z_{oh} = 0.1$ m, $z_{oh} = 0.01$m) in predicting dryland LE and subsequently ET was poor with negative NSE, large RMSE, and an MAPD ranging from 38–44%. The kB^{-1} model performance was remarkably superior in the estimation of dryland LE, with no significant bias, positive NSE, and an MAPD of 25%. The importance of a variable kB^{-1} (from the kB^{-1} Model) was established in the case of dryland sparse vegetated surfaces, where the difference between T_o and T_s is amplified and the results of correction applied gets eminent. As in this

study, SEBAL applied with kB^{-1} = 2.3 or z_{oh} (z_1) = 0.1 m has shown large discrepancy in predicting LE or ET from sparse vegetated surfaces with errors reaching up to 50% (Elhaddad and Garcia, 2011; Timmermans et al., 2007; Gao and Long, 2008).

The performance statistics for instantaneous ET evaluated separately for dryland and irrigated fields and are provided in Table 3.7. Because ET is derived/converted from LE, its performance statistics are identical to the LE statistics.

The performance statistics of H in Table 3.5 and Table 3.6, clearly shows that H was being overestimated for the three approaches (kB^{-1} = 2.3 and z_{oh} = 0.1 m, z_{oh} = 0.01 m), but only the kB^{-1} model was unbiased. This observation agreed with the many studies reporting overestimation of H in SEBAL (French et al., 2005; Long and Singh 2012a, Choi et al., 2009) and in general from those single source resistance models, which provide inadequate consideration for excess resistance (Stewart et al., 1994). The direct implication of overestimation of H could be seen as underestimation errors in LE flux, provided the available energy was computed accurately. Under unstable conditions, T_s is frequently greater than T_o, (Troufleau et al., 1997; Stewart et al., 1994) particularly over surfaces with sparse vegetation, subsequently replacing T_o with T_s in Eq.(3.1), would straight-away result in overestimation of H if excess resistance (or kB^{-1}) is not adequately considered. In the present study , the overestimation of H from the three approaches (kB^{-1} = 2.3 and z_{oh} = 0.1 m , z_{oh} = 0.01 m) was a direct consequence of inadequate correction in terms of kB^{-1}. A spatially variable kB^{-1} value from a physical based kB^{-1} model incorporated into SEBAL generated H and LE fluxes without any bias error, proving that a realistic kB^{-1} value was required to adequately account for the differences between T_o and T_s.

3.6 Summary

The formulation of H from the MOS theory has some constraints that cannot be overridden by assumptions. The dT is based on aerodynamic temperature (T_o), which is linked to the aerodynamic resistance to heat transfer and the aerodynamic excess resistance. The adoption of T_s in the single source model by replacing T_o, modifies the role of excess resistance into a more or less empirical correction factor. Hence, the liberty to use T_s comes with the bottleneck of deducing a reasonable correction factor. SEBAL has an indigenous method to compute dT; however, this cannot and does not evade the computation of an appropriate correction factor in

terms of kB^{-1} or z_{oh}. We summarized below finding of this study where SEBAL was applied for irrigated and dryland conditions representing the two contrasting hydrological regimes using four different z_{oh} values, namely: (i) $z_{oh}=z_{om}/\exp(kB^{-1})$, where kB^{-1} is constant 2.3; (ii) z_{oh} = 0.1 m, where z_{oh} is a spatial constant and redefined as z_1; (iii) z_{oh} = 0.01 m, where z_{oh} is a spatial constant and redefined as z_1; and (iv) $z_{oh}=z_{om}/\exp(kB^{-1})$, where kB^{-1} is parameterized and thus spatially varying.

1. The kB^{-1} model produce distinctly and statistically different results than the constant kB^{-1} and constant z_1 (z_{oh}) approaches. Constant kB^{-1} (2.3) and constant z_1 (0.1 m and 0.01 m) approaches had similar performance trends.

2. Performance statistics from the pooled data (irrigated + dryland) reveals that the kB^{-1} model was superior in predicting LE compared with the other three approaches. The constant kB^{-1} (2.3) and constant z_1 (0.1 m and 0.01 m) approaches produced large overestimation errors in H, leading to greater underestimation errors in LE estimates.

3. SEBAL performance for irrigated fields (greater ET rates, limited soil water deficits, and complete ground cover) and dryland fields (lower ET rates, greater soil water deficits, and sparse ground cover) were markedly different.

4. Performances of the four approaches were comparable and excellent for the irrigated fields representing the greater ET, limited soil water deficits, and more complete ground cover. This conclusion derived for irrigated fields has several ramifications: (i) single source models like SEBAL generally produce good result for such surfaces, (ii) LE is significantly large for such surfaces, so H has a more limited role in LE accuracy (iii) H estimates are more accurate for such surfaces because dT is small and the errors in dT are small (since difference between T_o and T_s is small), and (iv) the need for a precise value of correction factor in terms of kB^{-1} or z_{oh} still exists for such surfaces.

5. The value of kB^{-1} (2.3) given by Garrat and Hicks (1973) and adopted in SEBAL was found to be too small for the irrigated fields. Instead, a kB^{-1} value of 7 given by Stewart et al. (1994) and used by Kustas et al. (1996) was found to be more suitable for the irrigated fields. As reported by other studies (Verhoef et al. 1997; Troufleau et al. 1997), we also found H to be more sensitive to a kB^{-1} value of 2.3 than a value of 7.

6. All four approaches performed poorly for dryland conditions, however the kB^{-1} model performed distinctly differently and significantly better compared to the other three approaches.

This result confirms that for sparse and greater soil water deficits conditions, the single-source resistance formulation have limited capability in predicting H and LE fluxes. Only the kB^{-1} model produced a positive NSE value indicating that it had the potential to improve ET or LE estimated for dryland conditions.

7. The absence of bias error in the kB^{-1} model runs for both dryland and irrigated fields, indicates that kB^{-1} parameter performed well as a correction factor and accounted for the difference between T_o and T_s. It also indicates that kB^{-1} model treated the smaller ET and greater ET crops surfaces appropriately.

8. SEBAL claimed that the dT from the hot and cold pixel approach would automatically consider the differences between T_o and T_s (Bastiaanssen et al., 1998; Jacob et al., 2002; Timmermans et al., 2007; Norman et al., 2006); however, in our study H was consistently overestimated with the constant kB^{-1} (2.3) and constant z_1 (0.1 m, 0.01 m) approaches, indicating that dT could not account for the differences between T_o and T_s. The hot and cold pixel selection approach governing the dT value had no intrinsic characteristics to consider for the inaccuracies generated as a consequence of replacing T_o with T_s.

9. The constant z_{oh} (z_1) values of 0.1 m, 0.01 m, and even 0.001 m produced similar results. The constant z_{oh} (z_1) redefines the dT and r_{ah} terms, and hence the constant z_{oh} (z_1) becomes merely an empirical term. Thus, the constant z_{oh} (roughness length for heat transport) should not be referred to as z_{oh} instead as z_1, an empirical height with no physical significance.

10. The limited role of H on the accuracy of LE for irrigated fields with complete ground cover (greater ET surface) negates the advantage received through the accurate estimation of H. On the contrary, under sparse vegetated (less ET crop surface), LE was sensitive to errors in H estimates, and apparently single resistance formulations like SEBAL performed poorly in estimating H for such surfaces.

11. Finally, SEBAL was sensitive to the value of z_{oh} or kB^{-1}. The approach of evading z_{oh} by adopting constant z_1 appeared to be a good option under the greater ET rates, limited soil water deficits, and greater ground cover; however, under sparse ground covers this would completely fail. The performance of constant kB^{-1} (2.3) approach was relatively poor under both sparse and full canopy cover conditions. As noted by Verhoef et al. (1997), a variable kB^{-1} is better for most surfaces as compared to a constant value; this was observed in the present study.

An uncalibrated kB^{-1} model incorporated into SEBAL performed better for both dryland and irrigated lysimeter fields, compared with other approaches.

3.7 Conclusion

SEBAL with all four approaches worked well for the irrigated fields with limited soil water deficits and greater ground cover. Agricultural systems are not always composed of irrigated system, and even if irrigation is provided, it is at some specific soil water deficit level, implying that crops would undergo soil water limiting conditions through their life cycle. If single-source algorithms such as SEBAL are to be applied to an agricultural system, it is necessary to modify these not only to provide good estimates for unstressed crops, but also to accommodate the water limiting conditions. The results of this study indicate an error range from 11% to 45%, where the lower limit denotes unstressed crop ET and the upper limit refers to sparse/stressed crop ET; this is a large range. The lower limit of 11% error could be considered a good performance considering that this evaluation was performed against lysimeters and because the comparison was with the instantaneous value; improvement is possible as time aggregation from hourly to daily and further seasonal ET is applied. Attempts to reduce the upper limit error of 45% arising from the more realistic scenario of the incomplete canopy cover and stressed crop is needed. The errors from the dryland conditions were reduced from 45% to 25% through the use of a physically based excess resistance model incorporated into SEBAL. The foundation of this improvement is based on the principle of arriving at the right correction factor, which could reduce the consequences of the discrepancy between radiometric and aerodynamic temperature. Although, parameter kB^{-1} defining the excess resistance (r_r) has a physical basis, with the adoption of the radiometric temperature, it (kB^{-1}) transforms into an empirical term acting as a correction factor. The SEBAL approach with spatially constant $kB^{-1} = 2.3$, z_{oh} (z_1) = 0.1 or z_{oh} (z_1) = 0.01, could not account for the spatial variability of the discrepancy between T_o and T_s, and hence underperforms in a realistic agricultural setting or even performs poorly for dryland agriculture system. This study categorically proves that a spatially variable kB^{-1} value derived from a physical model incorporated into SEBAL could generate good overall estimates and simultaneously deliver better performance under dryland agriculture systems.

3.8 Acknowledgments

This research was supported by the Ogallala Aquifer Program, a consortium between USDA−Agricultural Research Service, Kansas State University, Texas A&M AgriLife Research, Texas A&M AgriLife Extension Service, Texas Tech University, and West Texas A&M University. This is contribution number 13-064-J from the Kansas Agricultural Experiment Station.

3.9 References

Allen, R.G., Pereira, L.S., Howell, T.A., Jensen, M.E., 2011. Evapotranspiration information reporting: I. Factors governing measurement accuracy. Agric. Water Manage., 98, 899–920.

Allen, R.G., Tasumi, M., Trezza, R., 2007. Satellite-Based Energy Balance for Mapping Evapotranspiration with Internalized Calibration (METRIC)-Model. J. Irrig. Drain. Eng. 133, 380–394.

Allen, R.G., Bastiaanssen, W.G.M., Tasumi, M., Morse, A., 2001. Evapotranspiration on the watershed scale using the SEBAL model and landsat images. ASAE Meeting Paper No.01–2224 St. Joseph, Michigan.

Anderson, M.C., Allen, R.G., Morse, A., Kustas W.P., 2012. Use of Landsat thermal imagery in monitoring evapotranspiration and managing water resources. Remote Sens. Environ. doi:10.1016/j.rse.2011.08.025.

Bastiaanssen, W.G.M., Noordman, E.J.M., Pelgrum, H., Davids, G., Thoreson, B.P., Allen, R.G., 2005. SEBAL model with remotely sensed data to improve water-resources management under actual field conditions. J. Irrig. Drain. Eng. 131, 85–93.

Bastiaanssen, W.G.M., Ahmad, M.D., Chemin, Y., 2002. Satellite surveillance of evaporative depletion across the Indus Basin. Water Resour. Res. 38, 1273–1281.

Bastiaanssen, W.G.M., 2000. SEBAL-based sensible and latent heat fluxes in the irrigated Gediz Basin, Turkey. J. Hydrol. 229, 87–100.

Bastiaanssen, W.G.M., Menenti, M., Feddes, R.A., Holtslag, A.A.M., 1998. A remote sensing surface energy balance algorithm for land (SEBAL)–1. Formulation. J. Hydrol. 213, 198–212.

Bastiaanssen, W.G.M., 1995. Regionalization of surface flux densities and moisture indicators in composite terrain. Ph.D Thesis, Wageningen Agriculture University.

Batra, N., Islam, S., Venturini, V., Bisht, G., Jiang, L., 2006. Estimation and comparison of evapotranspiration from MODIS and AVHRR sensors for clear sky days over the Southern Great Plains. Remote Sens. Environ. 103, 1–15.

Beljaars, A.C.M., Holtslag, A.A.M., 1991. Flux parameterization over land surfaces for atmospheric models. J. Appl. Meteorol. 30, 327–341.

Blumel, K., 1999. A simple formula for estimation of the roughness length for heat transfer over partly vegetated surfaces. J. Appl. Meteorol. 38, 814–829.

Brutsaert, W., 1975. On a derivable formula for long-wave radiation from clear skies. Water Resour. Res. 11, 742–744.

Brutsaert, W., Sugita, M., 1996. Sensible heat transfer parameterization for surfaces with anisothermal dense vegetation. J. Atmos. Sci. 53, 209–216.

Brutsaert, W., 1982. Evaporation into the atmosphere. Holland: D. Reidel Pub. Co.

Chamberlain, A.C., 1968. Transport of gases to and from surfaces with bluff and wave-like roughness elements. Quart. J. Roy. Meteorol. Soc. 94, 318–332.

Chandrapala, L., Wimalasuriya, M., 2003. Satellite measurement supplemented with meteorological data to operationally estimate evapotranspiration in Sri Lanka. Agric. Water Manage. 58, 89–107.

Chávez, J.L., Gowda, P.H., Howell, T.A., Neale, C.M.U., Copeland, K.S., 2009. Estimating hourly crop ET using a two-source energy balance model and multispectral airborne imagery. Irrig. Sci. 28, 79–91.

Chehbouni, A., Seen, D.L., Njoku, E.G., Monteny, B.M., 1996. Examination of the difference between radiative and aerodynamic surface temperatures over sparsely vegetated surfaces. Remote Sens. Environ. 58, 177–186.

Choi, M., Kustas, W.P., Anderson, M.C., Allen, R.G., Li, F., Kjaersgaard, J.H., 2009. An intercomparison of three remote sensing-based surface energy balance algorithms over a corn and soybean production region (Iowa, U.S.) during SMACEX 2009. Agric. For. Meteorol.149, 2082–2097.

Cleugh, H.A., Leuning, R., Mu, G., Running, S.W., 2007. Regional evaporation estimates from flux tower and MODIS satellite data. Remote Sens. Environ. 106, 285–304.

Colaizzi, P.D., Evett, S.R., Howell, T.A., Tolk, J.A., 2004. Comparison of aerodynamic and radiometric surface temperature using precision weighing lysimeters. In: Wei Gao, D.R. Shaw, Remote sensing and modeling of ecosystems for sustainability, vol. 5544 (pp. 215–229). Bellingham, WA: SPIE.

Crow, W.T., Kustas, W.P., 2005. Utility of assimilating surface radiometric temperature observations for evaporative fraction and heat transfer coefficient retrieval. Boundary-Layer Meteorol. 115, 105–130.

Elhaddad, A., Garcia, L.A., 2011. ReSET-Raster: Surface Energy Balance Model for Calculating Evapotranspiration Using a Raster Approach. J. Irrig. Drain. Eng. 137, 203–210.

Field, R.T., Fritschen, L.J., Kanemasu, E.T., Smith, E.A., Stewart, J.B., Verma, S.B., Kustas, W.P., 1992. Calibration, comparison, and correction of net radiation instruments used during FIFE, J. Geophys. Res. 18, 681–695.

French, A.N., Jacob, F., Anderson, M.C., Kustas, W.P., Timmermans, W., Gieske, A., Su, Z., Su, H., McCabe, M.F., Li, F., Prueger, J., Brunsell, N., 2005. Surface energy fluxes with the Advanced Spaceborne Thermal Emission and Reflection radiometer (ASTER) at the Iowa 2002 SMACEX site (USA). Remote Sens. Environ. 99, 55–65.

Gao, Y., Long, D., 2008. Intercomparison of remote sensing-based models for estimation of evapotranspiration and accuracy assessment based on SWAT. Hydrol. Processes 22, 4850–4869.

Gowda, P.H., Chavez, J.L., Colaizzi, P.D., Evett, S.R., Howell, T.A., Tolk, J.A., 2008. ET mapping for agricultural water management: present status and challenges. Irrig. Sci. 26, 223–237.

Glenn, E.P., Huete, A.R., Nagler, P.L., Hirschboeck, K.K., Brown, P., 2007. Integrating remote sensing and ground methods to estimate evapotranspiration. Crit. Rev. Plant Sci. 26, 139–168.

Gonzalez-Dugo, M.P., Neale, C.M.U., Mateos, L., Kustas, W.P., Prueger, J.H., 2009. A comparison of operational remote sensing-based models for estimating crop evapotranspiration. Agric. For. Meteorol. 149, 1843–1853.

Garrat, J.R., Hicks, B.B., 1973. Momentum, heat and water vapour transfer to and from natural and artificial surfaces. Quart. J. Roy. Meteorol. Soc. 99, 680–687.

Gieske, A., Meijninger, W., 2005. High density NOAA time series of ET in the Gediz Basin, Turkey. Irrig. Drain. Syst. 19, 285–299.

Gokmen, M., Vekerdy, Z., Verhoef, A. Verhoef, W., Batelaan, O., van der Tol, C., 2012 . Integration of soil moisture in SEBS for improving evapotranspiration estimation under water stress conditions. Remote Sens. Environ. 121, 261–274.

Hall, F.G., Huemmrich, K.F., Goetz, S.J., Sellers, P.J., Nickerson, J.E., 1992. Satellite remote sensing of surface energy balance: Success, failures and unresolved issues in FIFE. J. Geophys. Res. D: Atmos. 97, 19,061–19,089.

Jia, L., Su, Z., van den Hurk, B., Menenti, M., Moene, A., De Bruin, H.A.R., Yrisarry, J.J.B., Ibanez, M., Cuesta, A., 2003. Estimation of sensible heat flux using the Surface Energy Balance System (SEBS) and ATSR measurements. Phys. Chem. Earth Pt. B 28, 75–88.

Jacob, F., Olioso, A., Gu, X.F., Su, Z., Seguin, B., 2002. Mapping surface fluxes using airborne visible, near infrared, thermal infrared remote sensing data and a spatialized surface energy balance model. Agronomie, 22, 669–680.

Kalma, J.D., McVicar, T.R., McCabe, M.F., 2008. Estimating land surface evaporation: A review of methods using remotely sensed surface temperature data. Surv. Geophys. 29, 421–469.

Kalma, J.D., Jupp, D.L.B., 1990. Estimation of evaporation from pasture using infrared thermometry: evaluation of a one-layer resistance model. Agric. For. Meteorol. 51, 223–246.

Kustas, W., Anderson, M., 2009. Advances in thermal infrared remote sensing for land surface modeling. Agric. For. Meteorol. 149, 2071–2081.

Kustas, W.P., Anderson, M.C., Norman, J.M., & Li, F., 2007. Utility of radiometric-aerodynamic temperature relations for heat flux estimation. Boundary-Layer Meteorol. 122, 167–187.

Kustas, W.P., Moran, M.S., Humes, K.S. Stannard, D.I., Pinter, P.J., Hipps, L.E., Swiatek, E., Goodrich, D.C., 1994. Surface energy balance estimates at local and regional scales using optical remote sensing from an aircraft platform and atmospheric data collected over semiarid rangelands. Water Resour. Res. 30, 1241–1259.

Kustas, W.P., Choudhury, B.J., Moran, M.S., Reginato, R.J., Jackson, R.D., Gay, L.W., Weaver, H.L., 1989. Determination of sensible heat flux over sparse canopy using thermal infrared data. Agric. For. Meteorol. 44, 197–216.

Kleinbaum, D.G., Kupper, L.L., Muller, K.E., 1988 Applied Regression Analysis and Other Multivariable Methods: Second Edition. Massachusetts: Duxbury Press.

Lhomme , J.P., Montes, C., Jacob, F., Prévot, L., 2012. Evaporation from Heterogeneous and Sparse Canopies: On the Formulations Related to Multi-Source Representations. Boundary-Layer Meteorol. 144, 243–262.

Lhomme, J.P., Chehbouni, A., Monteny, B., 2000. Sensible heat flux-radiometric surface temperature relationship over sparse vegetation: Parameterizing B^{-1}. Boundary-Layer Meteorol. 97, 431–457.

Li, Z. L., Tang, R., Wan, Z., Bi, Y., Zhou, C., Tang, B., 2009. A review of current methodologies for regional evapotranspiration estimation from remotely sensed data. Sensors 9, 3801–3853.

Long, D., Singh, V.P., Li, Z.L., 2011. How sensitive is SEBAL to changes in input variables, domain size and satellite sensor. J. Geophys. Res. D: Atmos. 116, D21107, doi: 10.1029/2011JD016542.

Long, D., Singh, V.P., 2012a. A modified surface energy balance algorithm for land (M-SEBAL) based on a trapezoidal framework. Water Resour. Res. 48, W02528, doi: 10.1029/2011WR010607.

Long, D., Singh, V.P., 2012b. A Two-source Trapezoid Model for Evapotranspiration (TTME) from satellite imagery. Remote Sens. Environ. 121, 370–388.

McCabe, M.F., Wood, E.F., 2006. Scale influences on the remote estimation of evapotranspiration using multiple satellite sensors. Remote Sens. Environ. 105, 271–285.

Massman, W.J., 1999. A model study of kB_H^{-1} for vegetated surfaces using ‘‘localized near-field’’ Lagrangian theory. J. Hydrol. 223, 27–43.

Marek, T.H., Porter, D.O., Howell, T.A., Kenny, N., Gowda, P.H., 2009. Understanding ET and its use in irrigation scheduling (a TXHPET Network series user manual). Texas AgriLife Research at Amarillo, Publication No. 09-02, Texas A&M University, Amarillo, 6 Texas, 60 p.

Moriasi, D.N., Arnold, J.G., Liew, M.W.V., Bingner, R.L., Harmel, R.D., Veith, T.L., 2007. Model evaluation guidelines for systematic quantification of accuracy in watershed simulations. Tran. ASABE 50, 885–900.

Mu, Q., Zhao, M., Running, S.W., 2011. Improvements to a MODIS global terrestrial evapotranspiration algorithm. Remote Sens. Environ. 115, 1781–1800.

Mu, Q., Heinsch, F.A., Zhao, M., Running, S.W., 2007. Development of a global evapotranspiration algorithm based on MODIS and global meteorology data. Remote Sens. Environ. 111, 519–536.

Norman, J.M., Anderson, M.C., Kustas, W.P., 2006. Are single-source, remote-sensing surface-flux models too simple? In: G. D'Urso, M.A.O. Jochum, & J. Moreno, (Eds.). Proceedings of the international conference on earth observation for vegetation monitoring and water management. American Institute of Physics, 852, 170–177.

Owen, P.R., Thomson, W.R., 1963. Heat transfer across rough surfaces. J. Fluid Mech. 15, 321–334.

Paul, G., Gowda, P.H., Prasad, P.V.V., Howell, T.A., Staggenborg, S.A., Neale, C.M.U., 2012. A comprehensive evaluation of SEBAL using high resolution airborne imagery from BEAREX08. In review in Adv. Water Res.

Paulson, C.A., 1970. The mathematical representation of wind speed and temperature profiles in the unstable atmospheric surface layer. J. Appl. Meteorol. 9, 856–861.

Singh, R.K., Irmak, A., Irmak, S., Martin, D.L., 2008. Application of SEBAL model for mapping evapotranspiration and estimating surface energy fluxes in south-central Nebraska. J. Irrig. Drain. Eng. 134, 273–285.

Sobrino, J.A., Jimenez-Muñoz, J.C., Sòria, G., Gómez, M., Ortiz, A.B., Romaguera, M., Zaragoza, M., Julien, Y., Cuenca, J., Atitar, M., Hidalgo, V., Franch, B., Mattar, C., Ruescas, A., Morales, L., Gillespie, A., Balick, L., Su, Z., Nerry, F., Peres, L., Libonati, R., 2008. Thermal remote sensing in the framework of the SEN2FLEX project: field measurements, airborne data and applications. Int. J. Remote Sens. 29, 4961–4991.

Sobrino, J. A., Jimenez-Muñoz, J. C., Zarco-Tejada, P. J., Sepulcre-Canto, G., de Miguel, E., Sòria, G., Romaguera, M., Julien, Y., Cuenca, J., Hidalgo, V., Franch, B., Mattar, C., Morales, L., Gillespie, A., Sabol, D., Balick, L., Su, Z., Jia, L., Gieske, A., Timmermans, W., Olioso, A., Nerry, F., Guanter, L. Moreno, J., Shen, Q., 2009. Thermal remote sensing from airborne hyperspectral scanner data in the framework of the SPARC and SEN2FLEX projects: an overview. Hydrol. Earth Syst. Sci. 13, 2031–2037.

Stewart, J.B., Kustas, W.P., Humes, K.S., Nichols, W.D., Moran, M.S., De Bruin H.A.R., 1994. Sensible heat flux-radiometric surface temperature relationship for eight semi arid areas. J. Appl. Meteorol. 33, 1110–1117.

Su, Z., 2002. The Surface Energy Balance System (SEBS) for estimation of turbulent heat fluxes. Hydrol. Earth Syst. Sci. 6, 85–99.

Su, Z., Schmugge, T., Kustas, W.P., Massman, W.J., 2001. An evaluation of two models for estimation of the roughness height for heat transfer between the land surface and the atmosphere. J. Appl. Meteorol. 40, 1933–1951.

Sverdrup, H.U., 1937. On the evaporation from the oceans. J. Mar. Res. 8, 2–14.

Tang, R., Li, Z.L., Jia, Y., Li, C., Sun, X., Kustas, W.P., Anderson, M.C., 2011. An intercomparison of three remote sensing-based energy balance models using Large Aperture Scintillometer measurements over a wheat–corn production region. Remote Sens. Environ. 115, 3187–3202.

Tasumi, M., Trezza, R., Allen, R.G., Wright, J.L., 2005. Operational aspects of satellite-based energy balance models for irrigated crops in the semi-arid U.S. Irrig. Drain. Syst. 19, 355–376.

Teixeira, A.H., Bastiaanssen, W.G.M., Ahmad, M.D., Bos, M.G., 2009. Reviewing SEBAL input parameters for assessing evapotranspiration and water productivity for the Low-Middle Sao Francisco River basin, Brazil Part A: Calibration and validation. Agric. For. Meteorol. 149, 462–476.

Thom, A.S., 1972. Momentum, mass and heat exchange of vegetation. Quart. J. Roy. Meteorol. Soc. 98, 124–134.

Timmermans, W.J., Kustas, W.P., Anderson, M.C., French, A.N., 2007. An intercomparison of the Surface Energy Balance Algorithm for Land (SEBAL) and the Two-Source Energy Balance (TSEB) modeling schemes. Remote Sens. Environ. 108, 369–384.

Tolk, J.A., Evett, S.R., Howell, T.A., 2006. Advection influences on evapotranspiration of Alfalfa in a semiarid climate. Agron. J. 98, 1646–1654.

Troufleau, D., Lhomme, J.P., Monteny, B., Vidal A., 1997. Sensible heat flux and radiometric temperature over sparse Sahelian vegetation. I. An experimental analysis of kB^{-1} parameter. J. Hydrol. 189, 815–838.

Wu, B., Yan, N., Xiong, J., Bastiaanssen, W.G.M., Zhu, W., Stein A., 2012. Validation of ETWatch using field measurements at diverse landscapes: A case study in Hai Basin of China. J. Hydrol. 437, 67–80.

Verhoef, A., De Bruin H.A.R., Van Den Hurk B.J.J.M., 1997. Some practical notes on the parameter kB^{-1} for sparse vegetation. J. Appl. Meteorol. 36, 560–572.

Van de Griend, A.A., Owe, M., 1993. On the relationship between thermal emissivity and normalized difference vegetation index for natural surfaces. Int. J. Remote Sens. 14, 1119–1131.

Wang, J., Sammis, T.W., Gutschick, V.P., Gebremichael, M., Miller, D.R., 2009. Sensitivity analysis of the Surface Energy Balance Algorithm for Land (SEBAL). Trans. ASABE 52, 801–811.

Willmott, C.J., & Matsuura, K., 2005. Advantages of the mean absolute error (MAE) over the root mean square error (RMSE) in assessing average model performance. Clim. Res. 30, 79–82.

Yang, D., Chen, H., Lei, H., 2010. Estimation of evapotranspiration using a remote sensing model over agricultural land in the North China Plain. Int. J. Remote Sens. 29, 3783–3798.

Table 3.1 Image Acquisition date and various weather parameters.

Date	Day of Year	AGL	MS Res. (m)	TIR Res. (m)	S ($W\ m^{-2}$)	T_a (°C)	RH %	BP (kPa)	Wind Speed ($m\ s^{-1}$)
06/25/07	176	1000	0.5	1.8	897	27.9	51	88.6	4.9
07/02/07	183	1000	0.5	1.8	789	25.7	51	88.8	2.6
07/10/07	191	1000	0.5	1.8	794	31.8	29	88.6	4.9
07/26/07	207	1000	0.5	1.8	901	28.6	43	88.6	4.8
07/27/07	208	1000	0.5	1.8	799	29.7	37	88.6	2.0
06/26/08	178	2000	1.0	3.0	827	29.8	34	88.4	7.8
07/12/08	194	2000	1.0	3.0	897	21.6	44	88.9	9.1
07/20/08	202	2000	1.0	3.0	805	27.5	44	89.0	4.5
07/28/08	210	2000	1.0	3.0	844	31.0	50	88.1	5.3
08/05/08	218	2000	1.0	3.0	834	31.9	28	88.9	2.4

S is Solar irradiance , T_a is air Temperature, RH is relative humidity, BP is barometric pressure, MS is multispectral, TIR is thermal infrared, Res. is spatial resolution, AGL is above ground level

Table 3.2 Performance statistics for T_s (Obs. Mean: 34.59C), R_n (Obs. Mean:574.6), and G_o (Obs. Mean:36.2); (no. of observations = 40).

Estimated parameter	Mean	MBE[1]	MAE[2]	RMSE[3]	MAPD[4]	NSE[5]	Regression		
							R^2	slope	y-intercept
T_s (^{o}C)	34.8	0.23	1.10	1.58	3.18	0.96	0.94	1.02	-0.58
R_N (W m^{-2})	571	-5.57	23.55	29.55	4.08	0.71	0.76	0.92	39.83
G_o (W m^{-2})	35	-1.97	13.16	16.82	35.38	0.21	0.23	0.28	24.69

[1] Mean bias error; $MBE = \frac{1}{n}\sum_{i=1}^{n}(M_i - O_i)$, [2] Mean absolute error; $MAE = \frac{1}{n}\sum_{i=1}^{n}|M_i - O_i|$,

[3] Root mean square error; $RMSE = \sqrt{\frac{1}{n}}\sum_{i=1}^{n}(M_i - O_i)^2$, [4] Mean absolute percent difference $MAPD = \frac{\sum_{i=1}^{n}|M_i - O_i|}{\sum_{i=1}^{n} O_i} \times 100$

[5] Nash-Sutcliffe efficiency; $NSE = \frac{\sum_{i=1}^{n}(O_i - \bar{O})^2 - \sum_{i=1}^{n}(M_i - O_i)^2}{\sum(O_i - \bar{O})^2}$

Where, O_i-observed value; M_i- Modeled value; $\bar{O}$-mean of the observed, $\bar{M}$- mean of the modeled

Table 3.3 Statistical significance testing for coincidence of the regression fits under the four model runs. The critical value for a two sided Student's t test with significance level α=0.05 is given by $t_{76,0.975}$=1.992.

Model Runs	z_{oh}=0.1 m		z_{oh}=0.01 m		kB^{-1} model	
	Slope	Intercept	Slope	Intercept	Slope	Intercept
kB^{-1}=2.3	|T|=0.306 P=0.763	|T|=0.267 P=0.789	|T|=0.485 P=0.629	|T|=0.064 P=0.949	|T|=2.762 P=0.008	|T|=3.416 P=0.001
kB^{-1} model	|T|=3.241 P=0.002	|T|=3.231 P=0.002	|T|=3.457 P=0.0009	|T|=3.472 P=0.0009		
z_{oh}=0.01 m	|T|=0.188 P=0.852	|T|=0.209 P=0.835				

Table 3.4 Performance statistics for Instantaneous ET (mm h^{-1}) for the complete dataset under four different z_{oh} values. The observed mean was 0.55 mm h^{-1} and the no. of observations were 40

Runs	Mean (mm h^{-1})	MBE (mm h^{-1})	MAE (mm h^{-1})	RMSE (mm h^{-1})	MAPD (%)	NSE	Regression		
							R^2	slope	y-interp.
kB^{-1}=2.3	0.42	-0.13	0.15	0.18	26.8	0.23	0.72	0.98*	-0.12
z_{oh}=0.1 m	0.47	-0.08	0.12	0.14	21.4	0.50	0.74	1.00*	-0.07
z_{oh}=0.01 m	0.47	-0.08	0.12	0.15	21.9	0.47	0.75	1.03*	-0.10
kB^{-1} model	0.55	0.00	0.09	0.10	16.5	0.72	0.74	0.63*	0.20

*significant at p value 0.001

Table 3.5 Performance statistics for Sensible Heat (Obs. Mean:170.11), and Latent Heat (Obs. Mean: 368.29) under four different z_{oh} values.

Estimated parameter	Mean ($W\ m^{-2}$)	MBE ($W\ m^{-2}$)	MAE ($W\ m^{-2}$)	RMSE ($W\ m^{-2}$)	MAPD (%)	NSE	Regression		
							R^2	slope	y-intercept
$H_{kB^{-1}=2.3}$	266	96.1	101.2	117.7	59.5	-0.29	0.61	0.85*	121
$H_{z_{oh}=0.1}$	228	57.6	72.2	88.7	42.4	0.26	0.64	0.87*	79
$H_{z_{oh}=0.01}$	234	63.4	75.3	91.6	44.2	0.21	0.65	0.89*	82
$H_{kB^{-1}=model}$	173	2.9	70.7	77.8	41.5	0.43	0.45	0.37*	110
$LE_{kB^{-1}=2.3}$	270	-97.8	104.0	124.2	28.2	0.20	0.73	0.95*	-80
$LE_{z_{oh}=0.1}$	309	-59.4	82.1	99.0	22.3	0.49	0.73	0.97*	-49
$LE_{z_{oh}=0.01}$	303	-65.2	83.6	101.9	22.7	0.46	0.75	1.00*	-66
$LE_{kB^{-1}=model}$	364	-4.7	62.2	72.3	16.9	0.73	0.75	0.62*	136

*significant at p value 0.05

Table 3.6 Performance statistics for H and LE presented separately for the two water regimes under four different z_{oh} values. The observed mean of H for the irrigated fields and dryland field are 126.6 W m^{-2} and 232.2 W m^{-2} respectively. The observed mean of LE for the irrigated and dryland field are 437.1 W m^{-2} and 284.4 W m^{-2} respectively.

Runs	n	Mean (W m^{-2})	MBE (W m^{-2})	MAE (W m^{-2})	RMSE (W m^{-2})	MAPD (%)	NSE	Regression		
								R^2	slope	y-interp.
$H_{kB^{-1}=2.3}$	20▲	203	76.1	79.5	92.0	62.8	0.32	0.81	0.98	79
	20■	330	116.1	122.9	136.8	57.5	-2.21	0.10	0.26^{ns}	274
$H_{z_{oh}=0.1}$	20▲	161	34.5	44.0	50.5	34.8	0.79	0.89	0.98	37
	20■	294	80.7	100.4	112.5	47.0	-1.20	0.11	0.30^{ns}	230
$H_{z_{oh}=0.01}$	20▲	164	36.9	45.8	53.0	36.2	0.77	0.89	0.98	39
	20■	304	89.9	104.7	115.9	49.1	-1.30	0.13	0.29^{ns}	240
$H_{kB^{-1}=model}$	20▲	147	20.1	62.5	71.7	49.4	0.58	0.67	0.48	86
	20■	199	-14.2	78.8	82.8	36.9	-0.18	0.01	0.03^{ns}	192
$LE_{kB^{-1}=2.3}$	20▲	373	-63.7	74.2	88.7	16.9	0.61	0.85	1.04	-83
	20■	167	-132.0	133.9	149.1	44.7	-1.25	0.33	0.31	75
$LE_{z_{oh}=0.1}$	20▲	415	-22.2	50.7	59.7	11.6	0.82	0.87	1.04	-42
	20■	203	-96.7	113.5	124.2	37.9	-0.56	0.30	0.35	98
$LE_{z_{oh}=0.01}$	20▲	413	-24.6	51.3	60.9	11.5	0.82	0.88	1.06	-53
	20■	194	-105.9	115.9	128.1	38.7	-0.66	0.36	0.37	82
$LE_{kB^{-1}=model}$	20▲	429	-7.7	48.8	60.9	11.2	0.82	0.85	0.68	132
	20■	298	-1.69	75.5	81.3	25.2	0.33	0.48	0.21	235

▲ Irrigated fields, ■Dryland fields, *significant at p value 0.05

Table 3.7 Performance statistics for Instantaneous ET (mm h^{-1}) presented separately for the two water regimes under four different z_{oh} values. The observed mean for the irrigated and dryland fields were 0.66 mm h^{-1} and 0.44 mm h^{-1} respectively.

Runs	n	Mean (mm h^{-1})	MBE (mm h^{-1})	MAE (mm h^{-1})	RMSE (mm h^{-1})	MAPD (%)	NSE	Regression		
								R^2	slope	y-interp.
kB^{-1}=2.3	20▲	0.58	-0.08	0.10	0.13	15.9	0.61	0.83	1.06*	-0.12
	20■	0.25	-0.19	0.19	0.22	44.5	-1.23	0.33	0.30*	0.11
z_{oh}=0.1	20▲	0.63	-0.02	0.07	0.09	11.5	0.81	0.86	1.05*	-0.06
	20■	0.30	-0.14	0.17	0.18	37.8	-0.55	0.28	0.34*	0.15
z_{oh}=0.01	20▲	0.63	-0.02	0.07	0.09	11.7	0.80	0.87	1.08*	-0.08
	20■	0.29	-0.15	0.17	0.19	38.6	-0.64	0.35	0.36*	0.12
kB^{-1} model	20▲	0.65	-0.00	0.07	0.09	11.0	0.80	0.83	0.69*	0.20
	20■	0.44	-0.00	0.11	0.12	25.4	0.31	0.46	0.20*	0.35

▲ Irrigated fields, ■Dryland fields, *significant at p value 0.05

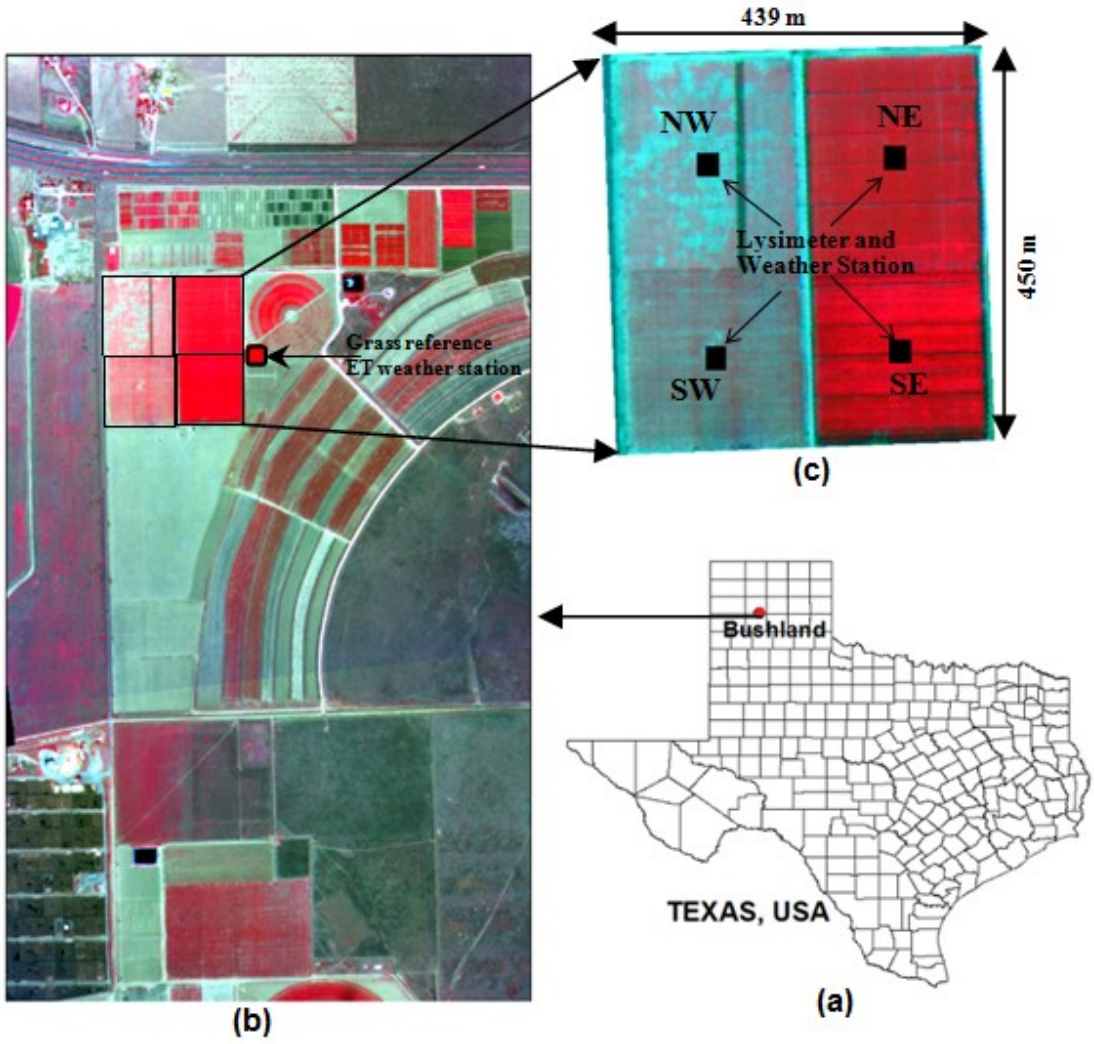

Figure 3.1 False color composite aircraft image of 5 August, 2008, showing the BEAREX08 study region. (a) location of the study area in reference to the state of Texas, USA. (b) aircraft scene covering a region of close to 5km^2 and (c) exploded view of the lysimeter field.

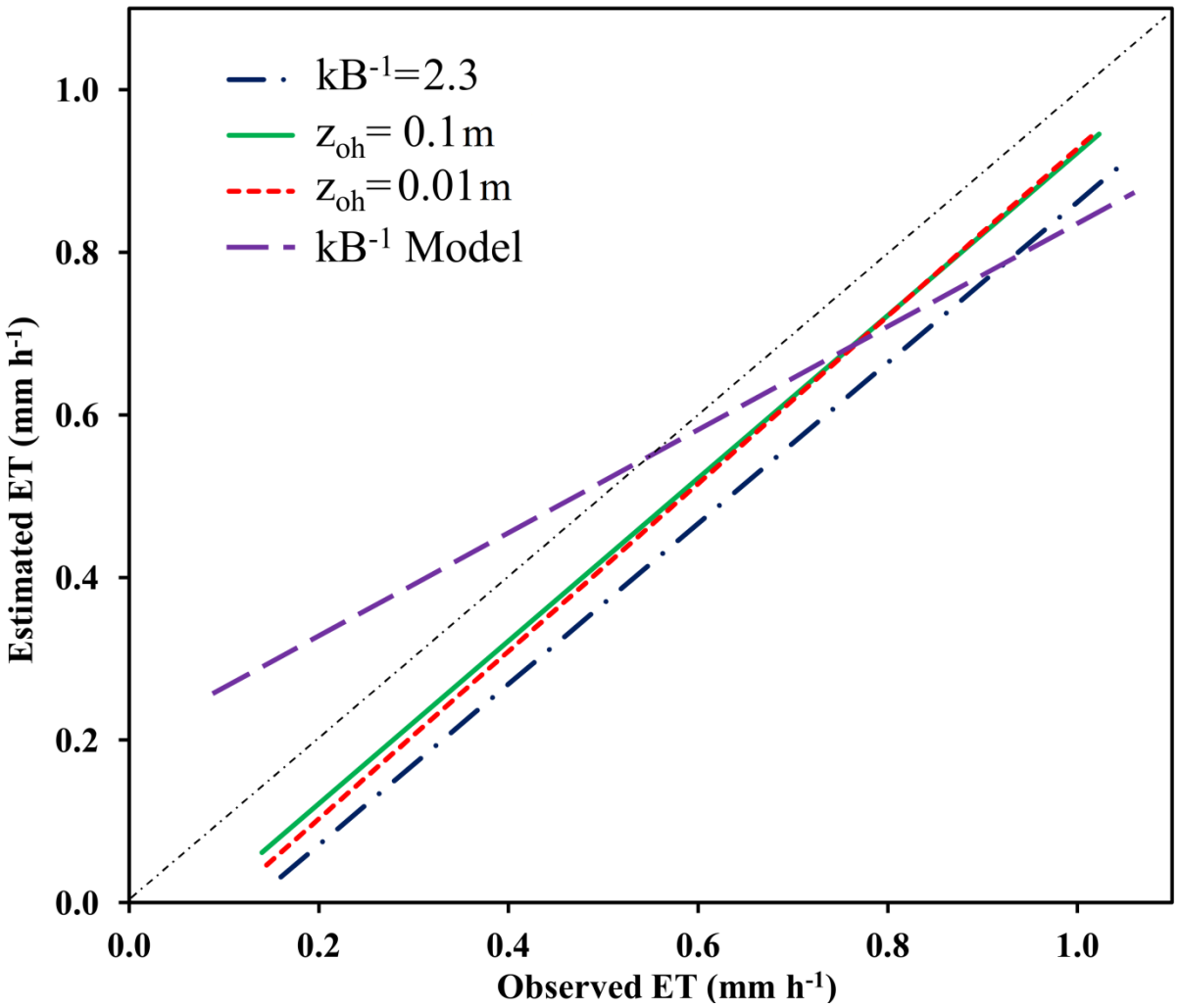

Figure 3.2 Linear fitted relationship between the observed and estimated ET under four different zoh runs.

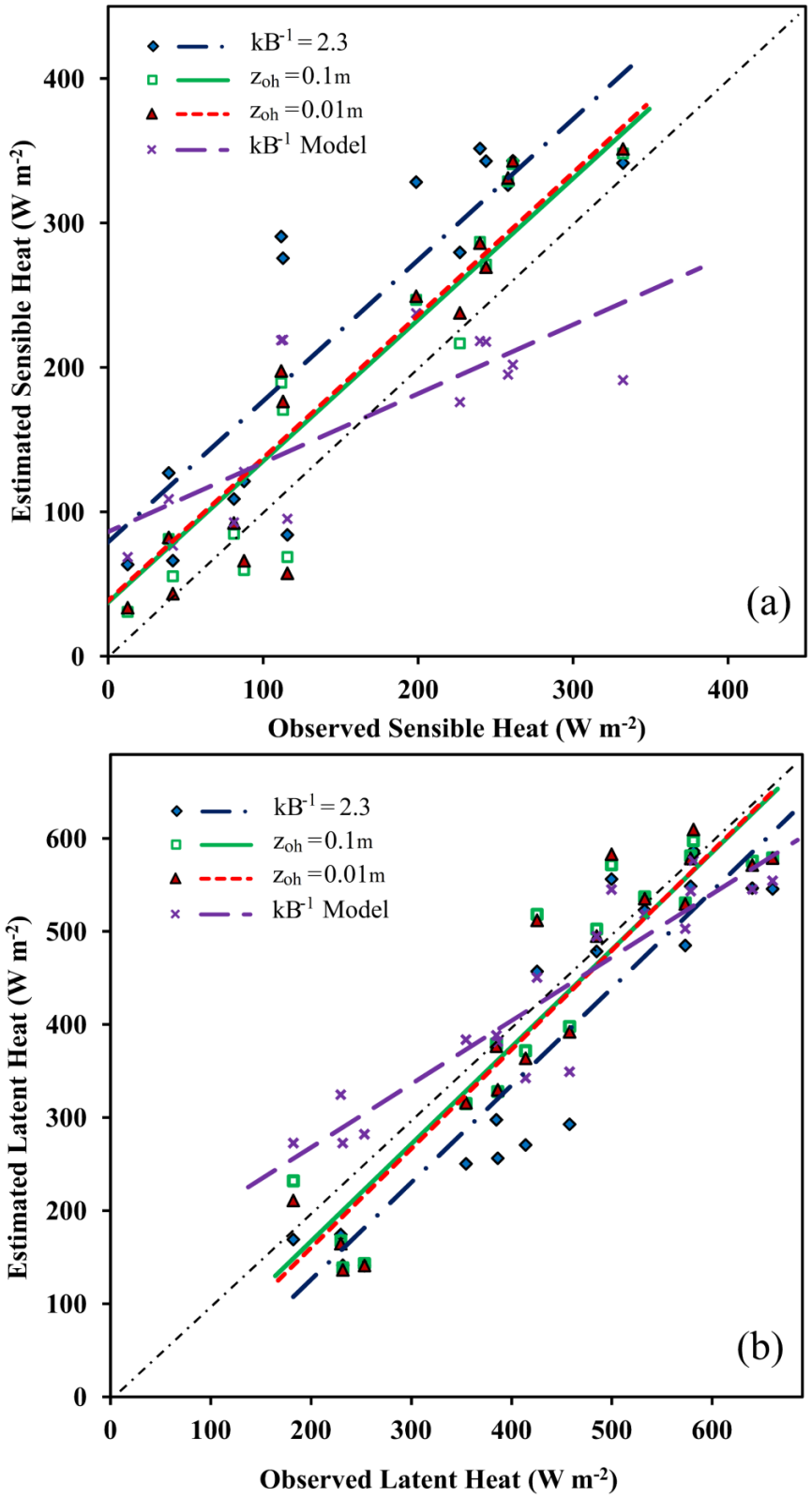

Figure 3.3 . Modeled versus observed (a) sensible heat and (b) latent heat for the irrigated fields.

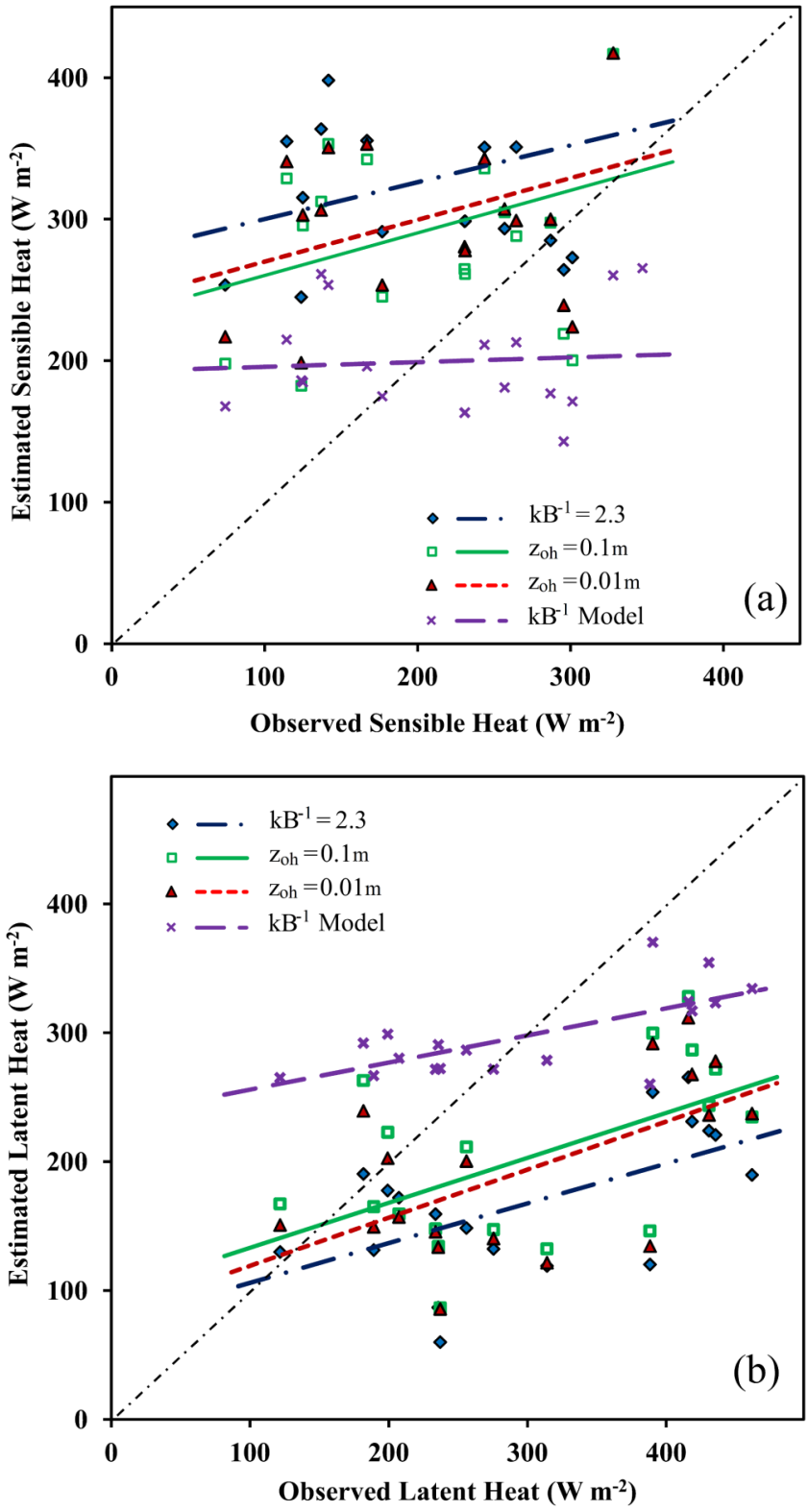

Figure 3.4 Modeled versus observed (a) sensible heat and (b) latent heat for the dryland fields.

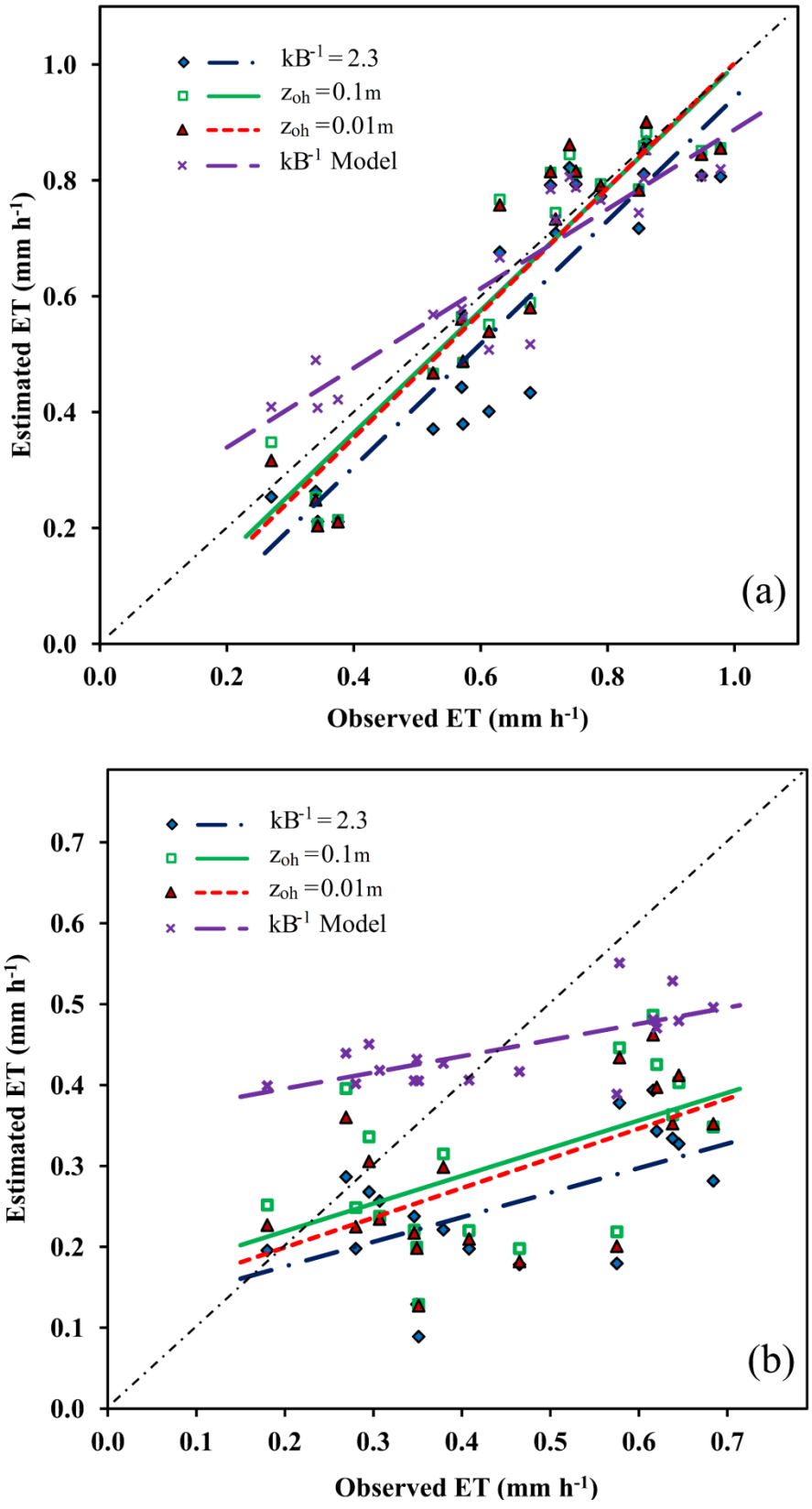

Figure 3.5 Modeled versus observed ET for (a) irrigated field and (b) dryland field

Chapter 4 - Role of hot and cold pixel concept in remote sensing based single source surface energy balance algorithms

4.1 Abstract

Evapotranspiration (ET) mapping with thermal remote sensing data garnered a renewed interest with the inception of SEBAL (Surface Energy Balance Algorithm for Land). Since then, numerous models have been developed along similar concepts that derive near surface temperature gradient, dT, from a single linear function of surface temperature. The dT function was derived from two anchor pixels denoting the hydrological extremes, and coined as the hot (dry) and the cold (wet) pixels. Although this concept was revolutionizing, the effects of numerous assumptions and pitfalls associated with it were not well understood. In this study, eight high resolution airborne images acquired during the BEAREX07-08 (Bushland Evapotranspiration and Agricultural Remote Sensing Experiment) campaigns over irrigated and dryland agricultural fields equipped with large precision lysimeters was utilized to test the hot and cold pixel concept. METRIC^{TM} (Mapping Evapotranspiration at high Resolution and with Internalized Calibration), a variant of SEBAL was compared with a generic single source (GSS) algorithm which does not use the hot and cold pixel concept and only differed in its definition and computation of the dT parameter. METRIC derived ET flux generated an overall relative error of 24%, whereas the GSS produced an 18% relative error. For irrigated conditions, METRIC produced a relative error of 11% against 18% with GSS-ET estimates. However, relative error with METRIC was greater (45%) than that with GSS (20%) for dry land conditions. These results clearly indicated that the use of the dT function as opposed to the use of classical MOS (Monin-Obukhov similarity) theory while dropping the aerodynamic excess resistance may not perform well for estimating ET over sparse and water limited cropping conditions.

4.2 Introduction and Theory

Evapotranspiration (ET) is one of the major processes driving the water balance and surface energy balance of earth's hydrosphere, biosphere, and atmosphere. Surface Energy Balance Algorithm for Land (SEBAL) was developed in the early 90's (Bastiaanssen, 1995) for estimating ET using remotely sensed visible and thermal infrared spectral reflectance with

auxiliary ground measurements. SEBAL became a widely used algorithms with several variant models such as METRIC (Mapping Evapotranspiration at high Resolution and with Internalized Calibration; Allen et al., 2005), SSEB (Simplified Surface Energy Balance; Senay et al., 2007), ReSET (Remote Sensing of Evapotranspiration; Elhaddad and Garcia, 2008), SEBTA (Surface Energy Balance with Topography Algorithm; Gao et al., 2011), and M-SEBAL (Modified SEBAL; Long and Singh, 2012) built along similar philosophy. A common feature in these algorithms was the concept of deducing the near surface temperature gradient, dT, as a linear function of surface radiometric temperature. The dT function was derived from two anchor points (pixels) denoting the hydrological extremes, and coined as the hot (dry) and the cold (wet) pixels. This concept was floated as revolutionizing; however, numerous associated assumptions and pitfalls were never thoroughly examined. The issues related to the dT concept in SEBAL and it variants could be understood better by investigating the generic bulk parameterizations of sensible heat flux (H) based on the Monin and Obukhov (1954) similarity theory (MOST),

$$H = \rho_a C_p \frac{T_o - T_a}{r_{ah}} \tag{4.1}$$

$$r_{ah} = \frac{1}{k u_*}\left[ln\left(\frac{z_{ref} - d_o}{z_{oh}}\right) - \psi_h\right] \tag{4.2}$$

where ρ_a is the density of air (kg m^{-3}), C_p is the air specific heat at constant pressure (~1,004 J kg^{-1} K^{-1}), r_{ah} (s m^{-1}) is the aerodynamic resistance to heat transfer, and T_a is the air temperature (°C). In Eq.(1), T_o (°C; aerodynamic temperature) is defined as the extrapolation of T_a down to an effective height within the canopy at which the vegetation component of H and latent heat (LE) fluxes arise given by d_o+z_{oh} (Chehbouni et al., 1996), where d_o is zero plane displacement height and z_{oh} (m) is roughness length for heat transport. The other terms in Eq. (4.2) are von Karman's constant (k ; ~0.41), the friction velocity (u_* in m s^{-1}) and stability correction function for heat (ψ_h) as a function of Monin-Obukhov length (L). In Eq. (4.1) the temperature gradient (dT) is defined as the difference between T_o and T_a. The absence of direct measurement and theoretical nature of T_o and z_{oh} made the implementation of Eq. (4.1) a challenge. The only approach, as an alternative to this limitation was to adopt the radiometric temperature (T_s) derived from the thermal sensors and apply required correction to account for inherent differences between the two temperatures.

SEBAL defined dT as the near-surface temperature difference between level z_1 and z_2 where z_1 was taken as 0.1 m and z_2 was the reference level (T_a measurement level usually 2 m) (Bastiaanssen et al., 2005; Allen et al., 2007). This is a serious deviation from the original definition where the position of effective heat source is given by z_{oh} and not by any arbitrary value of z_1. How an arbitrary value of 0.1 m for z_1 was reached upon is never found in the SEBAL/METRIC literature. At the same time, numerous studies have reported that z_{oh} is a highly sensitive parameter when using a MOST formulation (Steward et al., 1994; Liu et al., 2007). The dT was computed in SEBAL through an indigenous method popularly known as the 'hot and cold pixel' concept. Following Fig.4.1, dT is computed for two points marked as the hot and cold pixel by inverting Eq. (4.3) and the resulting linear relationship is applied over the study region. There are several assumptions and limitations to this concept which are listed here under two categories: (1) assumptions in the validity of dT vs T_s relationship across the landscape and (2) assumptions in the selection of hot and cold pixel used for developing the dT vs T_s relationship. The first category of assumptions builds the conceptual framework of SEBAL and has several sub-assumptions: (a) a prior existence of relationship between dT and T_s; (b) dT vs T_s relationship accounts for the spatial variability of z_{oh}; (c) the dT vs T_s relationship accounts for the spatial variability of T_a; and (d) the dT vs T_s relationship accounts for the atmospheric contamination of acquired remote sensing data. The second category of assumptions pertains to the implementation of the concept and has also several sub-assumptions: (a) there exists a hot and a cold pixel in the image; (b) there exists a criteria for the selection of hot and cold pixel; and (c) the selection of hot and cold pixel is invariant of the domain size.

In SEBAL literature, several selection criterias could be found for the selection of hot and cold pixel, example (a) for hot pixel: dry sandy soil (Chandrapala and Wimalasuriya, 2003), bare soil (Allen et al., 2007), maximum temperature (Jacob et al., 2002), scatter plot (Choi et al., 2009, Long and Singh, 2012), and (b) for cold pixel: water body (Bastiaanssen et al., 2005), full vegetation (Allen et al., 2007), minimum temperature (Jacob et al., 2002), scatter plot (Choi et al., 2009, Long and Singh, 2012). Interestingly all these studies generated similar levels of ET accuracy. The METRIC algorithm may be considered as more conceptually evolved in the hot and cold pixel concept for its physical treatment of end members (Fig 4.1B), because the METRIC algorithm attempts to attach physical meaning to the hot and cold pixel by stating that at hot pixel some residual moisture is present ($LE \neq 0$) and at cold pixel, vegetation is transpiring

at 1.05 times the reference ET (H≠0). These are deviations from SEBAL (Fig. 4.1). However, there is no study comparing SEBAL and METRIC to conclude that the physical treatment given to the end member pixels improved performance. Formulation for estimating sensible heat (H) flux in METRIC is given as follows:

$$H = \rho_a C_p \frac{dT_{1-2}}{r_{ah,1-2}} \tag{4.3}$$

$$\mathrm{r_{ah,1-2}} = \frac{1}{\mathrm{k u_*}}\left[ln\left(\frac{\mathrm{z_2}}{\mathrm{z_1}}\right) - \psi_\mathrm{h}\right] \tag{4.4}$$

where, $r_{ah,1\text{-}2}$ is aerodynamic resistance (s m^{-1}) between two near-surface heights, z_1 and z_2 taken as 0.1 and 2 m, respectively, above the zero-plane displacement height. The $dT_{1\text{-}2}$ parameter (K) represents the near-surface temperature difference between $z_1$and z_2. The $dT_{1\text{-}2}$ parameter is computed for the study area using the linear function developed from the hot and cold pixel concept (Fig 4.1B). The METRIC approach is to fix the source/sink height (z_1=0.1 m) and rely on the dT from the hot and cold pixel concept to accommodate for the differences between T_o and T_s. The $r_{ah,1\text{-}2}$ is computed using z_1 (0.1 m) defined to be at an elevation above z_{oh}, and thus it eliminates the use of z_{oh}.

A generic single source (GSS) model formulation is similar to Eq. 4.1 and 4.2, except T_o would be replaced by T_s and the source/sink height (z_{oh}) would be defined as radiometric roughness length for heat.

$$\mathrm{H} = \rho_\mathrm{a} \mathrm{C_p} \frac{\mathrm{T_s - T_a}}{\mathrm{r_{ah}}} \tag{4.5}$$

$$\mathrm{r_{ah}} = \frac{1}{\mathrm{k u_*}}\left[ln\left(\frac{\mathrm{z_{ref} - d_o}}{\mathrm{z_{oh}}}\right) - \psi_\mathrm{h}\right] \tag{4.6}$$

METRIC and GSS differed only in their approach of defining and computing dT and corresponding r_{ah}, which would have direct influence on the estimation of H fluxes. The z_{oh} in Eq. 4.6 is related to a radiometric excess resistance parameter, kB^{-1}, (Garratt and Hicks, 1973) as:

$$\mathrm{z_{oh}} = \mathrm{z_{om}}/\exp\left(\mathrm{kB^{-1}}\right) \tag{4.7}$$

It needs to be clarified here that aerodynamic excess resistance parameter (kB_a^{-1}) is strictly an aerodynamic term related to the aerodynamic surface temperature. However, it

becomes merely a fitting parameter that is no longer connected to its theoretical background when T_o is replaced with T_s (Troufleau et al., 1997; Lhomme et al., 2000). Remote sensing algorithms that use the bulk transfer equations are required to use kB^{-1} (Verhoef et al., 1997; Lhomme et. al, 2000); however, the value of kB^{-1} can highly vary spatially and diurnally, and parameterization is not easy. Reported kB^{-1} values ranged between 1–12 (Su et al., 2001) and largerer values found to be less sensitive (Troufleau et al., 1997; Verhoef et al., 1997). A widely used constant kB^{-1} value of 2 proposed by Garrat and Hicks (1973) was too small for most surfaces (Kustas et al., 1989; Stewart et al., 1994; Verhoef et al., 1997; Su et al., 2001; Lhomme et al., 2000) and the fact that the overestimation of kB^{-1} has less consequence than underestimating it (Troufleau et al., 1997; Verhoef et al., 1997), supports the usage of a value of around 6 (Steward et al., 1994). Recent developments in conceptualization and parameterization of kB^{-1} (Su et al., 2001) has proved to be promising in generating spatially variable kB^{-1} for accurate estimation of H using T_s (Kustas and Anderson, 2009). The objective of this study was to analyze the performance of a model that utilizes the hot and cold pixel concept (METRIC) and compares it against an algorithm (GSS) which utilizes the kB^{-1} parameter.

4.3 Materials and Methods

High resolution airborne imagery data from the Bushland Evapotranspiration and Agricultural Remote Sensing Experiments during 2007 and 2008 (BEAREX07 and BEAREX08) was used in this study. Both METRIC and GSS were applied on eight high resolution airborne images acquired during two summer growing seasons for estimating hourly ET and validated against lysimeter data.

4.3.1 Study area and instrumentations

The BEAREX07 and BEAREX08 field campaigns were conducted at the USDA-ARS Conservation and Production Research Laboratory (CPRL) Bushland, Texas, during the 2007 and 2008 summer growing seasons. This is a semi-arid region with geographic coordinates of 35º 11' N, 102º 06' W and elevation of 1170 m above mean sea level. The CPRL has four large weighing lysimeters (3 m long x 3 m wide x 2.4 m deep) each located in the middle of approximately 4.7 ha fields arranged in a block pattern. The two lysimeter fields located in the east (NE and SE) were managed under irrigated conditions, and the other two lysimeter fields in the west (NW and SW) were under dryland management. Each lysimeter field was equipped

with an automated weather station that provided net radiation (R_n), T_s, soil heat flux (G_o), T_a, relative humidity, and wind speed measurements (refer to Chávez et al., 2009 for details of field instrumentation). In addition, a grass reference ET weather station (0.31 ha), which is a part of the Texas High Plains ET Network, was located on the eastern edge of the SE irrigated lysimeter field (Marek et al., 2009). During the BEAREX07 (2007), the NE field was planted with forage sorghum (on 30 May), the SE field was planted to corn (on 17 May). The NW field was planted with grain sorghum in rows (on 6 June), and the SW field was planted with grain sorghum in clumps (on 6 June). During the BEAREX08 (2008), cotton was planted on all lysimeter fields. The planting was done on 21 May and 5 June on irrigated and dryland lysimeters, respectively.

4.3.2 Airborne Remote Sensing Data

Flying expeditions were conducted during the summer field campaign to acquire high resolution remotely sensed imagery using the Utah State University (USU) airborne digital multispectral system. It acquired high resolution imagery in the green (0.545–0.555 μm), red (0.665–0.675 μm), near-infrared (0.790–0.810 μm), and thermal infrared (8–12 μm) portions of the electromagnetic spectrum. Visible and near infrared images were acquired at 0.5–1 m spatial resolution, and the thermal images were acquired at 1–3 m. Eight images, four in each year, that were acquired close to 12 Noon CST during the mid-cropping season were used in this study. The acquisition dates were 2 July (183), 10 July (191), 26 July (207), 27 July (208) in 2007 and 12 July (194), 20 July (202), 28 July (210), and 5 August (218) in 2008. Description of the post processing including geometric corrections, radiometric calibration, and atmospheric correction that can be found in Neale et al. (2012). Crops in the irrigated field attained a near complete canopy by the last image acquisition date, whereas the dryland fields exhibited relatively less canopy cover. A 12 x 12 (m^2) pixel grid covering the lysimeter location was used in all four lysimeter fields to extract average values of estimated ET, R_n, G_o, T_s and aerodynamic parameters for evaluating the performances of METRIC and GSS algorithms.

4.3.3 Evaluation Statistics

Standard and regression statistics (mean, slope, intercept and coefficient of determination), error index statistics (MBE: mean bias error, MAE: mean absolute error and RMSE: root mean square error), and a dimensionless performance statistic (NSE: Nash-Sutcliffe efficiency) were used for model evaluation. All three error indices provide errors in the

constituent's unit and could also be expressed as relative error with respect to the mean. These three error indices served a unique purpose and were used in combination to diagnose the performances of the METRIC and GSS algorithms. The MBE was used as the indicator of under/overestimation error, the MAE was used as the primary indicator for average error, and the RMSE was reported as a conventional measure of error, and the MAPD (mean absolute percent difference) was used as a relative error indicator expressed as percentage deviation. Apart from these, the difference between RMSE and MAE was used as an indicator of variance in the individual errors of the dataset. The NSE indicated how well the plot of observed versus model estimated data fit the 1:1 line. Values between 0.0 and 1.0 are generally considered as acceptable levels of performance, whereas values <0.0 indicate unacceptable model performance (Moriasi et al., 2007). Formulations of performance statistics used in this study are provided as footnote in Table 4.1.

4.3.4 Remote Sensing Based Surface Energy Balance Algorithm

Most algorithms utilize the widely applied residual approach of surface energy balance to estimate ET at different temporal and spatial scales. The net energy coming from the sun and atmosphere in the form of short- and long-wave radiation is transformed and used for (a) heating the soil (G_o; soil heat flux into the ground), (b) heating the surface environment (H; sensible heat flux to the atmosphere), and (c) transforming water into vapor (LE; latent heat from the crop/soil surfaces). All the energy involved in the soil-vegetation-atmosphere interface can be given as the Energy Balance (EB) equation:

$$R_n = G_o + H + LE \tag{4.8}$$

where all units expressed in W m^{-2}. Latent heat flux can be expressed as hourly ET (mm) (by dividing LE by the latent heat of vaporization and the density of water). In METRIC, net radiation (R_n) is expressed as an electromagnetic balance of all incoming and outgoing fluxes, and soil heat flux is computed using an empirical relationship developed by Bastiaanssen et al. (1998). Sensible heat flux is estimated as discussed in the previous section using the METRIC approach and the generic approach. METRIC algorithm with all sub-models and step-wise procedures was adopted as reported in published literature (Allen et al., 2005; Allen et al., 2007; and Allen et al., 2011). The algorithms were coded using Python programming language and executed in Arc-GIS 10.0.

4.4 Results and Discussion

Performance statistics for estimating T_s, R_n and G_o are given in Table 4.1. Estimated R_n and retrieved T_s, accuracies were within the typical error limits of instrument measurement uncertainty (5%). A RMSE of 16 W m^{-2} in estimating G_o amounted to a high relative error of 35% (MAPD); however, the positive NSE (0.12) indicated model's satisfactory performance. Soil heat flux was smallest and relatively low in magnitude as compared with the other components of the energy balance for the present study domain, hence any error in G_o had minimal influence on the LE estimation.

Modeled ET from METRIC algorithm plotted against observed instantaneous ET (Fig. 4.2) showed a lag and large scatter along the regression line in the estimated values. However, a relatively small scatter and a small lag between the GSS-derived ET and observed data points were observed in the regression plot of the GSS model (Fig. 4.3). Comparison of the METRIC- and GSS-derived ET for irrigated and dryland lysimeter fields indicated a distinct difference in the performance of METRIC in estimating ET (Fig. 4.2). However, no such distinction could be made for GSS (Fig. 4.3). Statistical comparison of METRIC-estimated irrigated and dryland ET separately against observed data revealed the performance biases between the two water regimes with relative error of 11% and 45% respectively. The relative errors were 18% and 20% with GSS-estimated ET for irrigated and dryland fields, respectively. In dryland fields with sparsely vegetated surface undergoing frequent water stress, the difference between T_s and T_o could exceed 10°C (Chehbouni et al., 1996) whereas, in an irrigated field with well-watered dense homogeneous crops, the differences between T_s and T_o is minimal (1–2°C; Kustas et al., 1989). Accounting for the large difference between T_s and T_o in sparse vegetation water stressed condition is more critical for the model's performance than for the small difference arising under irrigated full canopy cover condition. Thus, dT is a more sensitive parameter for sparsely vegetated condition than for a dense non-water stressed vegetated condition.

Overall performance of estimated H fluxes from METRIC and GSS were compared against H derived as the residual of the observed components of the energy balance Eq. (4.8) and tabulated in Table 4.2. The H estimated from METRIC is marked by a large overestimation error of 98 W m-2 (MBE), a high relative error of 75% (MAPD) and a NSE value of -0.19, indicating poor performance. The performance of GSS model in predicting H was significantly better with an underestimation error of -44 W m-2, relative error of 42.6% and a positive NSE value of 0.63.

The overestimation error in the METRIC-estimated H fluxes translated into same magnitude of underestimation error in the estimation of LE fluxes. Interestingly, the greater relative error of 75% in the METRIC-estimated H fluxes corresponded to a nominal error of 24% in the estimated LE fluxes, and this is attributed to the unequal partitioning of the available energy into the H (mean: 144 W m-2) and LE (mean: 405 W m-2) fluxes under the energy non-limiting and water sufficient conditions. The GSS overestimated LE with a relative error of 18% which had its origin traced back to the underestimation in corresponding H estimates. (Table 4.2). The GSS-LE estimates outperformed the METRIC-LE estimates in all the performance measures. The difference between RMSE and MAE (RMSE – MAE) was almost double in the case of the METRIC-estimated LE fluxes as compared with GSS estimates indicating a larger variance in the individual errors, substantiating the large scatter illustrated in Fig. 4.2. The LE or ET underestimation errors in SEBAL and SEBAL-like algorithms is reported by various studies (French et al., 2005; Long and Singh 2012, Choi et al., 2009) and is the direct consequence of overestimation of H fluxes. Transformation of overestimation errors in METRIC-H to underestimation error in GSS-H (evident from Figs. 4.1 and 4.2, and Table 4.2) provides an adequate reason to conclude that dT is the parameter responsible for this biased behavior. The performance statistics for instantaneous ET evaluated for METRIC and GSS are provided in Table 4.2.

Table 4.3 gives the dT and r_{ah} values from METRIC and GSS approaches for two soil moisture regimes on two image acquisition dates. The H is a function of dT and r_{ah} as described by Eqs. 4.3 and 4.4 for METRIC and Eqs. 4.5 and 4.6 for GSS. Both dT and r_{ah} are intrinsically related, hence only a qualitative analysis is possible for the dT and r_{ah} values derived from the two approaches and reader may refer to Liu et al. (2007) for their ranges. Nevertheless, it could be concluded that GSS derived dT and r_{ah} are more accurate since it produced significantly better H estimates. Some of the critical observations inferred from Table 4.3 are: (a) negative dT for the irrigated field in the GSS model (b) dT for irrigated fields are always smaller than that for dryland field, (c) the differences in the magnitude of dT and r_{ah} between the two models and (d) relatively small values of z_{oh} in GSS model compared with a constant value of z_1 (0.1) used in METRIC.

4.5 Summary

The dT as defined in METRIC and computed from the hot and wet pixel concept may not represent and account for the non-unique relationship existing between T_o and T_s. The GSS model with an empirical correction in the form of excess resistance parameter, kB^{-1}, accounts for the difference between T_o and T_s. Hence an improvement in the overall performance and negligible bias between irrigated and dryland fields can be achieved.

The influence of dT cannot be seen under well-watered, densely cropped, energy non-limiting conditions. Because under such a condition, the LE fluxes are much greater than H fluxes and errors in H fluxes would have limited influence on the LE estimation. In other words, H is relatively insensitive parameter for the estimation of LE flux in irrigated conditions.

The overall relative error in METRIC-estimated ET was 24% whereas from GSS it was 18%, while this difference might not seem large yet this difference is solely the attribute of the dT parameter and got modulated depending on the partitioning of available energy (between H and LE). For dryland fields, the relative error in ET from METRIC was 45% whereas from GSS it was 20%, once again indicating the uncertainty in using the hot and cold pixel based dT parameter. More profound and direct impact of dT is seen in the H flux estimation were METRIC performance was poor with negative NSE values.

The dT is linked to r_{ah} physically; however, the non-availability of T_o and the theoretical nature of z_{oh} forces adoption of empiricism. The accuracy of H fluxes depends on appropriate dT and corresponding r_{ah}. METRIC approach fails in producing appropriate dT/r_{ah} under heterogeneous, sparse and water limited vegetation conditions. Meanwhile, the GSS approach of adopting a constant radiometric excess resistance parameter (kB^{-1}) not only produced significantly improved results but also reduced bias between irrigated and dryland fields proving that this approach accommodates for the discrepancy between T_o and T_s.

The selection criteria of hot and cold pixel or even the physical treatment of the hot and cold pixels has limited and uncertain influence on the performance of METRIC and SEBAL-like models. However, the developers have put great emphasis on this highly subjective selection process, adding that the algorithm should be executed by trained experts alone (Allen et al., 2007; Batiaanssen et al., 2010; Allen et al., 2011), again a subjective requirement. The process of selection of the hot and cold pixel is highly uncertain and operator dependent, hence it becomes

difficult to ascertain any form of sensitivity for the dT parameter. Often a trial and error method is adopted to select the pixels to match the requirements.

4.6 Conclusions

The two algorithms (METRIC and GSS) examined in this study only differed in their approach of computing the dT value. Hence any inconsistency in model performance in estimating ET should solely be attributed to the approaches used in calculating this parameter. The GSS model outperformed METRIC in all the performance statistics. The claims that the dT parameter computed using the hot and cold pixel concept considers for the atmospheric attenuations, T_o–T_s difference, spatially variability of z_{oh}, and spatial variability of T_a is implausible especially when the existence of dT versus T_s relationship is questionable and never been tested thoroughly. Too much is at stake from a regression equation developed from merely two subjective points. Numerous studies reported the high sensitivity of dT and termed it as the backbone of SEBAL and SEBAL-like models; however, the large subjectivity and uncertainty attached to dT computation cannot allow a fair sensitivity analysis. SEBAL-like models including the METRIC model never fully evaluated independently the validity of dT versus T_s relationship. The high degree of ambiguity in the selection of hot and cold pixel lead to large variations in the dT function, thus making the process a trial and error method. The approach of hot and cold pixel should only be considered as an empirical method for estimating the dT parameter over a relatively homogeneous and well managed landscape, and any physical treatment given to the end member pixel may not warrant performance augmentation. Finally, the approach of deducing dT from the hot and cold pixel concept has been exploited beyond its limited capacity and detail studies should be carried out to address the several drawbacks and uncertainties when applying over heterogeneous spatial domain.

4.7 Acknowledgments

This research was supported by the Ogallala Aquifer Program, a consortium between USDA−Agricultural Research Service, Kansas State University, Texas A&M AgriLife Research, Texas A&M AgriLife Extension Service, Texas Tech University, and West Texas A&M University. This is contribution number 13-258-A from the Kansas Agricultural Experiment Station.

4.8 References

Allen, R.G., Irmak, A., Trezza, R., Hendrickx, J.M.H., Bastiaanssen, W., Kjaersgaard, J., 2011. Satellite-based ET estimation in agriculture using SEBAL and METRIC. Hydrol. Process., 25, 4011–4027.

Allen, R.G., Tasumi, M., Trezza, R., 2007. Satellite-Based Energy Balance for Mapping Evapotranspiration with Internalized Calibration (METRIC)-Model, J. Irrig. Drain. Eng., 133, 380–394.

Allen, R.G., Tasumi, M., Morse, A., Trezza, R., 2005. A Landsat-based Energy Balance and Evapotranspiration Model in Western US Water Rights Regulation and Planning, Irrig. Drain. Syst., 19, 251–268.

Bastiaanssen, W., Thoreson, B., Clark, B., David, G., 2010. Discussion of "Application of SEBAL Model for Mapping Evapotranspiration and Estimating Surface Energy Fluxes in South-Central Nebraska" by Ramesh K. Singh, Ayse Irmak, Suat Irmak, and Derrel L. Martin, J. Irrig. Drain. Eng., 134, 282–283.

Bastiaanssen, W.G.M., Noordman, E.J.M., Pelgrum, H., Davids, G., Thoreson, B.P., Allen, R.G., 2005. SEBAL model with remotely sensed data to improve water-resources management under actual field conditions, J. Irrig. Drain. Eng., 131, 85–93.

Bastiaanssen, W.G.M., 1995. Regionalization of surface flux densities and moisture indicators in composite terrain: A remote sensing approach under clear skies in Mediterranean climates, 273 pp., Ph.D. thesis, Wageningen Agric. Univ., Den Haag, Netherlands.

Bastiaanssen, W.G.M., Menenti, M., Feddes, R.A., Holtslag, A.A.M., 1998. A remote sensing surface energy balance algorithm for land (SEBAL)–1. Formulation, J. Hydrol., 212, 198–212.

Chandrapala, L., and Wimalasuriya, M., 2003. Satellite measurement supplemented with meteorological data to operationally estimate evapotranspiration in Sri Lanka, Agric. Water Manage., 58, 89–107.

Chehbouni, A., Seen, D.L., Njoku, E.G., Monteny, B.M., 1996. Examination of the difference between radiative and aerodynamic surface temperatures over sparsely vegetated surfaces, Remote Sens. Environ., 58, 177–186.

Chávez, J.L., Gowda, P.H., Howell, T.A., Neale, C.M.U., Copeland, K.S., 2009. Estimating hourly crop ET using a two-source energy balance model and multispectral airborne imagery, Irrig. Sci., 28, 79–91.

Choi, M., Kustas, W.P., Anderson, M.C., Allen, R.G., Li, F., Kjaersgaard, J.H., 2009. An intercomparison of three remote sensing-based surface energy balance algorithms over a corn and soybean production region (Iowa, U.S.) during SMACEX, Agric. For. Meteorol., 149, 2082–2097.

Elhaddad, A., and Garcia, L.A., 2008. Surface energy balance-based model for estimating evapotranspiration taking into account spatial variability in weather, J. Irrig. Drain. Eng., 134, 681–689.

French, A.N., Jacob, F., Anderson, M.C., Kustas, W.P., Timmermans, W., Gieske, A., Su, Z., Su, H., McCabe, M.F., Li, F., Prueger, J., Brunsell, N., 2005. Surface energy fluxes with the Advanced Spaceborne Thermal Emission and Reflection radiometer (ASTER) at the Iowa 2002 SMACEX site (USA), Remote Sens. Environ., 99, 55–65.

Garrat, J.R., and Hicks, B.B., 1973. Momentum, heat and water vapour transfer to and from natural and artificial surfaces, Quart. J. Roy. Meteorol. Soc., 99, 680–687.

Gao, Z.Q., Liu, C.S., Gao, W., Chang, N.B., 2011. A coupled remote sensing and the Surface Energy Balance with Topography Algorithm (SEBTA) to estimate actual evapotranspiration over heterogeneous terrain, Hydrol. Earth Syst. Sci., 15, 119–139.

Jacob, F., Olioso, A., Gu, X.F., Su, Z., Seguin, B., 2002. Mapping surface fluxes using airborne visible, near infrared, thermal infrared remote sensing data and a spatialized surface energy balance model. Agronomie, 22, 669–680.

Kalma, J.D., and Jupp, D.L.B., 1990. Estimation of evaporation from pasture using infrared thermometry: evaluation of a one-layer resistance model, Agric. For. Meteorol., 51, 223–246.

Kustas, W.P., Choudhury, B.J., Moran, M.S., Reginato, R.J., Jackson, R.D., Gay, L.W., Weaver, H.L., 1989. Determination of sensible heat flux over sparse canopy using thermal infrared data, Agric. For. Meteorol., 44, 197–216.

Kustas, W., and Anderson, M., 2009. Advances in thermal infrared remote sensing for land surface modeling, Agric. For. Meteorol., 149, 2071–2081.

Liu, S., Lu, L., Mao, D., Jia, L., 2007. Evaluating parameterizations of aerodynamic resistance to heat transfer using field measurements, Hydrol. Earth Syst. Sci., 11, 769–783.

Long, D., and Singh, V.P., 2012a. A modified surface energy balance algorithm for land (M-SEBAL) based on a trapezoidal framework, Water Resour. Res., 48, W02528, doi:10.1029/2011WR010607.

Lhomme, J.P., Chehbouni, A., Monteny, B., 2000. Sensible heat flux-radiometric surface temperature relationship over sparse vegetation: Parameterizing B^{-1}, Boundary-Layer Meteorol., 97, 431–457.

Monin, A.S., and Obukhov, A.M., 1954. Basic laws of turbulent mixing in the ground layer of the atmosphere, Tr. Akad. Nauk. SSSR Geofiz. Inst., 24, 163–187.

Moriasi, D.N., Arnold, J.G., Liew, M.W.V., Bingner, R.L., Harmel, R.D., Veith, T.L., 2007. Model evaluation guidelines for systematic quantification of accuracy in watershed simulations, Tran. ASABE, 50, 885–900.

Marek, T.H., Porter, D.O., Howell, T.A., Kenny, N., Gowda, P.H., 2009. Understanding ET and its use in irrigation scheduling (a TXHPET Network series user manual). Texas AgriLife Research at Amarillo, Publication No. 09-02, Texas A&M University, Amarillo, 6 Texas, 60 pp.

Neale, C.M.U., Geli, H., Kustas, W.P., Alfieri, J.G., Gowda, P.H., 2012. Modeling the Soil Water Content Profile using a Remote Sensing Based Hybrid Evapotranspiration Modeling Approach. Adv. Water Resour., 50, 152–161.

Norman, J.M., Anderson, M.C., Kustas, W.P., 2006. Are single-source, remote-sensing surface-flux models too simple? In: G. D'Urso, M.A.O. Jochum, & J. Moreno, (Eds.). Proceedings of the international conference on earth observation for vegetation monitoring and water management. American Institute of Physics, 852, 170–177.

Senay, G.B., Budde, M., Verdin, J.P., Melesse, A.M., 2007. A coupled remote sensing and Simplified Surface Energy Balance approach to estimate actual evapotranspiration from irrigated fields, Sensors, 7, 979–1000.

Su, Z., Schmugge, T., Kustas, W.P., Massman, W.J., 2001. An evaluation of two models for estimation of the roughness height for heat transfer between the land surface and the atmosphere, J. Appl. Meteorol., 40, 1933–1951.

Stewart, J.B., Kustas, W.P., Humes, K.S., Nichols, W.D., Moran, M.S., De Bruin H.A.R., 1994. Sensible heat flux-radiometric surface temperature relationship for eight semi arid areas, J. Appl. Meteorol., 33, 1110–1117.

Troufleau, D., Lhomme, J.P., Monteny, B., Vidal A., 1997. Sensible heat flux and radiometric temperature over sparse Sahelian vegetation. I. An experimental analysis of kB^{-1} parameter, J .Hydrol., 189, 815–838.

Verhoef, A., DeBruin H.A.R., Van den Hurk B.J.J.M., 1997. Some practical notes on the parameter kB^{-1} for sparse vegetation, J. Appl. Meteorol., 36, 560–572.

Table 4.1 Performance statistics for retrieved T_s (Obs. Mean: 33.3°C), R_n (Obs. Mean: 576 W m^{-2}) and G_o (Obs. Mean: 34 W m^{-2}). Total number of observations - 32.

Parameter	Estimated Mean	MBE[1]	MAE[2]	RMSE[3]	MAPD[4]	NSE[5]	R^2	slope	y-intercept
T_s (°C)	33.4	0.06	0.93	1.2	2.8	0.96	0.97	0.98	0.4
R_n (W m^{-2})	580	3.3	24	29	4.1	0.73	0.75	0.86	81
G_o (W m^{-2})	33	1.5	12	16	35.2	0.12	0.17	0.25	24

[1] $MBE = \frac{1}{n}\sum_{i=1}^{n}(M_i - O_i)$ [2] $MAE = \frac{1}{n}\sum_{i=1}^{n}|M_i - O_i|$ [3] $RMSE = \sqrt{\frac{1}{n}\sum_{i=1}^{n}(M_i - O_i)^2}$

[4] $MAPD = \frac{\sum_{i=1}^{n}|M_i - O_i|}{\sum_{i=1}^{n} O_i} \times 100$ [5] $NSE = \frac{\sum_{i=1}^{n}(O_i - \bar{O})^2 - \sum_{i=1}^{n}(M_i - O_i)^2}{\sum(O_i - \bar{O})^2}$

Table 4.2 Performance statistics for H (Obs. Mean: 144 W m^{-2}), LE (Obs. Mean: 405 W m^{-2}), and ET (Obs. Mean: 0.60 mm h^{-1})

Estimated Fluxes	Mean	MBE	MAE	RMSE	MAPD	NSE	R^2	slope	y-intercept
H_{METRIC}	242	98	108	125	75.1	-0.19	0.61	0.80	126
LE_{METRIC}	313	-92	97	122	23.9	0.34	0.76	0.93	-65
ET_{METRIC}	0.46	-0.14	0.14	0.18	23.9	0.34	0.76	0.93	-0.09
H_{GSS}	100	-44	61	70	42.6	0.63	0.85	1.1	-56
LE_{GSS}	459	53	75	87	18.5	0.67	0.85	1.08	18
ET_{GSS}	0.68	0.08	0.11	0.13	18.5	0.67	0.85	1.07	0.04

Table 4.3 Temperature gradient, dT, and aerodynamic resistance, r_{ah}, values from METRIC and GSS approach

Date	Field†	METRIC		GSS		
		dT	r_{ah}*	dT	r_{ah}	z_{oh}
July 28, 2008	NE	0.83	9.15	-3.54	34.85	0.00030
	SE	1.06	9.47	-2.74	36.81	0.00025
	NW	3.52	11.69	5.75	51.21	0.00003
	SW	3.01	11.34	3.98	47.44	0.00005
July 27, 2007	NE	1.30	11.05	-4.53	71.48	0.00067
	SE	1.24	9.88	-4.68	67.91	0.00071
	NW	3.40	13.85	1.31	70.94	0.00035
	SW	3.68	14.25	2.10	71.53	0.00029

*z_{oh} in METRIC is replaced by empirical level z_1 with a fixed value of 0.1 m.

† NE & SE are irrigated fields and NW & SW are dryland fields

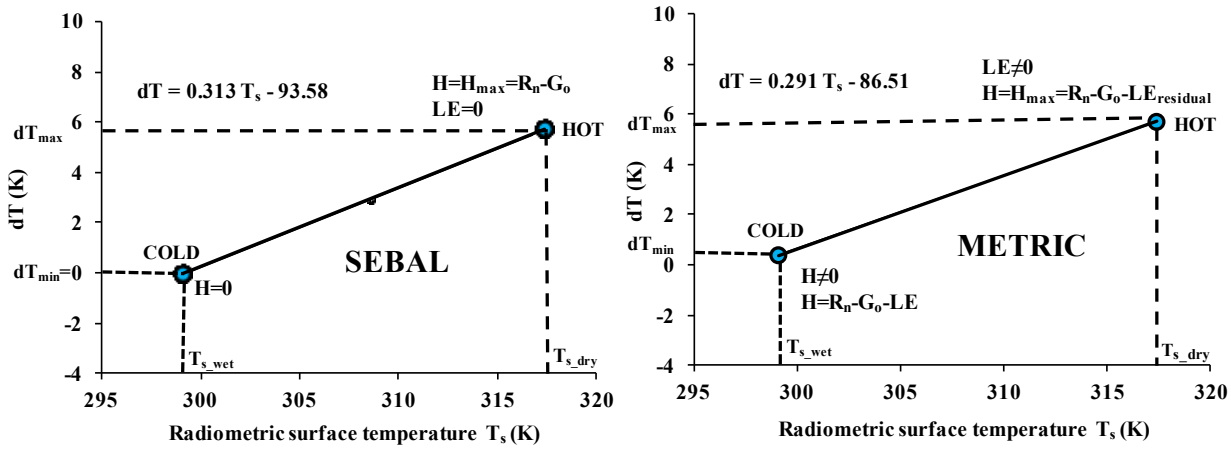

Figure 4.1 The dT formulation in SEBAL and METRIC for a July 28, 2008 image acquired over the USDA-ARS Conservation and Production Laboratory, Bushland, Texas. Note the change in the dT function from SEBAL to METRIC.

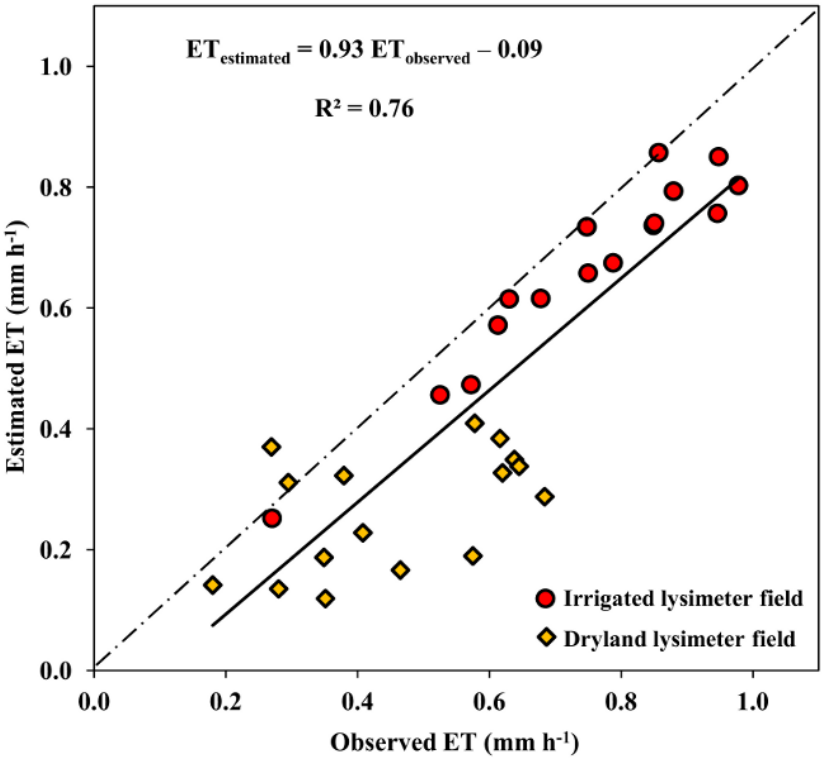

Figure 4.2 Observed versus METRIC-estimated instantaneous ET (mm h-1)

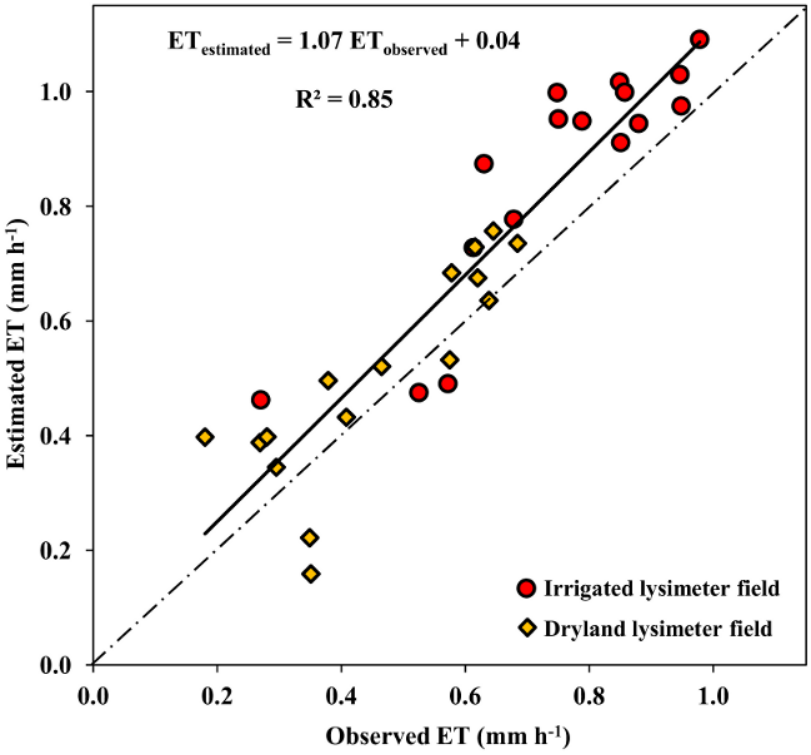

Figure 4.3 Observed versus GSS-estimated instantaneous ET (mm h-1)

Chapter 5 - Lysimetric evaluation of SEBS (Surface Energy Balance System) using high resolution airborne imagery

5.1 Abstract

Uses of spatial ET estimates are innumerable including hydrological modeling, irrigation scheduling, drought and flood monitoring and global climate change studies. The objective of this study was to evaluate the ability of the Surface Energy Balance System (SEBS) to estimate hourly ET fluxes using very high resolution (0.5-3 m) aircraft images acquired during the BEAREX07-08 (Bushland ET and Agricultural Remote Sensing Experiment 2007 and 2008). Accuracy of the predicted ET fluxes were investigated using observed data from 4 large weighing lysimeters, each located at the center of approximately 5 ha field in the USDA-ARS Conservation and Production Research Laboratory, Bushland, Texas. The uniqueness and the strength of this study come from the fact that it evaluates the SEBS for irrigated and dryland conditions simultaneously with each lysimeter field planted to tall and short crops over the two year period. Seventeen images acquired from early to mid cropping formation period were used in the study. SEBS algorithm performed equally well for both irrigated and dryland conditions in estimating the hourly ET with overall relative error of 12.6% .

5.2 Introduction

Surface Energy Balance System (SEBS) was developed by Su (2002) for the estimation of atmospheric turbulent fluxes using satellite earth observation data. SEBS adopts the concept from the SEBI (Surface Energy Balance Index) scheme (Menenti and Choudhury 1993). A better parameterization of turbulent heat transfer, bulk atmospheric similarity theory and algorithms to infer spectrally integrated hemispherical reflectance and brightness temperature has been integrated in SEBS (Menenti et al., 2003). At large spatial scales SEBS requires reference potential temperature and humidity of air at an appropriate height above heterogeneous land (Jia et al., 2003). This requirement of reference height taken at the planetary boundary layer (PBL) and observation values of potential temperature and humidity at this height can be seen as a bottleneck for application over heterogeneous land surfaces. Fields of wind, potential temperature and humidity of air generated by weather prediction model integrated over the planetary boundary layer has been used successfully to execute SEBS over large heterogeneous

land (Jia et al., 2003). Remote Sensing ET algorithms provides instantaneous ET value which are converted into daily, monthly, seasonal and yearly values by applying some conversion formulae. Better fit of the observed values were seen for long term ET estimation, from the fact that either conversion has components of observed variables or averaging smoothens/cancels out the errors. Validation using annual ET computed from simple water balance model suggested effective estimation of annual ET (Jin et al., 2009).

The aerodynamic resistance in a single source model is usually estimated on the basis of surface layer similarity theory. In single source models, the radiometric surface temperature, measured by the remote sensing thermal sensors, is assumed to be equivalent to the aerodynamic surface temperature. This approximation can be applied to heterogeneous land surfaces by adding an excess resistance term (kB^{-1}) to the aerodynamic resistance (Jia et al., 2003). SEBS provides a new parameterization of aerodynamic resistance to heat transfer (in terms of kB^{-1}) thus accounting for both aerodynamic excess resistance and radiometric excess resistance to relate sensible heat (H) to radiometric surface temperature.

SEBS was found to be sensitive to meteorological parameters (air temperature, air pressure and wind speed) and surface temperature (van der Kwast et al., 2009). SEBS have been used to estimate ET from data acquired with multiple sensors (ETM, ASTER, and MODIS) and evaluated using eddy covariance flux tower measurements. However, researchers have reported difficulty in evaluating large scale remote sensing results over heterogeneous terrain (McCabe and Wood, 2006). Also, SEBS has never been evaluated for its ability to estimate hourly ET fluxes from very high resolution remote sensing data in the semi-arid, highly advective, Texas High Plains. Therefore, the main objective of this study was to evaluate the Surface Energy Balance System (SEBS) to estimate hourly ET fluxes using very high resolution images in the Texas High Plains. Remote sensing data acquired during the Bushland Evapotranspiration and Agricultural Remote Sensing Experiment 2007 and 2008 (BEAREX07-08) was used for this purpose. An important aspect of the present study was that the SEBS algorithm was evaluated against the ET rates measured using four large weighing lysimeters, each located at the center of 4.7 ha field. The uniqueness and the strength of this study come from the fact that it evaluates SEBS algorithms for irrigated and dryland conditions simultaneously.

5.3 Materials and Methods

The Bushland Evapotranspiration and Agricultural Remote Sensing Experiment 2007 and 2008 (BEAREX07 and BEAREX08) provided a unique opportunity to evaluate the turbulent exchange of mass and energy over agricultural landscape. SEBS was executed for 17 high resolution airborne images acquired during the BEAREX07 and BEAREX08 (Table 5.1) field campaign and validated against large precision weighing lysimeters. Validation points consisted of two irrigated and two dryland fields located in the semi-arid Texas High Plains known for significant advection and nighttime ET (Tolk et al., 2006). Detailed information on the experimental set-up, algorithm description and evaluation process follows.

5.3.1 Study area and data acquisition

The BEAREX07 was conducted at the USDA-ARS Conservation and Production Research Laboratory during the 2007 summer cropping season to enhance understanding of land surface hydro-meteorological process in the semi-arid, highly advective, Texas High Plains and to develop a comprehensive dataset for rigorous testing of remote sensing based ET models.

The CPRL has four large weighing lysimeters (3 m long x 3 m wide x 2.4 m deep) each located in the middle of a 4.7 ha fields arranged in a block pattern. Two lysimeters fields located on the east (NE and SE) were managed under irrigation conditions and two lysimeters on the west (NW and SW) were managed under dryland conditions. In 2007 (BEAREX07), the NE field was planted with forage sorghum (on May 30), the SE field was planted with corn (on May 17) both being grown for silage. The NW field was planted with grain sorghum in rows (on June 6), and the SW field was planted with grain sorghum in clumps (on June 6). In 2008 (BEAREX08), the NE and SE fields were planted to cotton on May 21, and the NW and SW dryland lysimeters fields were planted to cotton on June 5 (Table 5.1). Cotton (variety Delta Pine 117) was seeded at 15.8 plants/m^2 on raised beds spaced at 0.76 m. Each lysimeter field was equipped with net radiometer, infra-red thermometer, soil heat flux plates and for measuring net radiation, radiometric surface temperature, and soil heat fluxes, respectively. In addition a grass reference ET weather station field (0.31 ha), which is a part of the Texas High Plains ET Network (TXHPET, 2006) is located on the eastern edge of the irrigated lysimeter fields.

Flying expeditions were carried out to collect remotely sensed imagery using the Utah State University (USU) airborne digital multispectral system. The system acquired high

resolution imagery in the visible, near infrared and thermal infrared portions of the electromagnetic spectrum. Visible and near infrared images were acquired at 0.5 m spatial resolution while the thermal images were acquired at 1.8 m. Seventeen images acquired during the early and mid cropping season were used to evaluate the SEBS algorithm in a GIS environment. Multiple images acquired during single day were included in the analyses to evaluate the capability of the algorithm in capturing the variations of energy fluxes and resistance terms. Image acquisition date and time, with various weather parameters at the time of image acquisition are presented in Table 5.2.

5.3.2 Surface Energy Balance System (SEBS)

Surface Energy Balance System (SEBS) is a single source land surface energy balance algorithm with a dynamic model for the thermal roughness and Monin-Obukhov Atmospheric Surface Layer (ASL) similarity for surface layer scaling. SEBS uses an excess resistance term that accounts for the fact that the roughness lengths for heat and momentum are different for canopy and soil surfaces. Primarily, three input data sets were utilized for executing the SEBS in this study: (1) albedo, emissivity, surface temperature and Normalized Difference Vegetation Index (NDVI) derived from remote sensing data (2) air pressure, air temperature, relative humidity, and wind speed measurements from weather stations, and (3) downward solar radiation.

Surface energy balance governs the water exchange and partition of the surface turbulent fluxes into sensible and latent heat in the soil-vegetation-atmosphere continuum. The residual method of surface energy balance is one of the most widely applied approaches to mapping ET at different temporal and spatial scales. In its simplest form the surface energy balance equation can be written as:

$$R_n = G_o + H + LE \tag{5.1}$$

where, R_n is the net radiation, G_0 is the soil heat flux into the soil, H is the sensible heat flux into the atmosphere, and LE is the latent heat flux (L is the latent heat of vaporization and E is the actual evapotranspiration).

Net radiation (R_n) is the dominant term in the energy balance equation as it represents the source of energy. It must be balanced by the thermodynamic equilibrium of other terms in the energy balance equation. The net radiation can also be expressed as an electromagnetic balance

of all incoming and outgoing fluxes reaching and leaving a flat horizontal and homogeneous surface as:

$$R_n = S\downarrow - S\uparrow + L\downarrow - L\uparrow = (1-\alpha_s)S\downarrow + \varepsilon_a\,\sigma\,T_a^4 - \varepsilon_s\,\sigma\,T_s^4 \quad (5.2)$$

where α_o is the broadband surface albedo, $S\downarrow$ is the incoming shortwave radiation, ε_a is the emissivity of air, T_a is the air temperature, ε_o is the surface emissivity, T_s is the surface temperature and σ is Stefan-Boltzmann constant.

SEBS requires accurate values of land surface albedo and land surface temperature (Jia et al., 2003). The broadband albedo was calculated as the total sum of the different in-band planetary albedos according to different weights for different bands. The band-pass solar exoatmospheric irradiance ($ESUN_\lambda$) is an average solar irradiance weighted by corresponding spectral band response function. It was computed from:

$$ESUN_\lambda = \frac{\sum\{E_o(\lambda)\times S(\lambda)\}\times\Delta\lambda}{\sum\{S(\lambda)\}\times\Delta\lambda} \quad (5.3)$$

where, $S(\lambda)$ is the wavelength dependent radiance spectral response also known as spectral response function for the sensor in W m^{-2} μm^{-1}, $E_o(\lambda)$ is the top of the atmosphere solar irradiance or the extraterrestrial solar irradiance in W m^{-2} μm^{-1}. The integration interval is within the pass band of the sensor; $\Delta\lambda$ is the wavelength interval taken as 0.005μm.The weight for each band was calculated and equation for broadband albedo (α_o) derived as :

$$\alpha_p = 0.303\,green + 0.400\,red + 0.296\,NIR \quad (5.4)$$

where green, red and NIR are the reflectance of the respective bands.

The remote sensing based variables that best explain the soil heat transport behavior are albedo, surface temperature and land cover vegetation index. The evaluation of G_o, usually presented as a ratio G_o/R_n, was adopted from Bastiaanssen et al. (1998):

$$\frac{G_o}{R_n} = \frac{(T_s - 273.15)}{100\alpha_s}(c_1\alpha_s + c_2\alpha_s^2)(1 - 0.98NDVI^4) \quad (5.5)$$

where c1 and c2 are locally calibrated coefficients with values of 0.12 and 0.42, respectively.

The apparent emissivity of the atmosphere was estimated from equations based on vapor pressure and temperature at the standard meteorological stations. For clear skies, the Brutsaert (1975) formulation was used as:

$$\varepsilon_a = 1.24\left(\frac{e_d}{T_a}\right)^{1/7} \tag{5.6}$$

where Ta is the air temperature [K], e_d is the vapor pressure [kPa]

In SEBS, the sensible heat flux (H) is estimated considering energy balance at limiting cases. Under dry-limit, the latent heat (LE_{dry}) becomes zero due to the limitation of soil moisture and the sensible heat flux (H_{dry}) is at maximum value. Therefore,

$$LE_{dry} = R_n - G_o - H_{dry} \equiv 0 \tag{5.7}$$

$$H_{dry} = R_n - G_o \tag{5.8}$$

Under wet limit evaporation takes place at potential rate (LE_{wet}) and the sensible heat flux (H_{wet}) value is at its minimum. Therefore,

$$\lambda E_{wet} = R_n - G_0 - H_{wet}, \;\; or\; H_{wet} = R_n - G_0 - \lambda E_{wet} \tag{5.9}$$

The sensible heat flux at wet limit is derived from an equation similar to the Penman-Monteith equation as:

$$H_{wet} = \left((R_n - G_0) - \frac{\rho C_p}{r_{ew}} \cdot \frac{e_{sat} - e}{\gamma}\right) / \left(1 + \frac{\Delta}{\gamma}\right) \tag{5.10}$$

The actual sensible heat flux (H) is given by the Equation 7.11 and is constrained in the range set by the sensible heat flux at wet (H_{wet}) and dry (H_{dry}) limits.

$$H = \rho C_p \frac{\Delta t}{r_{ah}} \tag{5.11}$$

where, ρCp is the volumetric heat capacity, r_{ah} is the aerodynamic resistance to heat transport and Δt is the difference between potential surface temperature and potential air temperature.

5.3.3 The Monin-Obukhov Similarity (MOS) stability correction functions

The MOS stability correction functions for momentum and sensible heat transfer Ψ_m and Ψ_h respectively are defined in the following integrated form

$$\Psi_i(y) = \int_0^y [1 - \phi_i(x)] \frac{dx}{x} \tag{5.12}$$

where y=-(z-d)/L. i equals m, or h for momentum and sensible heat transfer respectively.

$$y_1 = -\left[\frac{(100-d)}{L}\right] \tag{5.13}$$

$$y_2 = -\left[\frac{z_{om}}{L}\right] \tag{5.14}$$

$$x_1 = \left[\frac{y_1}{a}\right]^{1/3} \tag{5.15}$$

$$x_2 = \left[\frac{y_2}{a}\right]^{1/3} \tag{5.16}$$

$$\Psi_0 = \left(-\ln a + 3^{1/2} \cdot b \cdot a^{1/3} \cdot \pi/6\right) \tag{5.17}$$

$$\Psi_{m1} = \ln(a + y_1) - 3 \cdot b \cdot y_1^{1/3} + \frac{b \cdot a^{1/3}}{2} \ln\left[\frac{(1+x_1)^2}{(1 - x_1 + x_1^2)}\right] + 3^{1/2}.b.a^{1/3} \tan^{-1}\left[\frac{2x_1 - 1}{3^{1/2}}\right] + \Psi_0 \tag{5.18}$$

$$\Psi_{m2} = \ln(a + y_2) - 3 \cdot b \cdot y_2^{1/3} + \frac{b \cdot a^{1/3}}{2} \ln\left[\frac{(1+x_2)^2}{(1 - x_2 + x_2^2)}\right] + 3^{1/2}.b.a^{1/3} \tan^{-1}\left[\frac{2x_2 - 1}{3^{1/2}}\right] + \Psi_0 \tag{5.19}$$

$$\Psi_{h1} = \left[\frac{(1-d)}{n}\right] \ln\left[\frac{(c + y_1^n)}{c}\right] \tag{5.20}$$

$$\Psi_{h2} = \left[\frac{(1-d)}{n}\right] \ln\left[\frac{(c+y_2^n)}{c}\right] \tag{5.21}$$

On the basis of data reported by Högström (1988), and Kader and Yaglom (1990), Brutsaert (1999) assigned the constants in Equations (7.13–7.21) as a=0.33, b=0.41, m=1.0, c=0.33, d=0.057 and n=0.78.

5.3.4 Evaluation criterion

Coefficient of determination (R^2): It describes the proportion of the variance in measured data explained by the model; R^2 ranges from 0 to 1, with higher values indicating less error variance.

$$R^2 = \frac{\left(\sum_{i=1}^{n}(O_i - \bar{O})\,(M_i - \bar{M})\right)^2}{\sum_{i=1}^{n}(O_i - \bar{O})^2 . \sum_{i=1}^{n}(M_i - \bar{M})^2} \tag{5.22}$$

Nash-Sutcliffe efficiency (NSE): It indicates how well the plot of observed versus simulated data fits the 1:1 line. NSE is computed as shown in Equation 5.23. NSE ranges between $-\infty$ and 1.0 (1 inclusive), with NSE =1 being the optimal value. Values between 0.0 and 1.0 are generally viewed as acceptable levels of performance, whereas values <0.0 indicates unacceptable performance (Moriasi et al., 2007).

$$NSE = \frac{\sum_{i=1}^{n}(O_i - \bar{O})^2 - \sum_{i=1}^{n}(M_i - O_i)^2}{\sum(O_i - \bar{O})^2} \tag{5.23}$$

Mean bias error (MBE) and Percent bias (PBIAS): These indicate error in the units of the constituent of interest and also as percentage error, which facilitates result analysis. A value of zero or close to zero indicates good performance of the model. The optimal value of PBIAS is 0.0, with low-magnitude values indicating accurate model simulation. Positive values indicate model overestimation error, and negative values indicate model underestimation error.

$$MBE = \frac{1}{n}\sum_{i=1}^{n}(M_i - O_i) \tag{5.24}$$

$$PBIAS = \frac{\sum_{i=1}^{n}(M_i - O_i)}{\sum O_i} \times 100 \tag{5.25}$$

Root mean square error (RMSE) and percentage root mean square error (%RMSE): These are commonly used error index statistics with lower value range indicating better model performance.

$$RMSE = \sqrt{\frac{1}{n}\sum_{i=1}^{n}\{(M_i - O_i)\}^2} \tag{5.26}$$

$$Percent\ RMSE = \frac{RMSE}{\frac{\sum_{i=1}^{n} O_i}{n}} \times 100 \tag{5.27}$$

where in equations 20-25, n is the number of observations points, O_i and M_i are the observed and model predicted values at each comparison point i, and $\bar{O}$ and $\bar{M}$ are the arithmetic means of the observed and modeled values.

Mean absolute error (MAE) and Mean absolute percent error (MAPD): MAE is the most natural and unambiguous measure of average error magnitude, and recommended for all dimensioned evaluations and inter-comparisons of average model performance.

$$MAE = \frac{1}{n}\sum_{i=1}^{n}|M_i - O_i| \tag{5.28}$$

$$MAPD = \frac{\sum_{i=1}^{n}|M_i - O_i|}{\sum_{i=1}^{n} O_i} \times 100 \tag{5.29}$$

5.4 Results and Discussion

SEBS algorithm was applied on 17 high resolution aircraft imagery acquired during the BEARX07-08. Performance statistics for T_s, R_n, and G_o for the complete data set (n = 68) are provided in Table 5.3. Comparison of T_s retrieved from the airborne thermal images was validated against the measured data, showed good agreement with an MAE of 1.1°C representing 2.4% (MAPD) relative error. The performance of the airborne retrieved temperature was within the typical error of 1 to 1.5°C reported for satellite and airborne sensors. Net radiation was estimated with an average error of 23.0 W m^{-2} (MAE) and RMSE of 28.8 W m^{-2}. Evaluation statistics revealed good performance of the R_n model with a small relative error of 4% (MAPD), which was better than the reported range of 5 to 10% (~ 30–60 W m^{-2}) and most instrument measurement uncertainty. Soil heat flux was smallest amongst the energy balance components in the present agricultural location, where the observed mean of G_o was 38.7 W m^{-2} which was

significantly smaller than the observed means of R_n (577 W m^{-2}), H (171 W m^{-2}) and LE (374 W m^{-2}). Past studies have reported a large error range of 10–40 W m^{-2} (15–30%) in the estimation of G_o derived from the present parameterization involving fraction of R_n and a vegetative index formulation. Several reasons could explain the poor performance of the G_o model, including inadequate calibration of the empirical models and the model's incapability in capturing the large spatial variability. G_o was estimated with an overall error of 13.0 W m^{-2} (MAD), RMSE of 17 W m^{-2} and relative error of 33.6 % (MAPD). NSE value of 0.21 indicated average performance of the soil heat flux model. However, we articulate that the overall underperformance of G_o is not expected to influence the ET estimates because of the small magnitude of error which is evident from the plot of the energy balance components in Figure 5.1.

The hourly ET estimated by the SEBS algorithm showed strong correlation with the observed lysimeter data (Fig.5.2). Using all four lysimeter field data (68 data points), the overall error in SEBS-ET estimation was 0.01 mm h^{-1} (MBE), 0.10 mm h^{-1} (RMSE), 2.0% (PBIAS) and 16.8% (%RMSE) (Table 5.4). These results are comparable to prediction accuracy reported in Su (2002). It is known that the error tends to decrease as the instantaneous ET is interpolated into daily to seasonal values. Therefore, the error statistics in this study show good results for the estimated hourly ET compared with the lysimeter data. The R^2 and NSE values were 0.87 and 0.84, respectively, indicated good linear relationship and model performance. Model evaluation for the irrigated and dryland lysimeter fields separately is presented in Table 5.5 and Table 5.6. SEBS performed equally well for irrigated (NE and SE) and dryland (NW and SW) fields. Figure 5.3 shows the plot of observed versus estimated ET for the irrigated and dryland fields seperately. Evaluation statistics shows good performance in the prediction of sensible heat flux (Table 5.4–5.6). Stewart et al. (1994) reported that H can be estimated accurately using radiometric surface temperature when good estimation of kB^{-1} is available. The kB^{-1} parameterization in the SEBS algorithm, involving canopy structure in terms of canopy height, LAI and fractional vegetation cover could rightly estimate the roughness length for heat transfer (z_{oh}) for the dryland and irrigated fields thus providing good ET values for the dense and sparse vegetation conditions. Accurate radiometric surface temperature, estimation of roughness momentum transfer from canopy height measurements for each image and quality meteorological inputs, all contributed towards good estimation of hourly ET. Appendix A

provides the aerodynamic roughness parameters and temperature gradients estimated for the four fields.

5.5 Summary

SEBS algorithm was applied to eleven high-resolution airborne multispectral images acquired during early and mid summer cropping season of 2007 and 2008, and evaluated against lysimeter data. The performance of the algorithm was consistently good for irrigated (densely vegetated) and dryland (sparsely vegetated) conditions.

5.6 Acknowledgement

This research was supported in part by the Ogallala Aquifer Program, a consortium between USDA-Agricultural Research Service, Kansas State University, Texas AgriLife Research, Texas AgriLife Extension Service, Texas Tech University and West Texas A&M University.

5.7 References

Bastiaanssen, W.G.M., Menenti, M., Feddes, R.A., Holtslag, A.A.M., 1998. A remote sensing surface energy balance algorithm for land (SEBAL). 1. Formulation. Journal of Hydrology, 213, 198–212.

Brutsaert, W., 1975. On a derivable formula for long-wave radiation from clear skies. Water Resources Research, 11, 742–744.

Chávez, J.L., Gowda, P.H., Howell, T.A., Neale, C.M.U., Copeland, K.S., 2009. Estimating hourly crop ET using a two-source energy balance model and multispectral airborne imagery. Irrigation Science, 28, 79–91.

Gowda, P.H., Chavez, J.L., Colaizzi, P.D., Evett, S.R., Howell, T.A., Tolk, J.A., 2008. ET mapping for agricultural water management: present status and challenges. Irrigation Science, 26, 223–237.

Jia, L., Su, Z., Hurk, B.V.D., Menenti, M., Moene, A., De Bruin, H.A.R., Yrisarry, J.J.B., Ibanez, M., Cuesta, A., 2003. Estimation of sensible heat flux using the Surface Energy Balance System (SEBS) and ATSR measurements. Physics and Chemistry of Earth, Part B: Hydrology, Ocean & Atmosphere, 28,75–88.

McCabe, M.F., Wood, E.F., 2006. Scale influences on the remote estimation of evapotranspiration using multiple satellite sensors. Remote Sensing of Environment, doi:10.1016/j.rse.2006.07.006.

Menenti, M. and Choudhury, B.J., 1993. Parameterization of land surface evapotranspiration using a location dependent potential evapotranspiration and surface temperature range. In: Bolle, H.J. et al. (editors), Exchange processes at the land surface for a range of space and time scale, IAHS Publ. No., 212, 561–568.

Menenti, M., Jia, L., Su, L., 2003. On SEBI-SEBS validation in France, Italy, Spain, USA and China. In proceedings of ICID workshop on remote sensing of ET for large regions, 17 sep 2003.

Moriasi, D.N., Arnold, J.G., Liew, M.W.V., Bingner, R.L., Harmel, R.D., Veith, T.L., 2007. Model evaluation guidelines for systematic quatification of accuracy in watershed simulations. Transactions of ASABE, 50, 885–900.

Stewart, J.B., Kustas, W.P., Humes, K.S., Nichols, W.D., Moran, M.S., De Bruin, H.A.R., 1994. Sensible heat flux - radiometric surface temperature relationship for eight semi arid areas. Journal of Applied Meteorology, 33, 1110–1117.

Su, Z., Timmermans, W., Gieske, A., Jia, L., Elbers, J.A., Olioso, A., Timmermans, J., Vander Velde, R., Jin, X., Van Der Kwast, H., Nerry, F., Sabol, D., Sobrino, J.A., Moreno, J., Bianchi, R., 2008. Quantification of land–atmosphere exchanges of water, energy and carbon dioxide in space and time over the heterogeneous Barrax site. International Journal of Remote Sensing, 29, 5215–5235.

Su, Z., 2002. The Surface Energy Balance System (SEBS) for estimation of turbulent heat fluxes. Hydrology and Earth System Sciences, 6, 85–99.

Van der Kwast, J., Timmermans, W., Gieske, A., Su, Z., Olioso, A., Jia, L., Elbers, J., Karssenberg, D., de Jong, S., 2009. Evaluation of the Surface Energy Balance System (SEBS) applied to ASTER imagery with flux-measurements at the SPARC 2004 site (Barrax, Spain). Hydrology and Earth System Sciences, 13, 1337–1347.

Table 5.1 Image acquisition date and information on crops in the lysimeter field

No.	Year	Acquisition Date (DOY)	Time (CST)	Lysimeter Field			
				NE (Irrigated)	SE (Irrigated)	NW (Dryland)	SW (Dryland)
1	2007	June,24 (175)	10:20	Forage Sorghum May 30	Forage Corn May 17	Grain Sorghum June 6	Clumped Grain Sorghum June 6
2		June,25 (176)	11:33				
3		July,02 (183)	03:27				
4		July,10 (191)	09:53				
5		July,10 (191)	11:15				
6		July,10 (191)	02:50				
7		July,11 (192)	12:40				
8		July,26 (207)	11:37				
9		July,27 (208)	09:55				
10		July,27 (208)	11:16				
11		July,27 (208)	01:33				
12	2008	June,26 (178)	10:52	Cotton May 21	Cotton May 21	Cotton June 05	Cotton June 05
13		July,12 (194)	11:20				
14		July,20 (202)	11:06				
15		July,28 (210)	11:24				
16		Aug,05 (218)	11:43				
17		Aug, 13 (226)	11:25				

Table 5.2 Weather station parameters required as input to the model

Date	Time (CST)	Day of Year	S (Wm^{-2})	T_a (°C)	RH (%)	BP (kPa)	Wind Speed (ms^{-1})
06/26/08	10:52 AM	178	826.2	29.8	34	88.4	7.8
07/12/08	11:20 AM	194	897.3	21.6	44	88.9	9.1
07/20/08	11:06 AM	202	805.4	27.5	44	89.0	4.5
07/28/08	11:24 AM	210	844.3	31.0	50	88.1	5.3
08/05/08	11:43 AM	218	834.4	31.9	28	88.9	2.4
08/13/08	11:25 AM	226	825.7	25.9	53	88.6	4.8
06/24/07	10:20 AM	175	767.5	27.8	45	88.4	2.2
06/25/07	11:33 AM	176	896.9	27.9	51	88.6	4.9
07/02/07	03:27 PM	183	788.8	25.7	51	88.8	2.6
07/10/07	09:53 AM	191	653.1	29.3	37	88.5	1.4
07/10/07_1	11:15 AM	191	793.6	31.8	32	88.6	2.2
07/10/07_2	02:50 PM	191	883.0	33.6	26	88.6	4.0
07/11/07_3	12:40 PM	192	935.2	27.6	54	88.6	4.5
07/26/07	11:37 AM	207	900.6	28.6	43	88.6	4.8
07/27/07_1	09:55 AM	208	646.3	25.3	57	88.7	2.4
07/27/07_2	11:16 AM	208	798.8	29.7	37	88.6	2.0
07/27/07_3	01:33 PM	208	879.1	31.4	30	88.5	2.8

S is Solar irradiance , T_a is air Temperature, RH is relative humidity, BP is barometric pressure

Table 5.3 Performance statistics for T_s (Obs. Mean: 33.5 °C), R_n (Obs. Mean:577), and G_o (Obs. Mean:38.7); (no. of observations =68)

Estimated parameter	Mean	MBE	PBIAS %	MAE	MAPD %	RMSE	RMSE %	NSE	R^2
T_s (^oC)	33.5	0.03	0.08	0.80	2.4	1.1	3.3	0.96	0.96
R_N (W m^{-2})	571	-5.6	-1.0	23.0	4.0	28.8	5.0	0.86	0.87
G_o (W m^{-2})	31.9	-6.6	-17.5	13.0	33.6	17.0	43.8	0.21	0.34

Table 5.4 Performance statistics for Sensible Heat (Obs. Mean:171.2), Latent Heat (Obs. Mean: 374.6) and Evapotranspiration (Obs. Mean:0.56) for the complete data (N=68)

Estimated parameter	Mean	MBE	PBIAS (%)	RMSE	RMSE (%)	MAE	MAPD (%)	NSE	R^2
H ($W\ m^{-2}$)	170	-1.3	-0.8	64.7	37.8	50.8	29.7	0.69	0.75
LE ($W\ m^{-2}$)	381	6.8	1.8	63.4	16.9	47.6	12.7	0.84	0.87
ET ($mm\ h^{-1}$)	0.57	0.01	2.0	0.10	16.8	0.07	12.6	0.84	0.87

Table 5.5 Irrigated lysimeter field performance statistics for Sensible Heat (Obs. Mean:125.5), Latent Heat (Obs. Mean: 438.8) and Evapotranspiration (Obs. Mean:0.65) fluxes (N=38)

Estimated parameter	Mean	MBE	PBIAS (%)	RMSE	RMSE (%)	MAE	MAPD (%)	NSE	R^2
H ($W\ m^{-2}$)	131	5.9	4.7	74.6	59.4	56.3	44.8	0.63	0.74
LE ($W\ m^{-2}$)	456	17.3	3.9	73.4	16.7	55.9	12.7	0.79	0.84
ET ($mm\ h^{-1}$)	0.67	0.03	3.9	0.11	16.6	0.09	12.6	0.79	0.84

Table 5.6 Dryland lysimeter field performance statistics for Sensible Heat (Obs. Mean:208.8), Latent Heat (Obs. Mean: 310.4) and ET (Obs. Mean:0.46) (N=38)

Estimated parameter	Mean	MBE	PBIAS (%)	RMSE	RMSE (%)	MAE	MAPD (%)	NSE	R^2
H ($W\ m^{-2}$)	201	-7.4	-3.5	55.3	26.5	46.3	22.2	0.66	0.73
LE ($W\ m^{-2}$)	307	-3.7	-1.2	51.6	16.6	39.3	12.7	0.84	0.86
ET ($mm\ h^{-1}$)	0.46	-0.00	-0.73	0.08	16.6	0.06	12.6	0.84	0.86

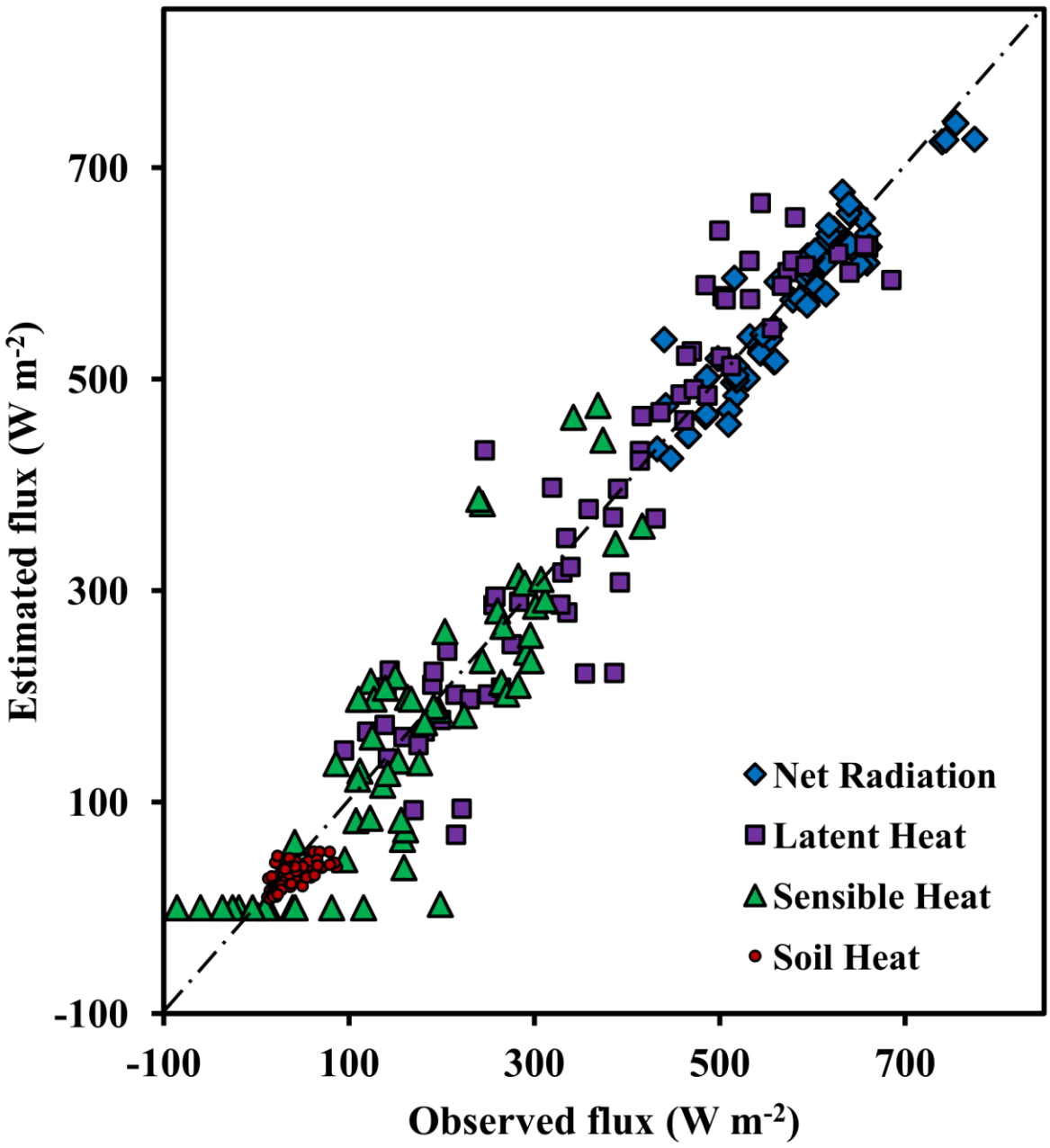

Figure 5.1 Energy balance components

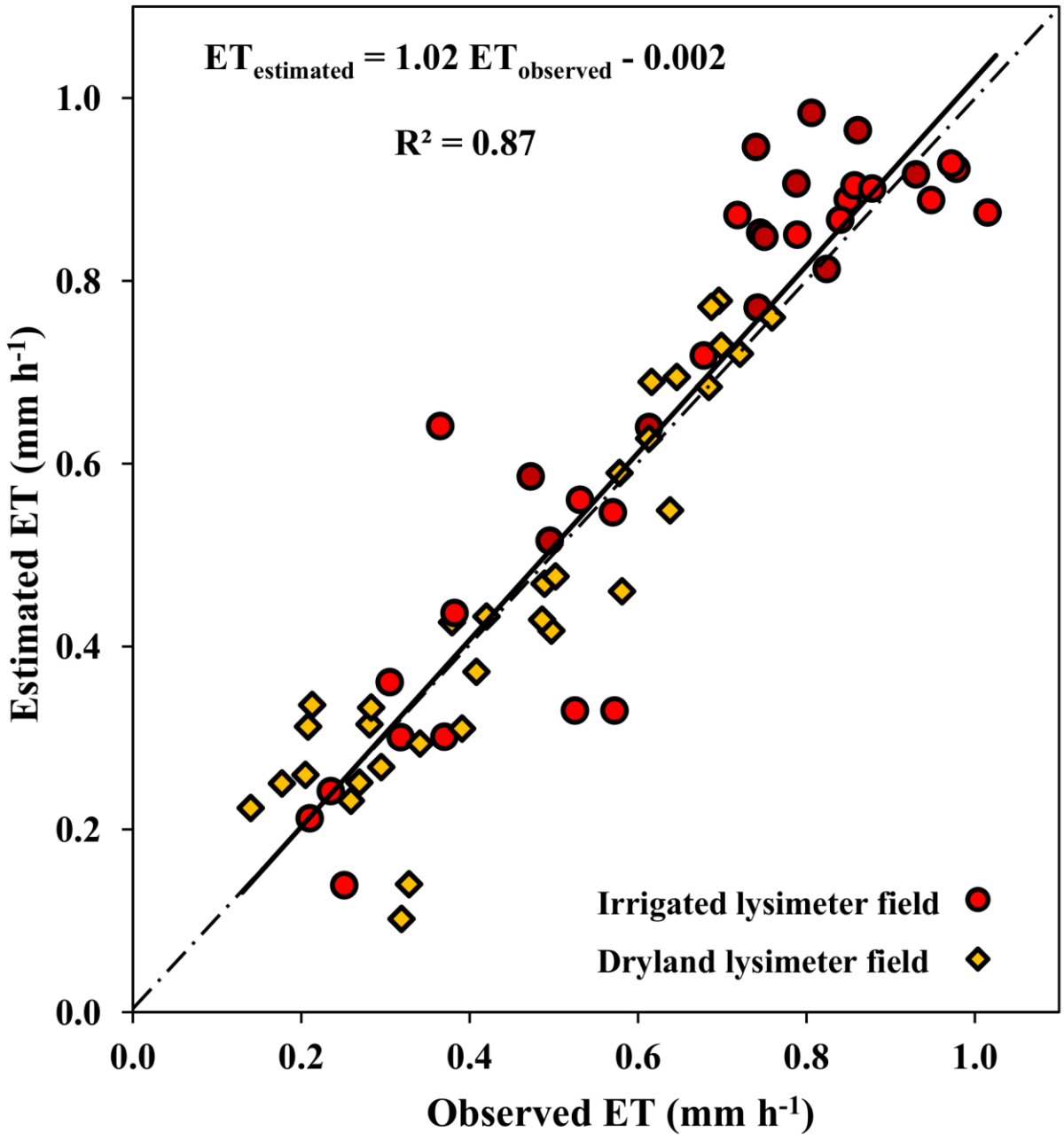

Figure 5.2 Observed versus estimated ET from SEBS for the complete data set (N=68)

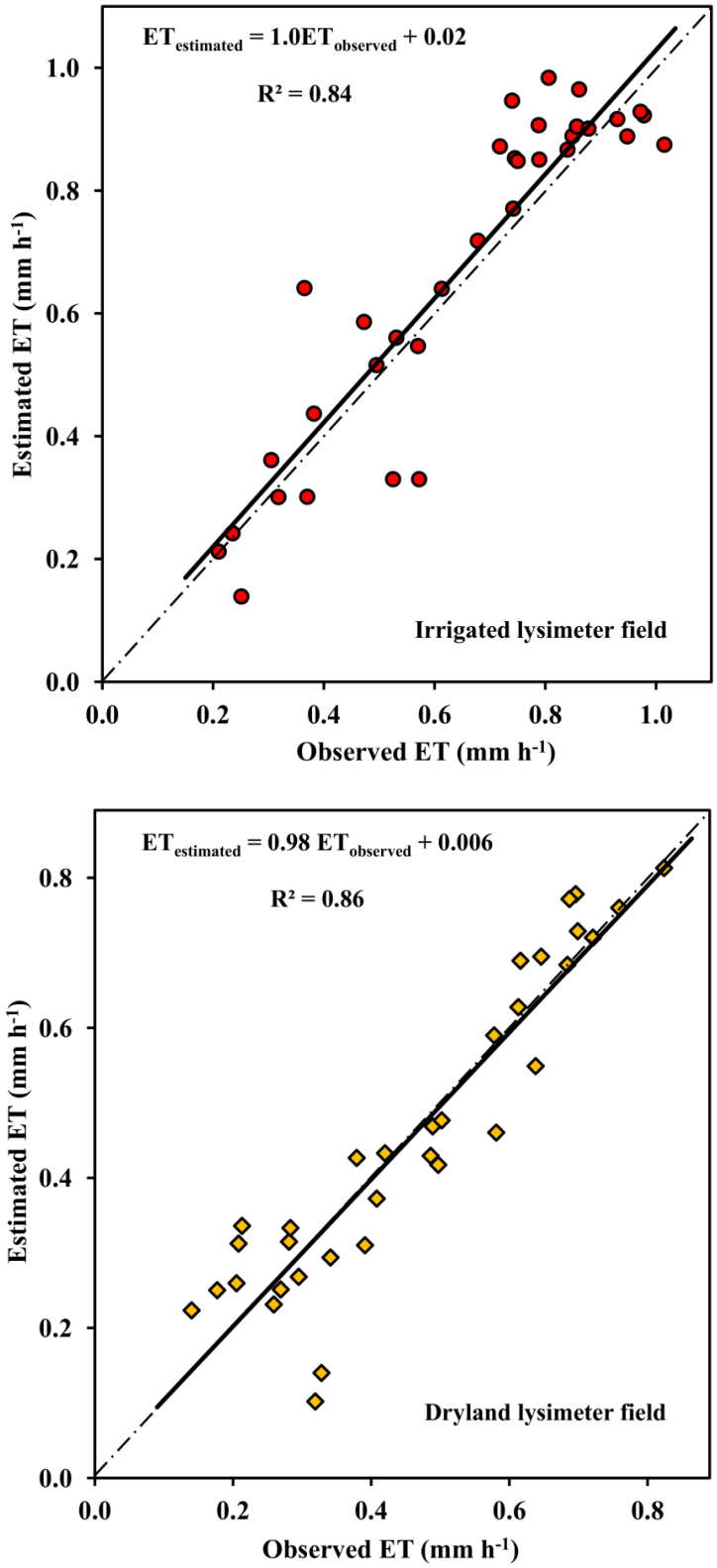

Figure 5.3 Performance of the SEBS for (a) irrigated and (b) dryland lysimeter fields (N=34)

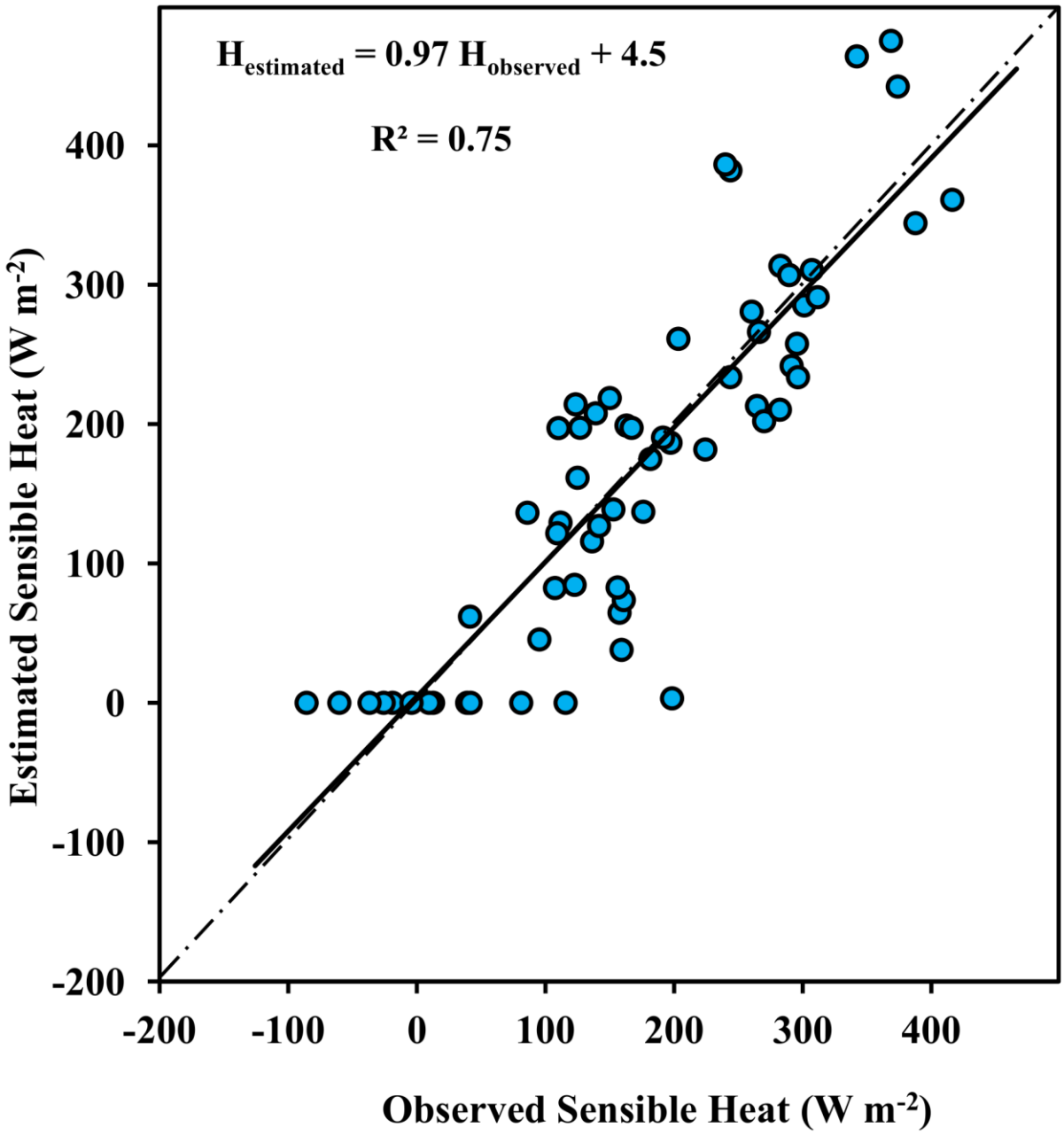

Figure 5.4 Observed versus estimated sensible heat flux for the complete data set (N=68)

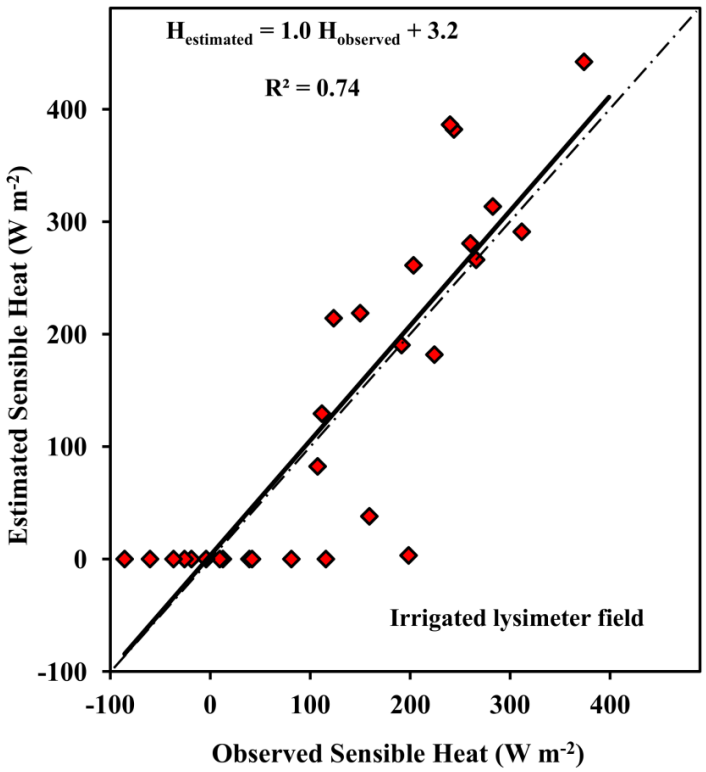

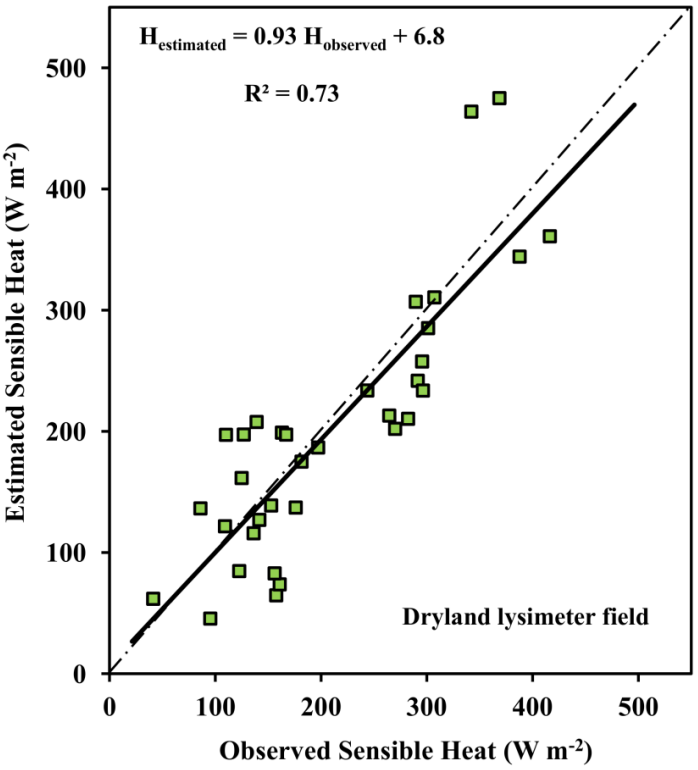

Figure 5.5 Observed versus estimated sensible heat flux for Irrigated and dryland fields (N=34)

Appendix C - Aerodynamic Roughness Parameters

Table 5.7 Aerodynamic roughness parameters and temperature gradient for the four fields under irrigation (NE and SE) and dryland (NW and SW) management.

Date	Field	z_{om} (m)	kB^{-1}	z_{oh} (m)	dT (°C)	r_{ah} (m s^{-1})
26 June, 2008	NE	0.012	19.6	0.00001	9.1	33.3
	SE	0.010	26.5	0.00001	8.8	33.7
	NW	0.009	49.3	0.00001	8.2	34.6
	SW	0.008	60.0	0.00001	8.0	34.9
12 July, 2008	NE	0.052	5.4	0.00026	6.4	17.7
	SE	0.045	5.7	0.00017	7.0	19.0
	NW	0.018	8.7	0.00001	12.3	27.2
	SW	0.024	7.3	0.00002	11.1	25.1
20 July, 2008	NE	0.085	3.4	0.00284	1.7	21.4
	SE	0.065	3.8	0.00152	2.9	23.5
	NW	0.008	14.0	0.00001	11.4	50.7
	SW	0.017	6.9	0.00005	8.7	42.8
28 July, 2008	NE	0.124	2.6	0.00813	-2.3	39.8
	SE	0.104	2.9	0.00551	-1.5	34.9
	NW	0.011	12.6	0.00001	7.3	46.1
	SW	0.018	7.5	0.00004	5.5	40.4
05 August, 2008	NE	0.152	1.9	0.01753	-3.9	430.5
	SE	0.201	1.9	0.02665	-4.0	420.3
	NW	0.014	11.6	0.00001	16.8	66.9
	SW	0.020	6.7	0.00007	14.7	46.9
13 Aug, 2008	NE	0.227	2.0	0.02988	-1.4	28.2
	SE	0.256	2.0	0.03457	-1.4	26.3
	NW	0.029	5.6	0.00016	2.5	39.3
	SW	0.061	3.9	0.00145	1.8	25.2
24 June, 2007	NE	0.015	6.2	0.00003	18.5	66.0
	SE	0.064	3.9	0.00131	6.1	29.9
	NW	0.011	7.4	0.00001	15.6	80.1
	SW	0.011	7.8	0.00001	16.5	80.9
25 June, 2007	NE	0.014	15.1	0.00001	18.6	43.2
	SE	0.073	4.1	0.00142	5.2	20.7
	NW	0.009	130.3	0.00001	15.5	46.2
	SW	0.009	78.4	0.00001	16.1	45.7

Table 5.7 continued

Date	Field	z_{om} (m)	kB^{-1}	z_{oh} (m)	dT (°C)	r_{ah} (m s^{-1})
02 July, 2007	NE	0.020	5.2	0.00012	14.09	46.6
	SE	0.157	2.3	0.01658	1.95	10.8
	NW	0.012	5.8	0.00003	17.30	58.4
	SW	0.013	5.7	0.00004	17.07	56.9
10 July, 2007 AM	NE	0.103	3.1	0.00092	4.4	23.03
	SE	0.227	1.7	0.00231	1.3	49.50
	NW	0.071	4.3	0.00054	6.7	37.23
	SW	0.070	4.3	0.00053	7.0	37.30
10 July, 2007 PM1	NE	0.114	2.8	0.00390	-1.7	46.6
	SE	0.178	1.7	0.02358	-4.1	10.8
	NW	0.067	5.5	0.00031	8.0	58.4
	SW	0.057	5.9	0.00014	8.7	56.9
10 July, 2007 PM2	NE	0.127	3.1	0.00443	-1.9	68.64
	SE	0.199	1.8	0.02757	-3.4	83.69
	NW	0.060	6.3	0.00013	6.9	35.50
	SW	0.052	6.7	0.00006	7.9	38.36
11 July, 2007 PM2	NE	0.157	3.4	0.00710	3.0	16.6
	SE	0.240	2.0	0.03121	0.4	12.2
	NW	0.088	6.4	0.00038	5.6	33.9
	SW	0.074	9.2	0.00008	5.6	42.4
26 July, 2007	NE	0.268	2.0	0.03436	-1.0	22.5
	SE	0.290	1.8	0.04339	-1.2	23.5
	NW	0.138	4.9	0.00159	2.4	22.2
	SW	0.116	5.7	0.00087	3.2	26.2
27 July, 2007 AM	NE	0.268	2.0	0.03613	0.4	6.8
	SE	0.285	1.9	0.04210	0.4	4.0
	NW	0.143	3.8	0.00460	2.6	23.0
	SW	0.124	4.2	0.00306	2.9	28.5
27 July, 2007 PM1	NE	0.270	1.6	0.04283	-4.7	1162.6
	SE	0.288	1.7	0.04619	-4.9	1207.8
	NW	0.141	3.6	0.00480	1.4	31.0
	SW	0.118	4.2	0.00253	2.2	35.4
27 July, 2007 PM2	NE	0.269	1.8	0.03505	-1.2	85.6
	SE	0.292	1.7	0.04495	-1.4	94.0
	NW	0.145	3.9	0.00348	1.9	24.7
	SW	0.124	4.5	0.00203	2.4	29.5

Chapter 6 - Conclusions, Recommendations and Future Directions

Algorithms utilizing remotely sensed data for estimating evapotranspiration (ET) was available from early 1980's and has since improved with enhanced capabilities of earth observation satellites and advances in parameterization of the soil-canopy-air heat exchange mechanism. ET is crucial as it links two fundamental processes; the surface energy balance budget and the water balance budget, both having highly and spatially variable attributes. Remote sensing based energy balance (EB) algorithms is one of the viable means for mapping ET at regional scale which has remarkable applications in agriculture, hydrology and climate studies. Enhancements to these algorithms are important to improve the accuracy of ET maps so that they can used as operational tools for managing water resources and understanding of carbon flux dynamics at regional and continental scales.

The research conducted here is aimed at utilizing finer resolution, high quality data set from BEAREX to evaluate widely used remote sensing based single source EB models. Results from the present study suggested that remote sensing based EB algorithms has the potential to estimate regional ET with adequate accuracy required for assessing crop water demand. A major conclusion derived from the evaluation of three single source energy balance models was the requirement of a mechanism to account for the differences between radiometric (T_s) and aerodynamic (T_o) temperatures. Performance bias was observed for dryland fields with SEBAL and METRIC indicating its inadequacy to address large T_s–T_o differences. SEBS algorithm with an excess resistance parameter (kB^{-1}) performed equally well for both irrigated and dryland conditions, which indicated that kB^{-1} parameter performed as a correction factor to account for the differences between T_o and T_s.

Specific Conclusions

Chapter 2

1. On an average 20% uncertainty in term of CV was observed as a result of subjectivity in the end member selection process. The sensitivity to end member pixel selection is crucial to the performance of SEBAL; hence, a clear methodology for the selection process is required to remove the subjective decision and make the process more robust. A rigorous sensitivity analysis of the 'a' and 'b' coefficients estimation in the temperature gradient relationship is necessary because this forms the backbone of SEBAL.

2. SEBAL ET_i estimates compared reasonably well against the lysimeter values with underestimation error and RMSE close to 0.15 mm h 1 (28%). Errors were relatively small for the irrigated fields as compared with the dryland fields.
3. Modifying the SEBAL algorithm by introducing kB^{-1} parameterization considerably improved the accuracy of ET_i estimation, with an overall RMSE of 0.08 mm h^{-1} (16%). It can be concluded that the temperature gradient (dT) and (T_a-T_o) linear relationship does not have any component to consider for the differences arising due to use of T_s for T_o and hence a realistic correction factor in the form of kB^{-1} has to be incorporated into SEBAL.
4. A kB^{-1} value of 2.3 would grossly underestimate ET for sparse vegetation conditions. Locally calibrated coefficients for the aerodynamic roughness parameters are crucial to the performance of the algorithm.

Chapter 3

1. The results of this study indicate an error range from 11% to 45%, where the lower limit denotes unstressed crop ET and the upper limit refers to sparse/stressed crop ET.
2. The errors from the dryland conditions were reduced from 45% to 25% through the use of a physically based excess resistance model incorporated into SEBAL. The foundation of this improvement is based on the principle of arriving at the right correction factor, which could reduce the consequences of the discrepancy between radiometric and aerodynamic temperature.
3. The SEBAL approach with spatially constant $kB^{-1} = 2.3$, $z_{oh}(z_1) = 0.1$ or $z_{oh}(z_1) = 0.01$, could not account for the spatial variability of the discrepancy between T_o and T_s, and hence underperforms in a realistic agricultural setting or even performs poorly for dryland agriculture system.
4. The kB^{-1} model produce distinctly and statistically different results than the constant kB^{-1} and constant z_1 (z_{oh}) approaches. Constant kB^{-1} (2.3) and constant z_1 (0.1 m and 0.01 m) approaches had similar performance trends.
5. SEBAL performance for irrigated fields (greater ET rates, limited soil water deficits, and complete ground cover) and dryland fields (lower ET rates, greater soil water deficits, and sparse ground cover) were markedly different.

6. The results confirm that for sparse and greater soil water deficits conditions, the single-source resistance formulation have limited capability in predicting H and LE fluxes.
7. The absence of bias error in the kB^{-1} model runs for both dryland and irrigated fields, indicates that kB^{-1} parameter performed well as a correction factor and accounted for the difference between T_o and T_s. It also indicates that kB^{-1} model treated the smaller ET and greater ET crops surfaces appropriately.
8. The limited role of H on the accuracy of LE for irrigated fields with complete ground cover (greater ET surface) negates the advantage received through the accurate estimation of H. Under sparse vegetated conditions (less ET crop surface), LE was sensitive to errors in H estimates, and apparently single resistance formulations like SEBAL performed poorly in estimating H for such surfaces.
9. An uncalibrated kB^{-1} model incorporated into SEBAL performed better for both dryland and irrigated lysimeter fields, compared with other approaches.

Chapter 4

1. The GSS model outperformed METRIC in all the performance statistics.
2. The approach of hot and cold pixel should only be considered as an empirical method for estimating the dT parameter over a relatively homogeneous and well managed landscape, and any physical treatment given to the end member pixel may not warrant performance augmentation.
3. The dT as defined in METRIC and computed from the hot and wet pixel concept may not represent and account for the non-unique relationship existing between T_o and T_s.
4. The GSS model with an empirical correction in the form of excess resistance parameter, kB^{-1}, accounts for the difference between T_o and T_s. Hence an improvement in the overall performance and negligible bias between irrigated and dryland fields can be achieved.
5. The influence of dT cannot be seen under well-watered, densely cropped, energy non-limiting conditions. Because under such a condition, the LE fluxes are much greater than H fluxes and errors in H fluxes would have limited influence on the LE estimation.
6. The accuracy of H fluxes depends on appropriate dT and corresponding r_{ah}. METRIC approach fails in producing appropriate dT/r_{ah} under heterogeneous, sparse and water limited vegetation conditions. Meanwhile, the GSS approach of adopting a constant

radiometric excess resistance parameter (kB^{-1}) not only produced significantly improved results but also reduced bias between irrigated and dryland fields proving that this approach accommodates for the discrepancy between T_o and T_s.

7. The selection criteria of hot and cold pixel or even the physical treatment of the hot and cold pixels has limited and uncertain influence on the performance of METRIC and SEBAL-like models.

Chapter 5

1. SEBS algorithm performed equally well for both irrigated and dryland conditions in estimating the hourly ET with overall relative error of 12.6% .
2. The excess resistance parameter values pooled across the irrigated and dryland fields for the 17 images generated an average value of 6. The aerodynamic resistance value ranged from 17–81 m s^{-1} form the SEBS formulation for the agricultural landscape.

Recommendations

The capabilities and limitations of the various remote sensing based EB algorithms evaluated in this study has paved the way for development of these techniques into an operational ET remote sensing program for management of water resources and monitoring of ecosystem. Two specific recommendations are provided here, which could also form basis for future studies:

1. SEBAL and METRIC: The temperature gradient (dT) derived from hot and cold pixel concept has several drawbacks and uncertainties when applied over heterogeneous landscape. One of the assumptions of this concept is that it accounts for the spatial variability of roughness length for heat transport (z_{oh}). Adoption of a parameterized excess resistance into SEBAL would reduce the dependence on dT parameter, subsequently reducing the uncertainty in the hot and cold pixel selection process.
2. SEBS: In the present study, SEBS was executed using the Monin-Obukhov Atmospheric Surface Layer (ASL) scaling utilizing ground weather station parameters. Accuracy of the weather station inputs especially air temperature value highly influence the performance of SEBS. Spatially interpolated fields of weather inputs should be used when applying SEBS on a regional scale.

Future direction

Future directions of remote sensing based ET mapping technique is driven by the challenges faced in crop production and climate change impacts on biosphere. Sporadic water availability being the major limiting factor for crop production across the globe, the emphasis is now on efficient water management. Prioritization of limited water could only be made through accurate estimation of crop water requirement (crop ET). Conventional irrigation scheduling based on reference ET and crop coefficient cannot cope with the new variety release brought through crop improvement programs. The use of ET maps for irrigation scheduling and in variable rate irrigation applications would bring a breakthrough to irrigation water management. The ratio between actual and potential evaporation, a measure of water deficits, has strong correlation with gross primary production (GPP). Spatially distributed ET incorporated into the carbon budget study would not only improve the understanding of ecosystem dynamics to water stress but also would enhance the capability of regional estimation of net ecosystem exchange (NEE). Hindrances in the operational development of this technique has almost remained the same over the past three decades and these could also be seen the prevailing bottlenecks of this technique. Satellite sensors provide only a snapshot, setting a limit to the potential accuracy of ET estimated by a single satellite overpass. Temporal scaling from instantaneous to daily and further to required resolution is a challenge, which is being worked upon by various research groups. The integration of course and fine spatial resolution imagery through appropriate downscaling technique and data assimilation protocols utilizing the numerous weather and flux tower observations is underway to generate seamless ET maps.